

Alma Mater Studiorum - Università di Bologna

Facoltà di Chimica Industriale
Dipartimento di Chimica Industriale e dei Materiali

Cluster-derived Gold/Iron catalysts for environmental applications

Tesi di Dottorato di Ricerca

Presentata da:
Dott.ssa **Rosa Bonelli**

Relatore:
Dott.ssa **Stefania Albonetti**

Co-relatore:
Dott. **Stefano Zacchini**

Coordinatore:
Prof. **Fabrizio Cavani**

Dottorato di Ricerca in
Chimica Industriale (settore CHIM/04)
ciclo XXII

Esame finale anno 2010

INDEX

ABSTRACT	1
1. AIM OF THE WORK.....	5
2. INTRODUCTION	7
2.1 Gold catalysts.....	7
2.1.1 Brief history of catalysis by gold	7
2.1.2 Gold properties and reactivity	8
2.1.3 Gold nanoparticles properties	9
2.1.4 Bimetallic catalysts containing gold.....	14
2.2 Au supported catalysts preparation	17
2.2.1 Most used techniques	18
2.2.2 Preparation of supported bimetallic systems containing gold	22
2.2.3 Use of carbonyl clusters.....	23
2.3 Reactions catalysed by gold	25
2.3.1 Selective oxidations	26
2.3.2 Reactions for environmental applications	27
2.4 References	33
3. EXPERIMENTAL	41
3.1 Catalysts preparation.....	41
3.1.1 TiO ₂ and CeO ₂ supported catalysts	41
3.2 Catalysts characterization	43
3.3 Catalytic activity measurements	46
3.3.1 Toluene combustion	46
3.3.2 Methanol combustion	47
3.3.3 PROX reaction	48
3.4 References	49
4. TITANIA CATALYSTS.....	51
4.1 Introduction.....	51
4.2 Catalysts preparation and characterization.....	51

4.2.1	Synthesis of Au/FeO _x and FeO _x catalysts	51
4.2.2	IR study during TiO ₂ catalysts preparation	53
4.2.3	Thermal study on cluster decomposition	58
4.2.4	ICP analyses	62
4.3	Catalysts characterization	65
4.3.1	Specific surface area and XRD	65
4.3.2	Study of catalysts thermal treatment	68
4.3.3	TEM study	69
4.3.4	XPS studies	73
4.3.5	Temperature programmed reduction (TPR)	75
4.4	Catalytic activity	78
4.4.1	Toluene combustion	78
4.4.2	Characterization of spent catalysts after toluene combustion reaction	84
4.4.3	Methanol combustion	89
4.4.4	PROX reaction	91
4.5	References	93
5.	CERIA CATALYSTS	95
5.1	Introduction	95
5.2	Catalysts preparation and characterization	95
5.2.1	Synthesis of Au/FeO _x and FeO _x ceria catalysts	95
5.2.2	IR study during CeO ₂ catalysts preparation	96
5.2.3	ICP analyses of ceria catalysts	98
5.3	Catalysts characterization	100
5.3.1	Specific surface area and XRD	100
5.3.2	TEM study	102
5.3.3	XPS studies	104
5.3.4	Temperature programmed reduction analysis	105
5.4	Catalytic activity	109
5.4.1	Toluene combustion	110
5.4.2	Characterization of spent catalysts after toluene combustion reaction	111
5.4.3	Methanol combustion	112
5.4.4	Reaction mechanism for toluene and methanol combustion over titania and ceria catalysts	115
5.4.5	PROX reaction	117
5.5	Effect of catalyst thermal treatment	119
5.5.1	Study on catalysts pretreatment conditions	123
5.6	Iron content effect	131

5.7 Bibliografia.....	139
6. CONCLUSIONS	141

ABSTRACT

During the last years we assisted to an exponential growth of scientific discoveries for catalysis by gold and many applications have been found for Au-based catalysts. In the literature there are several studies concerning the use of gold-based catalysts for environmental applications and good results are reported for the catalytic combustion of different volatile organic compounds (VOCs).

Recently it has also been established that gold-based catalysts are potentially capable of being effectively employed in fuel cells in order to remove CO traces by preferential CO oxidation in H₂-rich streams.

Bi-metallic catalysts have attracted increasing attention because of their markedly different properties from either of the constituent metals, and above all their enhanced catalytic activity, selectivity and stability.

In the literature there are several studies demonstrating the beneficial effect due to the addition of an iron component to gold supported catalysts in terms of enhanced activity, selectivity, resistance to deactivation and prolonged lifetime of the catalyst.

In this work we tried to develop a methodology for the preparation of iron stabilized gold nanoparticles with controlled size and composition, particularly in terms of obtaining an intimate contact between different phases, since it is well known that the catalytic behaviour of multi-component supported catalysts is strongly influenced by the size of the metal particles and by their reciprocal interaction.

Ligand stabilized metal clusters, with nanometric dimensions, are possible precursors for the preparation of catalytically active nanoparticles with controlled dimensions and compositions. Among these, metal carbonyl clusters are quite attractive, since they can be prepared with several different sizes and compositions and, moreover, they are decomposed under very mild conditions.

A novel preparation method was developed during this thesis for the preparation of iron and gold/iron supported catalysts using bi-metallic carbonyl clusters as

precursors of highly dispersed nanoparticles over TiO_2 and CeO_2 , which are widely considered two of the most suitable supports for gold nanoparticles.

Au/FeO_x catalysts were prepared by employing the bi-metallic carbonyl cluster salts $[\text{NEt}_4]_4[\text{Au}_4\text{Fe}_4(\text{CO})_{16}]$ ($\text{Fe}/\text{Au}=1$) and $[\text{NEt}_4][\text{AuFe}_4(\text{CO})_{16}]$ ($\text{Fe}/\text{Au}=4$), and for comparison FeO_x samples were prepared by employing the homometallic $[\text{NEt}_4][\text{HFe}_3(\text{CO})_{11}]$ cluster. These clusters were prepared by Prof. Longoni research group (Department of Physical and Inorganic Chemistry- University of Bologna).

Particular attention was dedicated to the optimization of a suitable thermal treatment in order to achieve, apart from a good Au and Fe metal dispersion, also the formation of appropriate species with good catalytic properties.

A deep IR study was carried out in order to understand the physical interaction between clusters and different supports and detect the occurrence of chemical reactions between them at any stage of the preparation. The characterization by BET, XRD, TEM, H_2 -TPR, ICP-AES and XPS was performed in order to investigate the catalysts properties, with particular attention to the interaction between Au and Fe and its influence on the catalytic activity.

This novel preparation method resulted in small gold metallic nanoparticles surrounded by highly dispersed iron oxide species, essentially in an amorphous phase, on both TiO_2 and CeO_2 . The results presented in this thesis confirmed that FeO_x species can stabilize small Au particles, since keeping constant the gold content but introducing a higher iron amount a higher metal dispersion was achieved.

Partial encapsulation of gold atoms by iron species was observed since the Au/Fe surface ratio was found much lower than bulk ratio and a strong interaction between gold and oxide species, both of iron oxide and supports, was achieved.

The prepared catalysts were tested in the total oxidation of VOCs, using toluene and methanol as probe molecules for aromatics and alcohols, respectively, and in the PROX reaction.

Different performances were observed on titania and ceria catalysts, on both toluene and methanol combustion.

Toluene combustion on titania catalyst was found to be enhanced increasing iron loading while a moderate effect on FeO_x -Ti activity was achieved by Au addition. In this case toluene combustion was improved due to a higher oxygen mobility

depending on enhanced oxygen activation by FeO_x and Au/FeO_x dispersed on titania.

On the contrary ceria activity was strongly decreased in the presence of FeO_x , while the introduction of gold was found to moderate the detrimental effect of iron species. In fact, excellent ceria performances are due to its ability to adsorb toluene and O_2 . Since toluene activation is the determining factor for its oxidation, the partial coverage of ceria sites, responsible of toluene adsorption, by FeO_x species finely dispersed on the surface resulted in worse efficiency in toluene combustion.

Better results were obtained for both ceria and titania catalysts on methanol total oxidation.

In this case, the performances achieved on differently supported catalysts indicate that the oxygen mobility is the determining factor in this reaction.

The introduction of gold on both TiO_2 and CeO_2 catalysts, lead to a higher oxygen mobility due to the weakening of both Fe-O and Ce-O bonds and consequently to enhanced methanol combustion. The catalytic activity was found to strongly depend on oxygen mobility and followed the same trend observed for catalysts reducibility.

Regarding CO PROX reaction, it was observed that Au/FeO_x titania catalysts are less active than ceria ones, due to the lower reducibility of titania compared to ceria. In fact the availability of lattice oxygen involved in PROX reaction is much higher in the latter catalysts.

However, the CO PROX performances observed for ceria catalysts are not really high compared to data reported in literature, probably due to the very low Au/Fe surface ratio achieved with this preparation method.

CO preferential oxidation was found to strongly depend on Au particle size but also on surface oxygen reducibility, depending on the different oxide species which can be formed using different thermal treatment conditions or varying the iron loading over the support.

1. AIM OF THE WORK

During the last years interest on gold catalysis has increased dramatically and many applications have been found for Au based catalysts.

A consistent number of applications have been found for selective oxidation of several compounds and the role of gold in total oxidation has also been extensively investigated, essentially for volatile organic compounds (VOCs) combustion. The removal of VOCs has received particular attention due to the fact that they have been associated with the increase of photochemical smog in urban environments, depletion of atmospheric ozone and the production of ground-level ozone.

Catalytic incineration is one of the most promising technologies for controlling VOCs emission, resulting in their complete destruction and for energy saving. Even if Pd and Pt based catalysts are the most efficient systems used for total oxidation of VOCs, cheaper catalytic materials are under investigation in order to find an alternative for this kind of applications. In the literature there are several studies concerning the use of gold-based catalysts for environmental applications and good results are reported for the catalytic oxidation of different molecules such as alcohols, acetone and toluene.

Recently it has also been established that gold-based catalysts are potentially capable of being effectively employed in fuel cells in order to remove CO traces by preferential CO oxidation in H₂-rich streams. This last technology is one of the most promising approaches to hydrogen purification for its application in polymer electrolyte membrane (PEM) fuel cells, which are the most technologically advanced energy conversion systems but are extremely sensitive to traces of CO contamination.

Bi-metallic catalysts have attracted big attention because of their markedly different properties from either of the constituent metals, and above all their enhanced catalytic activity, selectivity and stability. In the literature, there are several studies demonstrating the beneficial effect due to the addition of an iron component to gold

supported catalysts in terms of enhanced activity, selectivity, resistance to deactivation and prolonged lifetime of the catalyst.

Since it is well known that the catalytic behaviour of multi-component supported catalysts is strongly influenced by the size of the metal particles and by their reciprocal interaction, we tried to develop a methodology for the preparation of iron stabilized gold nanoparticles with controlled size and composition, particularly in terms of obtaining an intimate contact between different phases. A novel preparation method was developed for the preparation of iron and gold/iron supported catalysts using bi-metallic carbonyl clusters as precursors of highly dispersed nanoparticles over TiO_2 and CeO_2 , which are widely considered two of the most suitable supports for gold nanoparticles.

The aim of this preparation method using carbonyl Fe-Au clusters with a well defined structure was, in fact, to anchor gold nanoparticles to the support via an iron layer. In this way we tried to stabilize gold particles and, at the same time, exploit the beneficial effect of gold on iron oxide since it is well known that gold enhances iron oxide reducibility promoting the formation of anionic vacancies where oxygen can chemisorb.

The prepared catalysts were tested in the total oxidation of VOCs, using toluene and methanol as probe molecules for aromatics and alcohols compounds, and in the PROX reaction.

The characterization by BET, XRD, TEM, H_2 -TPR, ICP-AES and XPS was performed in order to investigate the catalysts properties, with particular attention to the interaction between Au and Fe and its influence on the catalytic activity.

2. INTRODUCTION

2.1 Gold catalysts

2.1.1 Brief history of catalysis by gold

In the past gold had been generally regarded as a poor catalyst due to its chemical inertness when it is in a bulk form. Nevertheless during the last years we assisted to an exponential growth of scientific discoveries for catalysis by gold and hundreds of scientific papers are published on this topic every year due to the discovery that when it is subdivided down to the nanoscale it shows a surprisingly reactivity [1].

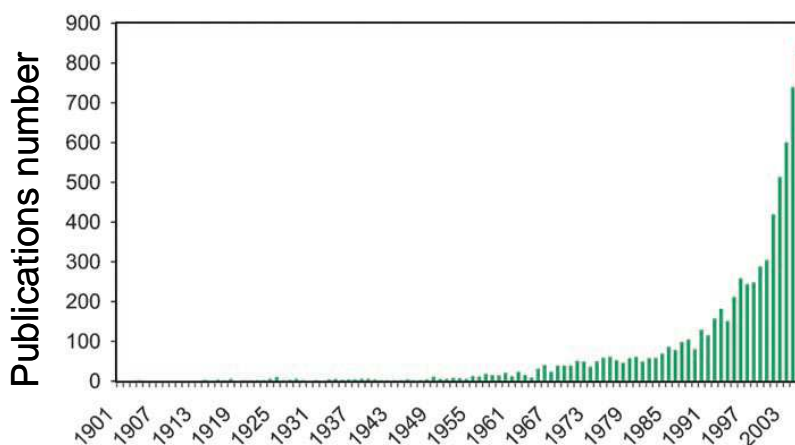


Figure 2.1: Number of publications on gold catalysis during last century.

Gold catalysis had received big attention since Haruta and co-workers reported that some gold catalysts were particularly active for low temperature CO oxidation [2]. Previously some other attempts were made in order to understand if there was any gold catalytic activity when dispersed as small particles. In the 1970s Bond and Sermon [3] [4] reported some interesting results on the hydrogenation of alkenes

and alkynes over Au/SiO₂, while Paravano and co-workers demonstrated an appreciable activity of Au/MgO and Au/Al₂O₃ catalysts in oxygen and hydrogen transfer reactions [5] [6]. Another approach was followed in the late 1970s by Ozin et al. [7] in order to understand the Au size effect starting from a single cluster of atoms; they reported that atomic Au species could react with a CO + O₂ matrix at 10K and form a complex that at higher temperature (30-40K) decomposes to CO₂. These studies demonstrated that small gold nanoparticles exhibited high catalytic activity for hydrogenation and oxidation reactions, but at that time only few researchers recognised the importance and the implications that such discoveries could imply. The attention on gold catalysis was renewed some years later, when Hutchings discovered that Au was the most active catalyst for the hydrochlorination of acetylene to vinyl chloride [8] and the pioneer work on CO oxidation conducted by Haruta showed the great potential of gold as a catalyst. From then on a remarkable growth in the exploration of gold catalytic properties was observed and its application are always increasing.

2.1.2 Gold properties and reactivity

The fact that Au was usually viewed as a poor catalyst is due to its small chemisorption ability compared to the platinum group metals (PGM). The Tanaka-Tamaru Rule [9] had shown that there is a parallelism between the strength of oxygen chemisorption and any related molecules and the enthalpies of formation of the most stable oxides or the analogous bulk compounds where these exists. Looking at calculated oxygen chemisorption energies on a selection of transition metals showed in Figure 2.2 it can be seen that:

- the metals located above and to the left of Au in the periodic table have increasingly large chemisorption energies;
- the metals closer to Au can bind oxygen weakly,
- Au is the only one with an endothermic chemisorption energy.

Cr	Mn	Fe -6,30	Co -5,07	Ni -3,90	Cu -2,51
Mo -7,48	Tc	Ru -4,62	Rh -4,03	Pd -1,20	Ag -0,65
W -8,62	Re	Os	Ir -4,65	Pt -2,17	Au +0,54

Figure 2.2: The dissociative chemisorption energies for oxygen on transition metalsurfaces with respect to a molecule in vacuum calculated by density functional theory (DFT).

In order to understand the catalytic properties of gold, it must be compared with Group 11 elements. The chemistry of gold ($5d^{10}6s^1$) is due to highest first ionization energy, thus the easier tendency to acquire a further electron to complete the $6s^2$, rather than lose the single electron on the 6s orbital and exist in the Au^{+1} form. The differences between the 4d and 5d elements (Cu and Ag) and their compounds have been ascribed to the difference in the first ionization energy.

Due to the large mass of its nucleus the relativistic effects are very important for Au [10] [11] [12]. Because of the increased mass of the nucleus, the s and p orbitals are contracted, whereas the d and f orbitals are expanded [13], thus the 6s orbital is more contracted and stabilized. Au optoelectronic properties are also different from its antecedent metals in Group 11. The yellow colour of Au is similar to that of Cu but different from that of silver and it due to the optical absorption in the visible region of the spectrum, depending on the smaller gap between the 5d band and 6s level [11] [14]. In the absence of this effect, gold would be white like silver and show the same propensity to tarnish. Gold can also be obtained in red, blue and violet colloidal forms by addition of various reducing agents to very dilute aqueous solution of gold(III) chloride.

2.1.3 Gold nanoparticles properties

Factors affecting the activity of supported gold nanoparticles are basically four:

1. particle size and shape;

2. interaction with the support;
3. presence of ionic gold;
4. preparation method and pre-treatment conditions.

The last factor will be discussed later.

2.1.3.1 Particle size effect

For many reactions the high activity of gold catalysts is due to Au particles size. Except for H₂ oxidation and hydrocarbon hydrogenation, most reactions are remarkably structure-sensitive over supported Au catalysts [15]. Thus, for all other reactions the average size of gold particles should be below 5 nm.

In general when the particle size decreases there is a series of effects due to the higher dispersion degree of the metal over the support:

- the fraction of atoms at the surface increases; consequently they can vibrate more freely, the melting temperature decreases and surface mobility increases;
- the coordination number of the atoms is lower then their reactivity is higher; moreover, the overlap of electron orbitals is smaller and the band structure resulted weakened;
- a larger fraction of the atoms comes in contact with the support, and the length of the perimeter metals is longer;
- more steps, edge and kink sites are formed on the particles.

In the literature there are many examples that highlight the role of the Au particle size in various reactions. In order to investigate why the size of Au nanoparticles influences so much their catalytic activity, theoretical calculations have been used. It was proposed that the high activity results from a quantum size effect with respect to the thickness of gold layer, based on the onset of a metal-to-non-metal transition that was observed to occur for very small Au particles (below 5 nm) [16]. For example the specific rate of CO oxidation in PROX reactions is strongly dependent on Au particle size, turnover frequencies increasing with Au dispersion [17] [18].

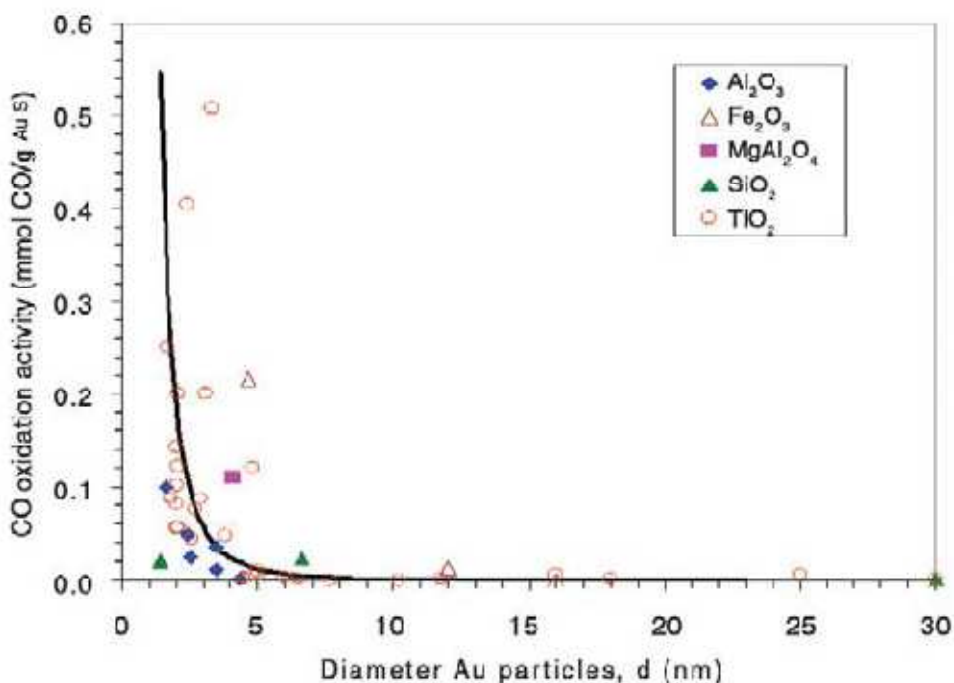
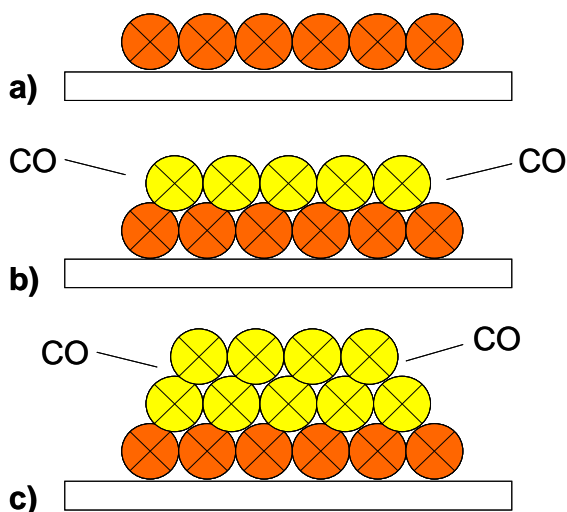


Figure 2.3: Reported catalytic activities for CO oxidation at 273 K as a function of Au particle size for different support materials.

Other studies showed that low coordinated Au atoms found on small particles have been suggested to play an important role in the activity of supported Au [19] [20]. Moreover it is often stressed that external gold atoms in contact with the support differ in some significant way from the others, and those at the edge play a paramount role in catalysis [21] [22] [23]. It has recently been claimed that structures described as bilayers, with no more than two layers of gold atoms, have greater activity than either thinner particles or larger multilayer particles for which many of the surface atoms are ineffective [24] [25] [26]. Menegazzo et al showed by volumetric measurements that the ratio of CO(ads) to Au(surface) is sometimes quite small (~10-15%) [27]. This effect can be explained looking at the Figure 2.4, where it is assumed that CO molecules can only be adsorbed with sufficient stability on atoms of low coordination number, and that on large particles these are too distant from the first layer atoms to be useful.



2.4: Variation of CO oxidation activity with particle size

a): small particle, low or zero activity; b): bilayer particle, maximum activity; c), large particle, CO molecules too far from first layer, low activity

2.1.3.2 Gold-support interaction

The choice of the most suitable support for gold nanoparticles is a fundamental factor. In fact, the physical and catalytic effects depending on particle size are strongly correlated by the contact with the support. Moreover the shape of a gold particle depends on the interaction between the gold and the support varying the amount of edge and corner atoms and strongly affecting Au catalysts activity. Generally the role of the support is to stabilize small gold particles during the preparation and further thermal treatments [28] [29] but there are also evidences for electronic effects on Au nanoparticles by the support. With model catalysts prepared by vapour-deposition of gold atoms onto MgO(100) [30] or TiO₂(110) [26] surfaces, the particles appear to become electron rich by electron transfer from F-centres on which they are nucleated; in this method Au⁰ atoms arrive at a dehydrated surface, and if mobile migrate to the nucleating centre. Au nanoparticles can also affect the

properties of the support. This effect is seen most clearly by the easier reduction of supports such as CeO_2 and Fe_2O_3 [31] [32] [33] [34]; with the former the interaction between metal and oxide can be quite complex, with Au^{3+} ions entering the oxide lattice and creating additional anion vacancies and easier O^{2-} mobility [35] [35] [36]. With oxide supports that are to some degree reducible under pre-treatment or reaction conditions (i.e. by CO or H_2) the resulting anion vacancies close to gold particles have been suggested as the site of oxygen adsorption and activation [37]; this will not happen to any significant extent with the ceramic oxides (MgO , SiO_2 , Al_2O_3), so that gold on these supports must rely on another type of mechanism for its activity. Other aspects of the support that influence performance include surface area [38], particle size and crystal habit. From a practical point of view, the choice of the support depends on which kind of reaction should be catalysed by Au.

2.1.3.3 The nature of gold active sites

The nature of the active sites was mostly a matter of debate in CO oxidation, the most frequently studied reaction over Au-based catalysts. However, until now there is no general consensus about this. As already mentioned in the previous paragraph, for some systems it is clear that the size of the Au crystallites is not sufficient to explain the high activity. Therefore, it has been proposed that the perimeter or gold-support interface [39] [40] [41] [42] or small Au clusters that have nonmetallic electronic properties due to a quantum-size effect [16], or step sites on the surface and strain defects [43] are more important than only Au nanoparticles with a size between 2 and 5 nm. On the other hand, other groups are convinced that Au^{3+} is responsible for the high activity in reactions such as CO oxidation [44], hydrogenation of ethene [45] [46], ethyne hydrochlorination [8] [47] [48], or water-gas shift [49]. An intermediate model was proposed: an ensemble of metallic Au atoms and Au cations with hydroxyl ligands [50] [51]. This model suggests that the Au cations must be stable in a reducing environment and also in the neighborhood of metallic gold. It was further concluded that Au^+ would be able to satisfy these requirements, rather than Au^{3+} and $[\text{Au}^+-\text{OH}]$ has been proposed as the cationic component. It has also been suggested that the active site for gold catalysis is anionic gold, Au^- . These species are mainly formed if Au is deposited on a defect-rich support, i.e. with an increased concentration of F-centres [52] [53] [54]. Another

factor that is believed by some authors to have a great influence during the catalytic reactions is water. According to some studies, the moisture effect is directly connected with CO activation and the nature of the support [55]. More water is required to promote CO oxidation over Au/Al₂O₃ or Au/SiO₂, compared to Au/TiO₂. H₂O was also found to be responsible for the stabilization of Au⁺ [17] [56], as well as for the deactivation of the catalyst, thus a detrimental role of H₂O [41] [57] [58] [59]. It was, for example, suggested that in the presence of water the dissociation of oxygen on gold particles may be activated and that oxygen reacts with water to produce an oxygen radical available for reaction and two surface hydroxyl groups [60]. A beneficial effect of water on the activation of O₂ was also proposed by Bond and Thompson [50]. Their reaction mechanism proceeds via a reaction between an OH group that spilled over from the support to Au³⁺ and the CO adsorbed on the gold particle, via a carboxylate group. The existence of OH groups was used to explain the negative activation energy found for Au/Mg(OH)₂ tested under ultra-dry reaction conditions in CO oxidation [61]. Water was even proposed as an easy way to regenerate the Au/Al₂O₃ catalyst [62]. For other reactions, reports on the effect of water on the catalytic activity of Au-based catalysts are rather scarce. However, Haruta reported that some Au-based catalysts were tolerant against moisture in NO reduction by CO [63] [64], and in reduction of NO with C₃H₆ in the presence of oxygen [65].

2.1.4 Bimetallic catalysts containing gold

In the field of heterogeneous catalysis a very large use has been made of catalysts containing two or more metals; bimetallic catalysts have attracted big attention because of their markedly different properties from both of the constituent metals, and above all their enhanced catalytic activity, selectivity and stability [66]. The addition of a second metal can favour the reduction of the first, increase the dispersion of a metal which has tendency to form large particles or decrease its fritting [67]. Some bimetallic systems have industrial applications, like Pt-Ir and Pt-Re for petroleum reforming, Pt-Sn for alkanes dehydrogenation and much of academic work has focussed on catalysts containing a metal of Group 8-10 plus one of Group 11.

In the literature there are several instances of gold improving the activity of palladium in reactions involving only hydrogen; bimetallic catalysts containing gold show activities that are superior to those of both components separately in the synthesis of hydrogen peroxide, vinyl acetate, and in a certain number of selective oxidations but also combustion reactions.

It was found that the selective oxidation of hydrogen to hydrogen peroxide, the combination of palladium with gold worked better than gold used alone and a 1:1 ratio was usually used [68]. The best catalyst is composed of Au-Pd-core shell particles. In the case of Au-Pd/Al₂O₃ this structure appeared to be generated during the reaction and may be the result of a sort of extractive chemisorption: basically both reactants (H₂ and O₂) will chemisorb more strongly on palladium and hence draw the particle to the surface [69]. Bimetallic Pd–Au supported on sulphated zirconia was successfully tested for the direct synthesis of hydrogen peroxide under very mild conditions (1 bar and 293 K) and outside the explosion range. The addition of gold in a relatively high amount (1/1 wt) to palladium improved the productivity and the selectivity of the process, producing a hydrogen peroxide concentration already useful for industrial applications [70].

A promotional effect of gold on palladium was also observed in the synthesis of vinyl acetate; its positive influence has been assigned to an electronic interaction which modifies the adsorption strength of various species on the palladium complexes and increases the rate of vinyl acetate desorption [71].

Pd-Au and Pt-Au catalysts supported on graphite (Pd, Pt : Au = 1 : 1) showed higher activity than the single metals for glycerol oxidation [72] [73] and for D-sorbitol oxidation [74] [75]. Au and Pd supported on mesoporous TiO₂ was found to be very active for catalytic combustion of propene and toluene [76]. The authors explained the promotional effect of gold on palladium partly by the presence of small metallic particles but mainly by Au-Pd-core shell particles.

The addition of Au to copper has been proposed for CO oxidation [77] [78], but also for propene epoxidation [79] and, recently, the selective oxidation of benzyl alcohol to benzaldehyde catalysed by bimetallic AuCu catalysts has been reported [80]. The inclusion of iron in gold supported catalysts has been also reported in the literature in order to increase catalyst's stability during CO oxidation and other applications. A separate and more detailed section about Au-Fe catalysts is reported following.

2.1.4.1 Iron addiction to gold catalyst

The use of mixed oxides in catalysis offers the opportunity of tuning the material properties to obtain specific sites that influence catalytic activity. Doping a reducible oxide, like TiO_2 , could lead to modifications of electronic properties or changes in the structure; consequently an improved catalytic activity and increased lifetime can be obtained [81].

In the literature there are several studies demonstrating the beneficial effect due to the addition of an iron component to gold supported catalysts in terms of enhanced activity, selectivity, resistance to deactivation and prolonged lifetime of the catalyst. For example the effect of iron on the activity of $\text{Au}/\text{Al}_2\text{O}_3$ in propene total oxidation was investigated [82]. The catalytic activity was improved by the addition of FeO_x species, that were found to act as structural promoter but also as co-catalyst. In this work it was proved that the gold particles were stabilized against sintering and that the lattice oxygen of the oxide plays an active role via the Mars-van Krevelen mechanism.

FeO_x is also one of the most promising promoters to enhance the catalytic performance of $\text{Au}/\text{Al}_2\text{O}_3$ for methane oxidation [83].

Moreau and Bond [84] demonstrated that the addition of iron during catalyst preparation lowered the rate of deactivation in CO oxidation when TiO_2 , SnO_2 , and CeO_2 were used as supports. Both the higher activity and the improved stability are linked to the ability of FeO_x phase to provide hydroxyl groups that are needed for the catalytic cycle and to form anion vacancies at which oxygen can chemisorb [85]. Shou and co-workers showed that the introduction of iron as additive of Au/TiO_2 catalysts increased the activity and stability even if this material did not have appreciable activity at temperature below 20°C [86].

$\text{Au}/\text{TiO}_2\text{-FeO}_x$ was found to be active in the partial oxidation of methanol. In this case the role of FeO_x additive was twofold: it was found to stabilize the gold particles against sintering and to provide active oxygen for the reaction system, thereby inhibiting the complete reduction of ionic gold, which is necessary for higher catalytic activity [87].

Corma et al. demonstrated that the addition of iron to high surface area TiO_2 leads to an increased number of oxygen defect sites that can react with O_2 forming peroxide and superoxide species. They observed that in the presence of gold

nanoclusters on the TiO_2 surface, the superoxide species become highly reactive and the activity of the supported gold catalyst for CO oxidation resulted strongly increased. Other studies also indicated a strong interaction between gold and the support and the presence of iron near their interface. The high activity was attributed to the enhanced oxygen activation on defects in this kind of sites that generate oxygen vacancies [88].

The influence of iron additive on redox, electronic and catalytic properties of gold incorporated into zeolite catalysts have been studied by Pestryakov [89]. In fact the structure of zeolites favours the formation of small gold nanoparticles (< 2 nm) that are very active for low-temperature CO oxidation. These species are unstable in zeolites and may be deactivated by oxidative pretreatments; however iron oxides was found to be one of the most efficient additives for Au/Fe/Y-zeolite catalyst in CO oxidation. The interaction of gold with iron in these materials leads to mutual influence on redox properties of Fe and Au ionic species and facilitates their reduction; this effect is explained by partial reduction of Fe species and Au clusters with CO at high temperature. Fe additive stabilizes the low-temperature gold active species and makes them insensitive to redox treatments.

Recently a Au/FeO_x/CeO₂ catalyst was found to be very active for CO oxidation at room temperature. The reason of such good performance has been attributed to the easy change of Au oxidation state; it appeared that the nature of the support and the presence of Fe³⁺/Fe²⁺ and Ce⁴⁺/Ce³⁺ couples facilitate gold oxidation, supporting the hypothesis that Au⁺/Au⁰ redox couple operate in the CO catalytic oxidation [90].

2.2 Au supported catalysts preparation

The properties of gold catalysts depend on the preparation method, which strongly influences Au particle size.

The precursors used in preparing supported gold catalysts are salts or complexes where gold is usually in + 3 oxidation state, while few of them are in +1 oxidation state, that is more unstable. The most used Au(III) precursor is the chloroauric acid (H[AuCl₄] · 3H₂O), which is an orange solid commercially available. This compound in water solution is a strong acid capable of dissolving alumina and magnesia.

Gold chloride (AuCl_3) is also occasionally used.

For most of the preparation methods gold is in +3 oxidation state after drying but it can be easily reduced to the metallic state by thermal treatments which can be performed either in oxidising or reducing atmospheres. Thermal treatments are often carried out in air but it is very important to operate under controlled conditions because parameters such as the nature of the gas, the flow rate, the final temperature and the heating rate, all influence the particle size.

The preparation method, the thermal treatment and the nature of the support may also affect the morphology of the particles.

2.2.1 Most used techniques

Many different techniques can be used in order to prepare supported gold catalyst and several methods have been developed to obtain systems with good performance. The most used techniques are listed below.

2.2.1.1 Impregnation

Impregnation is the simplest method which can be used with any kind of support. However, this method is not suitable for Au for at least two reasons. The first reason is that Au(III) has a relatively low affinity for metal oxides and, thus, the interaction with the support is weak. Secondly, during calcination of HAuCl_4 , because of the presence of chloride ions, the coagulation of Au particles is greatly enhanced and the result is an inactive Au-based catalyst, due to the formation of large, inactive Au ensembles. However, recently, a modified impregnation method was reported by Datye et al. [91]. According to their results, it is possible to obtain Au-based catalysts with an average particle size around 2.4 nm with a good activity in CO oxidation.

2.2.1.2 Coprecipitation

Coprecipitation is a single step method very easy to carry out by which the support and the gold precursors are formed at the same time [92]. Usually it is performed adding sodium carbonate to aqueous solution of HAuCl_4 and the nitrate of the metal precursor of the support. This method usually leads to good gold dispersion (< 10

nm) and to oxide surface area larger than in the absence of gold, even if some of the gold particles could be embedded in the bulk of support. Au on iron oxide is one of the most studied catalyst prepared by this method, because of the many possible structures that the support can adopt. However, this method works well only for certain metal oxide because the rates of precipitation of the two hydroxides and their affinity determine the gold particle size.

2.2.1.3 Deposition-precipitation (DP)

This method implies a process whereby the hydroxides or hydrated oxide are deposited onto the surface of the support as the result of gradually raising the pH of the solution in which the support is suspended. The precipitate may be nucleated by the support surface, and when properly performed, the whole of the active phase results attached to the support. Deposition-precipitation is the most widely used method for preparing active Au-based catalysts [15]. There are different ways to deposit Au onto the support: either by adjusting the pH of HAuCl_4 with Na_2CO_3 or NaOH and then adding the support, or by slowly increasing the pH of the HAuCl_4 solution in the presence of the support [93]. After washing with water to remove as much of the chlorine and sodium as possible, the product is dried and thermally treated under the desired conditions. This basic method has many variations, such as pH, temperatures of preparation and washing and use of other bases, such as ammonia. [94] [95] [96]. Some of these parameters have been systematically investigated; no significant differences were observed but there are often problems of reproducibility. Anyway it is claimed that very small Au particles are obtained, highly dispersed over the support.

Good results have been obtained using urea as base in the DP procedure, with the advantage that all the gold in solution is deposited onto the support. The use of urea requires a longer preparation time. In fact urea hydrolysis occurs only when it is heated above $60\text{ }^\circ\text{C}$, whereby there is a gradual and homogeneous release of hydroxyl ions and increase of the solution pH. Setting the temperature and a proper DP time it is possible to obtain very small Au particle size, which value can be tuned by varying the reaction time [97].

2.2.1.4 Deposition of organogold complexes

The advantage of using organogold complexes, such as phosphines, is that they do not contain chloride and the counter-ion is easily decomposed or eliminated. On the other hand, the complex has to be synthesized and generally nonaqueous solutions are needed, which means that the support must be dehydrated, the solvent dried and the finished catalyst stored in proper and controlled conditions, very often under vacuum.

Gold-phosphine complex $[\text{Au}(\text{PPh}_3)\text{NO}_3]$ and the cluster $[\text{Au}_9(\text{PPh}_3)_8](\text{NO}_3)_3$ have been used to prepare supported gold catalysts [98]. The supports were impregnated with a solution of the precursors in dichloromethane, that was removed by evaporation. Large particles were obtained after thermal treatment, but smaller particles were obtained by impregnation of freshly precipitated hydroxide with an acetone solution of the precursors [99]. In fact, during thermal treatment, the precursor ion and the hydroxide decompose simultaneously and this facilitates the gold-support interaction, which reduces mobility of the gold species during heating, thus preventing their sintering. More recently $[\text{Au}_6(\text{PPh}_3)_6](\text{BF}_4)_2$ was used to prepare Au/TiO_2 having small gold particles [100]. Other complexes used to obtain supported gold particles are the isonitrile gold (I) nitrate $[\text{Au}^{\text{I}}(\text{NO}_3)(\text{CN-Bu}^{\text{I}})]$ to prepare $\text{Au}/\text{Fe}_2\text{O}_3$ [101] and dimethylgold acetylacetonate $\text{Me}_2\text{Au}(\text{acac})$ which was used to deposit gold on magnesia, titania, alumina and NaY zeolite [102] [103] [104] [105] [106] [107].

2.2.1.5 Chemical vapour deposition (CVD)

In chemical vapour deposition (CVD) a volatile organogold compound, such as dimethylgold acetylacetonate, reacts with the surface of a support, on which it decomposes to metallic particles or a coherent film if the support is a flat surface. In this way small gold particles can be obtained, but with a broad size distribution [108]. This is probably one of the most successful methods for obtaining small gold particles on silica, with the further advantage of absence of chloride ions.

2.2.1.6 Deposition of colloids

The advantage of using the colloidal route for preparing supported gold catalysts lies in the way that conditions of preparation can be manipulated to give particles that have a narrow size distribution about the desired mean, which can be very small and particle shape can also be controlled in this way.

Gold particles can be dispersed on supports by dipping the supports in the prepared gold suspension, followed by washing and drying. In order to obtain supported particles which size is not much larger than they were in the colloidal suspension various parameters must be controlled, such as the nature and concentration of the stabilizer, the stabilizer/gold ratio, and the nature of support.

Au sols have been used to support gold nanoparticles on different materials such as titania, silica, alumina, zirconia and activated carbon, and can be obtained also by microwave synthesis [109] [110] [111] [112].

2.2.1.7 Less conventional methods

The above mentioned methods for preparing gold supported nanoparticles are the most used ones, but there are also many others under investigation. They include

- sol-gel technique, which involves the hydrolysis of a metal alkoxide in a water-alcohol solution of HAuCl_4 and it is mostly used for preparing gold-containing films oxide supported on wafers [113] [114]; photochemical deposition, during which Au is reduced on a support with a suitable bandgap by UV irradiation (usually semiconductors) [115];
- sonochemical techniques, which allow to deposit gold nanoparticles on the surface of supports by ultrasound, which induces chemical changes due to the cavitation phenomena caused by the formation, growth and implosive collapse of bubbles in a liquid [116] [117];
- spray techniques, atomising by ultrasonic devices the solutions containing both gold and support precursors, i. e. for preparing Au/TiO_2 catalyst [118]; more raffinate techniques such as cluster or atom beam deposition, or direct oxidation of bulk alloy and solvated metal atom dispersion or impregnation.

2.2.2 Preparation of supported bimetallic systems containing gold

Gold-based supported bimetallic catalysts have found numerous applications due to their superior performances compared to simple gold catalysts, as described previously.

The preparation of a supported bimetallic catalyst is not trivial: you have to ensure that the components reside in the same particle in the finished catalysts, because a synergistic effect between the two metals can be obtained only if they have proper size and they are in intimate contact.

The classical methods used for the preparation of supported Au catalysts are very difficult to be applied for the preparation of bimetallic small particles unless the precursors in solution interact strongly with each other.

In order to prepare gold-containing bimetallic catalyst three different routes can be followed:

1. To use metal precursors in solution that do not interact each other
2. To perform a series of surface reactions in order to create the interaction between the two metals;
3. To use directly bimetallic precursors.

2.2.2.1 Methods with non interacting precursors in solutions

Methods for preparing bimetallic supported gold catalysts that do not involve any kind of interaction between the precursors in solution are co-impregnation, co-adsorption of cations, co-deposition-precipitation and photoreduction.

Co-impregnation of a support by a solution containing precursors of the two metals is the simplest and most employed method that can be used, but if chloride salts are used there could be the problem of sintering during the following thermal treatment.

Pt-Au on silica was prepared by incipient wetness impregnation with chloride precursors, but large particles (> 20 nm) and a phase separation was observed [119] [120] [121]. PdAu/TiO₂ and PdAu/Fe₂O₃ have been prepared by Edwards and co-workers by co-impregnation of chloride precursors giving core-shell particles with a bimodal distribution of size with a Pd-rich shell [68]. Co-adsorption of cations gave good results in the case of Pd-Au and Pt-Au bimetallic particles inside Y zeolites prepared by simultaneous or sequential exchange with the appropriate ethylenediamine complex ions and various thermal treatments. [67]

Pd-Au and Pt-Au on titania-silica supports have been successfully prepared by co-deposition-precipitation, but poorest results have been obtained with Pd-Au/CeO₂ catalysts.

Sequential photoreduction has been used to prepare PdAu/Nb₂O₅ catalyst [122] and AuPt/TiO₂ have also been made by irradiation of platinum acetylacetonate in the presence of Au/TiO₂ made by DP [123].

2.2.2.2 Use of bimetallic precursors

Supported bimetallic catalyst can be prepared starting from bimetallic precursors: molecular cluster compounds, colloidal particles or dendrimer-stabilized particles can be used.

Bimetallic molecular cluster containing gold can adsorb intact on supports and the ligands can be removed by heating. The most used bimetallic cluster compounds are the ones stabilized by phosphine ligands, while is not diffuse the use of bimetallic carbonyl cluster containing gold, even if they were discovered and studied some time ago.

The use of bimetallic colloid is more diffuse since their composition can be easily tuned using mixed chloride precursors solutions which can be reduced in several ways after addition of a stabilizer.

In the literature several catalysts prepared in this way are reported: Pd-Au on titania [124], silica [125] [126] or carbon [72], Pt-Au on carbon [127] and Ag-Au/MCM-41 [128].

The use of dendrimer-stabilized bimetallic particles is another elegant method in order to prepare supported catalysts, by which particles size are perfectly controlled because after removing the dendrimer their size is generally retained.

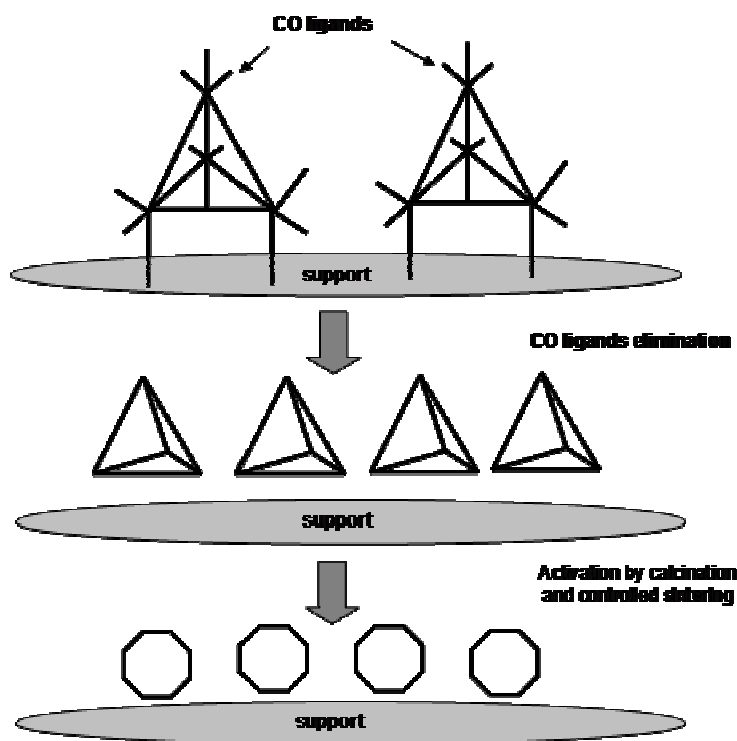
Cluster deposition using laser vaporization can also be used for this purpose.

2.2.3 **Use of carbonyl clusters**

Metal clusters of nanometric sizes stabilised by ligands are possible precursors for the preparation of catalytically active nanoparticles of controlled sizes [129]. These offer the advantage of having sizes and composition perfectly controllable and uniform and, finding the conditions to avoid agglomeration and sintering of the

nanoparticles, may be used for the preparation of catalytic materials with high activity and/or selectivity.

In particular, metal carbonyl clusters (MCC) have attracted great attention thanks to their structural, chemical-physical and bonding properties [130] [131] [132] [133]. If MCCs are mounted on a support surface, the ideal way to get metal particles is to remove the CO ligands maintaining the unperturbed metal framework that could be a building block in the controlled aggregation step (see Scheme 1).



Elimination of the carbonyl ligands can be carried out by different treatments (for example thermal treatment). The effect of decarbonylation treatment is strongly influenced by the nature of the cluster and the support and by the cluster–support interaction. The real transformations taking place are very complex, i.e. it was observed for ruthenium and iron–ruthenium bimetallic carbonyl clusters on silica and alumina. To obtain the supported MCCs, $\text{Ru}_3(\text{CO})_{12}$ and $\text{H}_2\text{FeRu}_3(\text{CO})_{13}$ molecular clusters were deposited on partially dehydrated SiO_2 and Al_2O_3 by impregnation with pentane solution of the carbonyl clusters, then they were dried in vacuum.

The stability of the cluster deposited depends also on its own nature. For example, $\text{Fe}_3(\text{CO})_{12}$ was highly reactive towards oxidation, and iron oxide were formed on both silica and alumina in a fast reaction, however, Ru-dicarbonyls were stable intermediates bound to the surface. Finally, how the conditions of decarbonylation affect the final metal dispersion is mentioned: depending on the gas atmosphere, highly dispersed metallic Ru or support bonded Ru-oxide can be formed. [134]

Some examples of materials obtained introducing carbonyl clusters in mesoporous silica have appeared recently in literature and the results obtained in terms of catalytic performances, selectivity, stability and recovery candidate these catalysts as new materials for clean technologies [135]. In order to avoid sintering, the catalytic reactions must be carried out under mild conditions, compatibly with activity. This limitation may be overcome acting on the composition of the metal nanoparticles and on the nature of the support. Several elements of the main group may be introduced on the surface or as interstitial atoms within the clusters, increasing their stability. Further developments may be obtained by employing bimetallic clusters [136], in particular coupling a catalytically active metal with a second one which may form an oxide layer strengthening the interaction between metal nanoparticle and support.

The chemistry of metal carbonyl clusters is extremely developed at the molecular level, regarding their synthesis, chemical, physical and structural properties [137]. Several species differing in sizes and composition may be prepared, including Fe-Co, Fe-Ni, Fe-Pd, Fe-Pt, Fe-Ag, Fe-Au, Ni-Co, Ni-Pd, Ni-Pt, Co-Pt bimetallic clusters. Moreover, playing on their charge and on the counter-ion, is possible to make these species soluble in common organic solvents but also in water. In this way, they may be easily transferred onto the supports or printed on surfaces with interesting applications in nanochemistry [138].

2.3 Reactions catalysed by gold

Gold catalysts with selected support materials can promote many reactions that usually occur at much lower temperature or with higher selectivity towards the desired products over gold catalyst than over other metal catalysts. The most studied reaction catalyzed by gold is CO oxidation, that has attracted so great attention for the number of possible applications at ambient temperature (such as

gas sensors, respirators and carbon dioxide laser) and for the ease in the following the reaction, even if the interpretation of the mechanism is not so simple. Strictly connected to CO oxidation there is PROX reaction (PReferential CO OXidation) in order to purify Hydrogen for PEM fuel cells application. Anyway in the literature there are many reactions in which gold catalysts can be used i.e partial oxidations, hydrogenations, Water Gas Shift (WGS) and several reactions to reduce environmental pollution such as NO_x reduction, VOC removal, dioxins destruction.

2.3.1 Selective oxidations

The discovery of the remarkable effectiveness of gold as a catalyst for selective oxidation of hydrocarbons and for further oxidation of organic molecules containing oxygenated groups has been a surprise comparable with its ability in CO oxidation at low temperature. In this context, beside the commercial interest in applying a more abundant noble metal, some features of gold catalysis appear unique. Gold appears as a very promising catalyst for sustainable processes based on the use of clean reagents, particularly O₂, often in aqueous solution or in the absence of solvent, under mild conditions, considering other fundamental peculiarities, such as biocompatibility, availability and easy recovery. Among the selective oxidations of hydrocarbons the most studied are propene oxidation to propene oxide over Au supported on TiO₂, SiO₂-TiO₂ or TS1, with good selectivity but only at low conversion values, and oxidation of cyclohexane for the production of adipic acid. Gold represents a second generation of catalysts for alcohol and carbohydrate oxidation: they show a great improvement in selectivity and stability and thus represent challenging substitutes for platinum group metals [139]. Au on activated carbon has been used for the oxidation of reducing sugar as D-glucose and D-lactose showing a good resistance to poisoning compared to Pt catalysts. High conversions can be raised on Au-Pd/C catalyst in the oxidation of glyoxal to glyoxalic acid and good results were obtained for the oxidation of n-heptanal on Au/CeO₂. Among alcohols oxidation great attention is paid for the oxidative dehydrogenation of methanol to form hydrogen on Au/TiO₂ systems and for glycerol oxidation for which Au, Pd-Au and Pt-Au on carbon have been used. Big interest has also been showed for in-situ hydrogen peroxide production by selective oxidation of hydrogen; its formation is favoured over gold surface and high productivities are obtained on

Au/SiO₂, Au/Fe₂O₃, Au/ Al₂O₃ and Au/TiO₂ and even better results were observed using Au in combination with Pd.

2.3.2 Reactions for environmental applications

The general need to reduce pollution and preserve the quality of air and water leads to the introduction of worldwide legislations that continuously impose pollutants emission limits lower and lower. Many catalytic processes have been developed to meet these requirements: reduction of nitrogen oxides, removal of halocarbons, sulphur dioxide, dioxins and volatile organic compounds (VOCs) and catalytic wet air oxidation of organic molecules in water. Gold catalysts also find application in all these mentioned reactions.

2.3.2.1 VOC combustion

Emission into the atmosphere of gaseous compounds derived from industrial or domestic activities leads to pollution that may be caused directly by those compounds or by secondary reactions that may occur in combination with sunlight or ozone. The so called "volatile organic compounds" are organic molecules having saturated vapour pressure above 10Pa at 20°C and include hydrocarbons, aromatic solvents, oxygenated compounds and chlorocarbons. They are often toxic and their large contribution to the formation of photochemical smog and ozone requires their abatement from the emission sources.

Catalytic combustion is the most promising technology for the destruction of VOC; it is preferred to thermal incineration due to the lower temperature required. In fact the concentration of pollutant in the gas streams are often very low (100-1000 ppm) and the reaction heat is not sufficient to raise catalyst's working temperature so an external heating is always required. Other advantages are the high selectivity to total oxidation and the possibility to operate with very dilute effluent streams.

For this reaction two kinds of catalysts are usually applied: i) supported noble metals and ii) metal oxides [140] [141].

Various reports have shown that supported Pt and Pd are very efficient catalysts for VOC total oxidation [142] [143], however cheaper catalytic materials are of ever increasing importance.

2.3.2.2 Gold catalysts for VOCs combustion

Since the pioneering work on Au catalysts by Haruta [63] many studies on gold catalysts and gold-supported catalysts for VOCs oxidation have been reported, with some reports of catalyst activities exceeding those of Pt/Al₂O₃ catalysts. The performance of gold catalysts for VOCs combustion is highly dependent on the size of the gold particles, as well as the nature of the support, and thus strongly affected by the preparation method and the pretreatment conditions [17] [32] [33] [144] [145]. Au/Fe₂O₃ [34], Au/Al₂O₃ and Au/CeO₂ have been recently reported as active catalysts for combustion of VOCs. This is basically due to the capacity of small gold nanoparticles to enhance the mobility of the lattice oxygen in the case of ferric oxide and for Au/CeO₂ to weak the surface Ce-O bonds close to gold atoms, thus activating the surface capping oxygen which is involved in a Mars-van Krevelen reaction mechanism.

Au supported on Co₃O₄ showed the highest catalytic activity among other supported metals for the complete oxidation (combustion) of hydrocarbons [146] [147] [148].

Carley et al. [149] studied the catalytic combustion of methane, ethane and propane over Au supported on different metal oxides such as CoO_x, MnO_x, CuO_x, Fe₂O₃ and CeO₂. A systematic enhancement of the catalytic activity in the combustion of this alkanes was observed adding gold to all this supports and the most active catalyst was found to be Au/CoO_x; a correlation between catalytic activity and reducibility was observed, the latter likely related to the improvement of the redox properties due to the introduction of defects into the surface of the support.

Cellier et al. prepared Au/MnO₂ and Au/TiO₂ as catalysts by the deposition-precipitation method [150] and investigated their activity in the total oxidation of n-hexane. The conversion of n-hexane into CO₂ on Au/MnO₂ is much higher than Au/TiO₂ for this reaction. However, Au/MnO₂ is also slightly less active than the original γ-MnO₂ support.

For total oxidation of propene, Au/Co₃O₄ was reported to be more active than Au deposited on NiFe₂O₄ or Fe₂O₃, but not as active as Pt/Al₂O₃ [144] [151]. Later, Kim et al. found some synergism between Pt/Al₂O₃ and Au/TiO₂ in low temperature oxidation of propene [152]. The authors observed that the addition of Au/TiO₂ to Pt/Al₂O₃ prevents CO formation and lowers the light-off temperature for C₃H₆ oxidation by ~540°C. A recent contribution in this field presents the influence of

additives such as transition metal oxides, ceria, and alkali (earth) metal oxides on the catalytic performance of Au/Al₂O₃ [28] [82]. The authors found that the role of metal oxides and ceria is twofold: 1) structural promoter for stabilizing small Au particles against sintering, and 2) co-catalyst by providing the active oxygen via a Mars and van Krevelen mechanism. On the other hand the alkali (earth) metal oxides are only structural promoters.

Au/V₂O₅ supported on titania and zirconia has been used for the total oxidation of benzene and a strong synergistic effect was observed between Au and V₂O₅ especially with titania. In this case activation of oxygen was thought to occur on the gold nanoparticles while benzene is activated on vanadium oxide surface.

Au/V₂O₅ supported on ceria was also found to be very active and stable for this reaction; in the presence of gold the reducibility of vanadia and ceria surfaces resulted enhanced and a lower reaction temperature was observed. The synergistic effect observed between gold and vanadia supported on ceria could be caused by a specific interaction between them and to the possibility of obtaining gold and ceria nanoparticles, that imply an increasing of the active oxygen species.

Studies on the support effect on Au/V₂O₅ using ceria-alumina, show that a 1:1 ceria :alumina ratio has higher activity than 1:4 ratio demonstrating that alumina increases the catalyst's stability.

Au supported on ceria or ferric oxide was found to be very active for oxygenated VOCs e.g. methanol, ethanol, 2-propanol and acetone as well as for aromatic molecules like toluene; in the last case gold catalysts showed lower activity compared to oxygenated compounds due to the much lower strength of the organic substrate adsorption on the catalyst surface.

Au/CeO₂ catalysts with low gold content have superior activity for formaldehyde oxidation at about 100°C and the catalytic activity of these materials is closely related to the crystal structure of gold in the catalysts: highly dispersed and poorly crystallized metallic gold and small amount of oxidized gold in the catalysts exhibits higher activity for HCHO combustion [153]. 1%Au/Fe₂O₃ is active for methanol combustion below 100°C and the comparison of T₅₀ values obtained with Au/Fe₂O₃ and the conventional combustion catalyst Pd/Al₂O₃ and Pt/Al₂O₃ gave the order activity



which is in contrast to that determined in earlier work, in which gold was found to be poorly active. Moreover the presence of gold improved the activity in the presence of moisture, probably because the adsorption of carbon monoxide results increased on Au/Fe₂O₃. Methanol can also be decomposed on Au supported over titania and ceria using non calcined supports with high surface area giving total conversion respectively at 230 °C and 80°C.

Ethanol was completely combusted on Pd-Au/ Al₂O₃ at 300°C and the presence of gold was found to stabilize Pd against oxidation.

The beneficial effect of gold on palladium supported on mesoporous TiO₂ was also reported by Siffert et al. for the reaction of catalytic oxidation of propene and toluene [76]. The authors explained the promotional effect of gold added to palladium partly by small metallic particles presence but mainly by metallic particles made up of Au-rich core with Pd-rich shell. In this case they demonstrated that gold also implies a protecting effect of the support under reduction atmosphere.

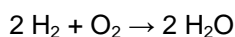
For the oxidative decomposition of nitrogen-containing organic molecules ferric oxide and NiFe₂O₄ show the highest activity owing to their strong affinities for nitrogen. The combustion of trimethylamine occurs below 100°C over Au/ NiFe₂O₄ with high selectivity to nitrogen and carbon dioxide, while over palladium and platinum systems nitrous oxide is the most abundant product even at higher temperature.

2.3.2.3 PROX

The large use of hydrogen in the chemical industry is due to many processes like ammonia synthesis, petroleum reforming and a multiplicity of hydrogenation processes. One of the most recent ways to use hydrogen is energy production by means of fuel cells. In fact fuel cell powered systems for transportation received increasing attention because of their theoretical high fuel efficiency and low environmental impact [154]. Among the numerous types of fuel cells that have already been developed, the proton exchange membrane fuel cell (PEMFC) is one of the most promising ones. The greatest hurdle to be overcome is finding a source of hydrogen of sufficient purity because trace amounts of CO poison the fuel cell Pt catalyst. Several approaches are currently applied: CO preferential oxidation, catalytic methanation, Pd-membrane separation. Among these, the preferential

oxidation (PROX) is the least expensive method to reduce CO to the desired level without excessive hydrogen consumption [155].

PROX catalysts need to be active and selective; the feed gas is usually composed by 1% CO, 1% O₂, 75% O₂ the rest being an inert gas and a successful catalyst should remove CO to less than 10 ppm and oxidize hydrogen less than 0,5% at the temperature of the fuel cell ~ 80°C.



The undesired reaction leads to a loss in fuel efficiency, so that the working temperature limitation becomes very important because the oxidation of hydrogen has the higher activation energy [156] and while very good selectivity can be obtained at ambient temperature, it falls down above 80-100°C. In addition, secondary reactions such as reverse water gas-shift (WGS) and methanation of CO can occur, depending on the temperature, O₂/CO ratio and contact time.

On the basis of these information the qualities that a successful catalyst ought to have can be summarized as follow:

- The adsorption of the reactants must be competitive, CO should adsorb much more strongly than hydrogen;
- Hydrogen and water should not inhibit CO oxidation but promote it limiting the carbonate ion formation;
- The oxidation of hydrogen should not be assisted by either of the carbon oxides or other intermediates (CO₃²⁻, HCOO⁻ etc);
- CO should not be reformed by the water-gas shift.

2.3.2.4 Gold catalysts for PROX reaction

Based on the high activity required to remove CO while maintaining a high CO oxidation selectivity, catalyst formulations used for PROX involve, in general, a high Pt group metal loading and high surface area supports, and are operated at temperatures between 70-200°C. The most extensively studied system so far

remains the Pt-based catalysts [157] [158] [159], but many studies reported Au as a potential catalyst for PROX. In fact Au-based catalysts are intrinsically more active for CO oxidation than for oxidation of hydrogen.

DFT calculations performed on Au(111), Cu(111) and Pt(111) have demonstrated that the barrier for CO oxidation on Au is 0.18 eV; the corresponding barrier for OH formation is much higher, 0.9 eV (at low temperatures) [160]. Similarly, Cu(111) shows a lower barrier for CO oxidation (0.82 eV) than for H₂ oxidation (1.28 eV), whereas Pt(111) shows a higher barrier for CO oxidation (0.96 eV) than for H₂ oxidation (0.83 eV). These calculations explain why Au and Cu are more selective than Pt for PROX at low temperatures and are consistent with experimental data [161]. In many studies, Au catalysts were most often supported on metal oxides such as Al₂O₃, Fe₂O₃, TiO₂, CeO₂, CoO_x, MnO_x, NiO_x, SnO₂ [162] [29] [163] [164] [165] [166] [167] [168] [169] [170] [171]. It is generally accepted that one decisive step of the reaction mechanism occurs at the metal/support interface on Au–O vacancy sites, where the reaction takes place between the O₂ activated predominantly on the oxygen vacancies of oxide and CO adsorbed predominantly on Au in close vicinity of each other [172]. In the literature many data can support this hypothesis. Widmann et al [173] reported a TAP study of CO oxidation over Au/CeO₂ that reveals that a preliminary oxygen removal by CO pulses (prior to CO + O₂ admission) enhances the CO conversion. Grisel et al. [29] reported the supply of active oxygen by MnO_x, Scirè and co-workers [174] concluded that on Au/iron oxide the reaction follows a Mars-van Krevelen mechanism which involves lattice oxygen provided by iron oxide while CO and H₂ are adsorbed on gold particles. Earlier Schumacher and co-workers studied the kinetics of the PROX process and the reaction mechanism over Au/TiO₂ [175] and found that H₂ affects the CO oxidation, most probably by competing hydrogen adsorption on the Au nanoparticles. Formate and carbonate species formed during the reaction represent side products/inhibitors, but they do not take part to the reaction as intermediates. A H₂-rich atmosphere inhibits the formation of formates. A variety of Au-based catalysts such as Au/Co₃O₄, Au/SnO₂, Au/Al₂O₃, Au/Fe₂O₃, Au/CeO₂, Au/NiO_x, Au/MnO_x, Au/Mg(OH)₂ and Au/TiO₂ has been studied by Schubert and co-workers [164]: the results showed that the presence of hydrogen does not have an important effect on the oxidation of CO and that an additional reaction path is created if a reducible support is present, by supplying oxygen, and that deactivation is caused by build-up

of surface carbonate species. The most active Au catalysts for PROX reaction are supported over reducible oxides, like CeO_2 or Fe_2O_3 , and several published results are in agreement with these data [174] [176] [177].

The role of the active supports have also been demonstrated by many studies in which an active oxide was added as promoter to an inactive support (i.e the less reducible Al_2O_3 or SiO_2). For instance, $\text{Au}/\text{Al}_2\text{O}_3$ was promoted by various oxides ($\text{Au}/\text{MO}_x/\text{Al}_2\text{O}_3$) resulting in enhanced activity [178]. The 6 wt% CoO_x added to Au/SiO_2 system [179] [180] resulted also in activity increase. Molybdenum oxide has similar effect [181]. Rare earth oxides are proved to be also excellent promoters [182]. However it has to be noted that the effect of the promoting oxides depends on the nature of the combination of additive and support and in most cases there are more beneficial effects: the promoter oxide can stabilize the gold particle size and the Au/promoter oxide interface can have a perimeter of increased activity.

Regarding the valence state of gold, there is still a debate about the nature of the active form in CO oxidation and PROX. In the literature, an important role was assigned to positively charged Au ions stabilised by the support oxide and the OH groups bonded to these Au or support surface hydroxyls close to the gold particles [37]. Naknam et al observed by DR/UV-vis spectroscopy that $\text{Au}^{\delta+}$ and Au^0 are dispersed on ZnO and ZnO/ Fe_2O_3 supports are active sites for the PROX reaction [183]. Other evidences that suggest cationic gold species are essential for CO oxidation and that may be preferentially found at the metal-support interface are provided by Fierro and Gates [184] [185]. On the contrary Manzoli et al. recently [186] investigated by FT-IR on gold catalysts supported on doped ceria. They modified ceria adding Sm^{3+} , La^{3+} and Zn^{2+} cations in order to create a defective fluorite structure with increased oxygen mobility that could result in higher activity and improved resistance towards deactivation caused by CO_2 and H_2O and found out that anionic gold is the active specie in the PROX reactions.

2.4 References

- [1] A. S. K. Hashmi, G. J. Hutchings, *Angew. Chem. Int. Ed.* 45 (2006) 7896.
- [2] M. Haruta, T. Kobayashi, H. Sano, N. Yamada, *Chem. Lett.* (1987) 405.
- [3] G. C. Bond, P. A. Sermon, *Gold Bull.* 6 (1973) 102.
- [4] G. C. Bond, P. A. Sermon, *J C S Chem. Comm* (1973) 444.

- [5] D. Y. Cha, G. Parravano, J. Catal. 18 (1970) 200.
- [6] D. S. Galvano, G. Parravano, J. Catal. 55 (1978) 178.
- [7] H. Huber, D. McIntosh, G. A. Ozin, Inorg. Chem. 16 (1977) 975.
- [8] G. J. Hutchings, J. Catal. 96 (1985) 292.
- [9] K. Tanaka, K. Tamaru, J. Catal. 2 (1963) 366.
- [10] G. C. Bond, Catal. Today 72 (2002) 5.
- [11] G. C. Bond, J. Mol. Catal. A 156 (2000) 1.
- [12] P. Pyykko, Angew. Chem. Int. Ed. 41 (2002) 3573.
- [13] R. Meyer, C. Lemire, S. K. Shaikhutdinov, H.-J. Freund, Gold Bull. 37 (2004) 72
- [14] I. A. H. Guerrero, H. J. Fasoli, J. L. Costa, J. Chem. Educ. 76 (1999) 200.
- [15] M. Haruta, CATTECH 6 (2002) 102.
- [16] M. Valden, X. Lai, D. W. Goodman, Science 281 (1998) 1647.
- [17] Haruta M, Tsubota T, Kobayashi T, Kageyama H, Genet M. J, Delmon, J. Catal: B 144 (1993) 175.
- [18] M. Haruta, Stud. Surf. Sci. Catal. 110 (1997) 123.
- [19] N. Lopez, J. K. Norskov, J. Am. Chem. Soc. 124 (2002) 11262.
- [20] Z.-P. Liu, P. Hu, A. Alavi, J. Am. Chem. Soc. 124 (2002) 14770.
- [21] T.V.W. Janssens, A. Carlsson, A. Puig-Molina, B.S. Clausen, J. Catal., 240 (2006) 108.
- [22] M.Okumura, S. Nakamura, S. Tsubota, T. Nakamura, M. Azuma, M. Haruta, Catal. Lett.,51 (1998) 53.
- [23] N.Ossipoff, N.W. Cant.,Topics Catal. 8 (1999) 161.
- [24] A.A. Herzing, C.J. Kiely, A.F. Carley, P. Landon and G.J. Hutchings, Science,321 (2008) 1331.
- [25] G.J. Hutchings, J. Mater. Chem. 19 (2009).
- [26] M. Chen, D.W. Goodman, Chem. Soc. Rev. 37(2008) 1860.
- [27] F. Menegazzo, F. Pinna, M.Signoretto, V. Trevisan, F. Boccuzzi, A. Chiorino, M. Manzoli, Appl. Catal. A:Gen. 356 (2009) 31.
- [28] A. C. Gluhoi, N. Bogdanchikova, B. E. Nieuwenhuys, J. Catal. 232 (2005) 96.
- [29] R. J. H. Grisel, B. E. Nieuwenhuys, J. Catal. 199 (2001) 48.
- [30] O. Meerson, G. Sitja, and C.R. Henry, Eur. Phys. J.:D 34 (2005) 119.
- [31] S.-P. Wang, T.-Y. Zhang, X.-Y. Wang, S.-M. Zhang,S.-R. Wang, W.-P. Huang and S.-H. Wu, J. Molec. Catal. A: Chem. 272 (2007) 45.
- [32] S. Minico`, S. Scire` , C. Crisafulli, R.Maggiore, S.Galvagno, Appl. Catal. B 28 (2000) 245.
- [33] S. Minicò, S. Scirè, C. Crisafulli, S. Galvagno, Appl. Catal. B 34 (2001) 277.
- [34] S. Scirè, S. Minicò, C. Crisafulli, S. Galvagno, Catal. Commun. 2 (2001) 229.
- [35] A.M. Venezia, G. Pantaleo, A. Longo, G. DiCarlo, M.P.Casaletto, F.L. Liotta and G. Deganello, J. Phys. Chem.B 109 (2005) 2821.
- [36] C.-J. Zhang, A. Michaelides, D.A King and S.J. Jenkins,J. Chem. Phys. 129 (2008) 194708.
- [37] G.C. Bond and D.T. Thompson, Gold Bull. 33 (2000) 41.
- [38] F. Moreau, G.C. Bond, Catal. Tod. 122 (2007) 215.
- [39] S. D. Lin, M. Bollinger, M. A. Vannice, Catal. Lett. 17 (1993) 245.
- [40] F. Boccuzzi, A. Chiorino, M. Manzoli, P. Lu, T. Akita, S. Ichikawa, M. Haruta, J. Catal. 202 (2001) 256.

- [41] M. Bollinger, M. A. Vannice, *Appl. Catal. B* 8 (1996) 417.
- [42] R. J. H. Grisel, C. J. Weststrate, A. Goossens, M. W. J. Craje, A. M. van der Kraan, B. E. Nieuwenhuys, *Catal. Today* 72 (2002) 123.
- [43] M. Mavrikakis, P. Stoltze, J. K. Norskov, *Catal. Lett.* 64 (2000) 101.
- [44] N. A. Hodge, C. J. Kiely, R. Whyman, M. R. H. Siddiqui, G. J. Hutchings, Q. A. Pankhurst, F. E. Wagner, R. R. Rajaram, S. E. Golunski, *Catal. Today* 72 (2002) 133.
- [45] J. Guzman, B. C. Gates, *Angew. Chem. Int. Ed.* 42 (2003) 690.
- [46] J. Guzman, B. C. Gates, *J. Phys. Chem. B* 106 (2002) 7659.
- [47] B. Nkosi, N. J. Coville, G. J. Hutchings, M. D. Adams, J. Friedl, F. E. Wagner, *J. Catal.* 128 (1991) 366.
- [48] B. Nkosi, M. D. Adams, N. J. Coville, G. J. Hutchings, *J. Catal.* 128 (1991) 378.
- [49] Q. Fu, H. Saltsburg, M. Flytzani-Stephanopoulos, *Science* 301 (2003) 935.
- [50] G. C. Bond, D. T. Thompson, *Gold Bull.* 33 (2000) 41.
- [51] C. K. Costello, M. C. Kung, S.-O. Oh, Y. Wang, H. H. Kung, *Appl. Catal. A* 232 (2002) 159.
- [52] A. Sanchez, S. Abbet, U. Heiz, W.-D. Schneider, H. Hakkinen, R. N. Barnett, U. Landman, *J. Phys. Chem. A* 103 (1999) 9573.
- [53] W. T. Wallace, R. L. Whetten, *J. Am. Chem. Soc.* 124 (2002) 7499.
- [54] L. D. Socaciu, J. Hagen, T. M. Bernhardt, L. Woste, U. Heiz, H. Hakkinen, U. Landman, *J. Am. Chem. Soc.* 125 (2003) 10437.
- [55] M. Date, M. Haruta, *J. Catal.* 201 (2001) 221.
- [56] M. Haruta, T. Kobayashi, N. Yamada, *Chem. Lett.* 2 (1987) 405.
- [57] J. D. Grunwaldt, C. Kiener, C. Wogerbauer, A. Baiker, *J. Catal.* 181 (1999) 223.
- [58] G. B. Hoflund, S. D. Gardner, D. R. Schryer, B. T. Upchurch, E. J. Kielin, *Langmuir* 11 (1995) 3431.
- [59] S. J. Lee, A. Gavriilidis, *J. Catal.* 206 (2002) 305.
- [60] F. Boccuzzi, A. Chiorino, *J. Phys. Chem. B* 104 (2000) 5414.
- [61] D. A. H. Cunningham, W. Vogel, and M. Haruta, *Catal. Lett.*, 63 (1999) 43.
- [62] H. H. Kung, M. C. Kung, C. K. Costello, *J. Catal.* 216 (2003) 425.
- [63] M. Haruta, *Catal. Today* 36 (1997) 153.
- [64] M. Haruta, *Catal. Surv. Jpn.* 1 (1997) 61.
- [65] A. Ueda, M. Haruta, *Gold Bull.* 32 (1999) 3.
- [66] M. A. C. Nascimento, *Theoretical Aspects of Heterogeneous Catalysis*, vol 8, Kluwer Academic Publishers, Dordrecht, Boston, MA, 2001.
- [67] G. Riahi, D. Guillemot, M. Polisset-Thfoin, A. A. Khodadadi, J. Fraissard, *Catal. Today* 72 (2002) 115.
- [68] J. K. Edwards, B. E. Solsona, P. Landon, A. F. Carley, A. Herzing, C.J. Kiely, G. J. Hutchings, *J. Catal.* 236 (2005) 69.
- [69] P. Landon, P. J. Collier, A. F. Carley, D. Chadwick, A. J. Papworth, A. Burrows, C.J. Kiely, G. J. Hutchings, *Phys. Chem. Chem. Phys.* 5 (2003) 1917.
- [70] G. Bernardotto, F. Menegazzo, F. Pinna, M. Signoretto, G. Cruciani, G. Strukul, *Appl. Catal. A: Gen.* 358 (2009) 129.
- [71] A. Abad, P. Concepcion, A. Corma, H. Garda, *Angew. Chem. Int. Ed.* 44 (2005) 4066.
- [72] C. L. Bianchi, P. Canton, N. Dimitratos, F. Porta, L. Prati, *Catal. Today* 102-103 (2005) 203.
- [73] N. Dimitratos, F. Porta, L. Prati, *Appl. Chem A: Gen.* 291 (2005) 210.

- [74] N. Dimitratos, L. Prati, *Gold Bull.* 38 (2005) 73.
- [75] N. Dimitratos, F. Porta, L. Prati, A. Villa, *Catal. Lett.* 99 (2005) 181.
- [76] M. Hosseini, S. Siffert, H.L. Tidahy, R. Cousin, J.-F. Lamonier, A. Aboukais, A. Vantomme, M. Roussel, B.-L. Su, *Catal. Today* 122 (2007), 391.
- [77] B. Zhu, Q. Guo, X. Huang, S. Wang, S. Zhang, S. Wu, W. Huang, *J. Mol. Catal. A: Chem.* 249 (2006) 211.
- [78] S. Kameoka and A. P. Tsai, *Catal. Lett.* 121 (2008) 337.
- [79] R. J. Chimentao, F. Medina, J. L. G. Fierro, J. Llorca, J. E. Sueiras, Y. Cesteros, P. Salagre, *J. Mol. Catal. A: Chem.* 274 (2007) 159.
- [80] C. Della Pina, E. Falletta, M. Rossi, *J. Catal.* 260 (2008) 384.
- [81] M. R. Hoffmann, S. T. Martin, W. Y. Choi, D.W. Bahnemann, *Chem. Rev.* 95 (1995) 69.
- [82] A. C. Gluhoi, N. Bogdanchikova, B. E. Nieuwenhuys, *J. Catal.* 229 (2005) 154.
- [83] A. C. Gluhoi, B. E. Nieuwenhuys, *Catal. Today* 119 (2007) 305.
- [84] F. Moreau, G.C Bond, *Catal Today* 114 (2006) 362.
- [85] F. Moreau, G.C Bond, *Top. Catal.* 44, 1-2, (2007) 95.
- [86] M. Shou, H. Takekawa, D. Y. Ju, T. Hagiwara, D.L. Lu, K. Tanaka, *Catal. Lett.* 108 (2006) 119.
- [87] F. W. Chan, H. Y. Yu, L. Selva Roselin, H. C. Yang, T. C. Ou, *Appl. Catal A: Gen.* 302 (2006) 157.
- [88] S. Carrettin, Y. Hao, V. Aguilar-Guerrero, B. C. Gates, S. Trasobares, J. J. Calvino, A. Corma, *Chem. Eur. J.* 13 (2007) 7771.
- [89] S. Carrettin, Y. Hao, V. Aguilar-Guerrero, B. C. Gates, S. Trasobares, J. J. Calvino, A. Corma, *Chem. Eur. J.* 13 (2007) 7771.
- [90] A. Penkova, K. Chakarova, O. H. Laguna, K. Hadjiivanov, F. Romaro Saria, M. A. Centeno, J. A. Odriozola, *Catal. Comm.* 10 (2009) 1196.
- [91] Q. Xu, K. C. C. Kharas, A. K. Datye, *Catal. Lett.* 85 (2003) 229.
- [92] M. Haruta, *Gold Bull.* 37 (2004) 27.
- [93] A. C. Gluhoi, M. A. P. Dekkers, B. E. Nieuwenhuys, *J. Catal.* 219 (2003) 197.
- [94] S.-J. Lee, A. Gavriilidis, *J. Catal.* 206 (2002) 305.
- [95] C.-K. Chang, Y.-J. Chen, C.-T. Yeh, *Appl. Catal A: Gen.* 174 (1998) 13.
- [96] F. Moreau, G.C Bond, *Appl. Catal A: Gen.* 302 (2006) 110.
- [97] R. Zanella, L. Delannoy, C. Louis, *Appl. Catal A: Gen.* 291 (2005) 62.
- [98] Y. Yuan, K. Asakura, H. Wan, K. Tsai, Y. Iwasawa, *Catal. Lett.* 42 (1996) 15.
- [99] Y. Yuan, A. P. Kozlova, K. Asakura, H. Wan, K. Tsai, Y. Iwasawa, *J. Catal.* 170 (1997) 191.
- [100] T. V. Choudhary, C. Sivadinarayana, C. C. Chusuei, A. K. Datye, J.P.F. Jr, D. W. Goodman, *J. Catal.* 201 (2002) 247.
- [101] T. J. Mathieson, A. G. Langdon, N.B. Milestone, B. K. Nicholson, *Chem. Commun.* (1998) 371.
- [102] M. Okumura, M. Haruta, *Chem. Lett.* (2000) 396.
- [103] J. Guzman, B.G. Anderson, C. P. Vinod, K. Ramesh, J. W. Niemantsverdriet, B. C. Gates, *Langmuir* 21 (2005) 3675.
- [104] J. C. Fierro- Gonzales, B. C. Gates, *J. Phys. Chem. B* 108 (2004) 16999.
- [105] J. C. Fierro- Gonzales, B. C. Gates, *J. Phys. Chem. B* 109 (2005) 7275.
- [106] J. Guzman, B. C. Gates, *Langmuir* 19 (2003) 3897.

- [107] J. C. Fierro- Gonzales, B.G. Anderson, C. P. Vinod, K. Ramesh, J. W. Niemantsverdriet, B. C. Gates, *Catal. Lett* 101 (2005) 265.
- [108] M. Okumura, S. Tsubota, M. Haruta, *J. Molec. Catal. A: Chem.* 199 (2003) 73.
- [109] F. Porta, L. Prati, M. Rossi, S. Coluccia, G. Martra, *Catal. Today* 61 (2000) 165.
- [110] S. Tsubota, T. Nakamura, K. Tanaka, M. Haruta, *Catal. Lett.* 56 (1998) 131.
- [111] D. Grunwaldt, M. Maciejewski, O.S. Becker, P. Fabrizioli, A. Baiker, *J. Catal.* 186 (1999) 458.
- [112] G. Martra, L. Prati, C. Manfredotti, S. Biella, M. Rossi, S. Coluccia, *J. Phys. Chem B* 107 (2003) 5453.
- [113] F. B. Li, X. Z. Li, *Appl. Catal. A* 228 (2002) 15.
- [114] E. Seker, E. Gulari, *Appl. Catal. A: Gen.* 232 (2002) 203.
- [115] D. Li, J. T. McCann, M. Gratt, Y. Xia, *Chem Phys. Lett.* 394 (2004) 387.
- [116] W. Chen, W. Cai, L. Zhang, G. Wang, L. Zhang, *J. Coll. Inter. Sci.* 238 (2001) 291.
- [117] T. Uematsu, I. Palinko, J. W. Seo, Z. Konya, k. Hernadi, I. Klricsi, *Chem. Phys. Lett* 372 (2003) 848.
- [118] T. Uematsu, L. Fan, T. Maruyama, N. Ichikuni, S. Shimazu, *J. Molec. Catal. A. Chem.* 182-183 (2002) 209.
- [119] B. D. Chandler, A.B. Shabel, C. F. Blanford, L. H. Pignolet, *J. Catal.* 187 (1999) 367.
- [120] A. Vazquez-Zavala, J. Garcia-gomez, A. Gomez-Cortes, *Appl. Surf. Sci.* 187 (2000) 177.
- [121] A. Sachdev, J. Schwank, *J. Catal.* 120 (1989) 353.
- [122] R. Brayner, D.d.S. Cunhab, F. Bozon-Verduraz, *Catal. Today* 78 (2003) 419.
- [123] F. Suzuki, S. Ito, T. Akita, K. Tanaka, T. Kawahara, H. Kobayashi, *J. Phys. Chem. B* 106 (2002) 8714.
- [124] H. Tada, F. Suzuki, S. Ito, T. Akita, K. Tanaka, T. Kawahara, H. Kobayashi, *J. Phys. Chem. B* 106 (2002) 8714.
- [125] A. M. Venezia, V. L. Parola, G. Deganello, B. Pawelec, J. L. G. Fierro, *J. Catal.* 215 (2003) 317.
- [126] T. Nakagawa, H. Nitani, S. Tanabe, K. Okitsu, S. Seino, Y. Mizukoshi, T. A. Yamamoto, *Ultrasonics Sonochem.* 12 (2005) 249.
- [127] J. Luo, M. M. Maye, V. Petkov, N. N. Kariuki, L. Wang, P. Njoki, D. Mott, Y. Lin, C.-J. Zhong, *Chem. Mater.* 17 (2005) 3086.
- [128] A.-Q Wang, J.-H. Liu, S. D. Lin, H.-p. Lin, C.-Y. Mou, *J. Catal.* 233 (2005) 186.
- [129] A. Schwarz et al., *Chem. Rev.* 95 (1995) 477.
- [130] M. Ichikawa, in *Metal Clusters in Chemistry*, P. Braunstein, L. A. Oro, P. R. Raithby Eds., Wiley-VCH, 1999, 1273.
- [131] E. Cariati, D. Roberto, R. Ugo, *Chem. Rev.* 103 (2003) 3707.
- [132] B. C. Gates, *Chem. Rev.* 95 (1995) 511.
- [133] R. Psaro, S. Recchia, *Catal. Today* 41 (1998) 139.
- [134] A. Beck, A. Horvath, A. Sarkany, L. Gucci, *Curr. Appl. Phy* 6 (2006) 200.
- [135] J. M. Thomas, B. F. G. Johnson, R. Raja, G. Sankar, P. A. Midgley, *Acc. Chem. Res.* 36 (2003) 20.
- [136] A. Siani, *Langmuir* 22 (2006) 5160.
- [137] C. Femoni, F. Kaswalder, M. C. Iapalucci, G. Longoni, Zacchini, *Coord. Chem. Rev.* 250 (2006) 1580.
- [138] P. Greco, M. Cavallini, P. Stoliar, S. D. Quiroga, S. Dutta, S. Zacchini, M. C. Iapalucci, V. Morandi, S. Milita, P. G. Merli, F. Biscarini, *J. Am. Chem. Soc* 130 (2008) 1177

- [139] L. Prati, M. Rossi, *J. Catal.* 176 (1998) 552.
- [140] S. C. Kim, *J. Hazard. Mater.* 91 (2002) 285.
- [141] R. Delaigle, D. P. Debecker, F. Bertinchamps, E. M. Gaigneaux *Top. Catal.* 52 (2009) 501.
- [142] G. Centi, *J. Mol. Catal. A* 173 (2001) 287.
- [143] K. Okumura, T. Kobayashi, H. Tanaka, M. Niwa, *Appl. Catal. B* 44, (2003) 325.
- [144] G.C. Bond, D.T. Thompson, *Catal. Rev.-Sci. Eng.* 41 (1999) 319.
- [145] M. Haruta, N. Yamada, T. Kobayashi, S. Iijima, *J. Catal.* 115 (1989) 301.
- [146] Haruta, M. *Now and Future* 7 (1992) 13.
- [147] R. D. Walters, J. J. Weimer, J. E. Smith, *Catal Lett* 30 (1995) 181.
- [148] M. Haruta, *Chem. Record* 3(2003) 75.
- [149] B.E. Solsona, T. Garcia, C. Jones, S.H. Taylor, A.F. Carley, G.J. Hutchings, *Appl. Catal. A: Gen.* 312 (2006) 67.
- [150] C. Cellier, S. Lambert, E.M. Gaigneaux, C. Poleunis, V. Ruaux, P. Eloy, C. Lahousse, P. Bertrand, J.-P. Pirard, P. Grange, *Appl. Catal. B* 70 (2007) 406.
- [151] M. Haruta, *Now and Future* 7 (1992) 13.
- [152] D. H. Kim, M. C. Kung, A. Kozlova, S. D. Yuan, H. H. Kung, *Catal. Lett.* 98 (2004) 11.
- [153] Y. Shen, X. Yang, Y. Wang, Y. Zhang, H. Zhu, L. Gao, M. Jia, *Appl. Catal. B: Env.* 79 (2008) 148.
- [154] A. Wootsch, C. Descorme, D. Duprez, *J. Catal.* 225 (2004) 259.
- [155] S. E. Golunski, *Plat. Met. Rev.* 42 (1998) 2. P. G. Gray, M. I. Petch, *Plat. Met. Rev.* 44 (2000) 108.
- [156] M. M. Schubert, A. Venugopal, M. J. Kahlich, V. Plzak and R. J. Behm, *J. Catal.* 222 (2004) 32.
- [157] O. Korotkikh, R. Farrauto, *Catal. Today* 62 (2000) 249.
- [158] H. Igarashi, M. Uchida, Y. Suzuki, M. Sasaki, M. Watanabe, *Appl. Catal. A* 159 (1997) 159.
- [159] M. M. Schubert, H. A. Gasteiger, R. J. Behm, *J. Catal.* 172 (1997) 256.
- [160] S. Kandoi, A. A. Gokhale, L. C. Grabow, J. A. Dumesic, M. Mavrikakis, *Catal. Lett.* 93 (2004) 93.
- [161] G. Avgouropoulos, T. Ioanides, C. Papadopoulou, J. Batista, S. Hocevar, H. K. Matralis, *Catal. Today* 75 (2002) 157.
- [162] G.K. Bethke, H.H. Kung, *Appl. Catal. A: Gen.* 43 (2000) 194.
- [163] J.H. Yang, C.K. Costello, Y.M. Wang, S.R. Bare, H.H. Kung, H.S. Oh,.
- [164] M.M. Schubert, V. Plzak, J. Garcke, R.J. Behm, *Catal. Lett.* 76 (3–4) (2001) 143.
- [165] M.M. Schubert, S. Hackenberg, A.C. van Veen, M. Muhler, V. Plzak, R.J. Behm, *J. Catal.* 197 (2001) 113.
- [166] C. Rossignol, S. Arrii, F. Morfin, L. Piccolo, V. Caps, J.L. Rousset, *J. Catal.* 230 (2005) 476.
- [167] M.J. Kahlich, H.A. Gasteiger, R.J. Behm, *J. Catal.* 182 (1999) 430.
- [168] M.M. Schubert, M.J. Kahlich, H.A. Gasteiger, R.J. Behm, *J. Power Sources* 84 (1999) 175.
- [169] W. Deng, J. De Jesus, H. Saltsburg, M. Flytzani-Stephanopoulos, *Appl. Catal. A: Gen.* 291 (2005) 126.
- [170] A. Jain, X. Zhao, S. Kjergaard, S.M. Stagg-Williams, *Catal. Lett.* 104(2005) 191.
- [171] R.M. Torres Sanchez, A. Ueda, K. Tanaka, M. Haruta, *J. Catal.* 168 (1997) 125.

- [172] G.C. Bond C. Louis, D.T. Thompson, *Catalysis by Gold*, Imperial College Press, 2006
- [173] D. Widmann, R. Leppert, R. J. Behm *J. Catal.* 251 (2007) 437.
- [174] S. Scire`, C. Crisafulli, S. Minico`, G. G. Condorelli, A. Di Mauro, *J. of Mol. Catal. A: Chem.* 284 (2008) 24.
- [175] Schumacher, Y. Denkwitz, V. Plzaak, M. Kinne, R. J. Behm, *J Catal* 224 (2004) 449. B.
- [176] A. Luengnaruemitchai, S. Osuwan, E. Gulari, *Int. J. Hydrogen Energy* 29 (2004) 429.
- [177] D. A. Bulushev, L. Kiwi-Minsker, I. Yuranov, E. I. Suvorova, P. A. Buffat, A. Renken, *J.Catal.* 210 (2002) 14.
- [178] R.J.H. Grisel, B.E. Nieuwenhuys, *Catal. Tod.* 64 (2001) 69.
- [179] K. Qian, W. Huang, Z. Jiang, H. Sun, *J. Catal.* 248 (2007) 137.
- [180] E.G. Szabó, M. Hegedüs, J.L. Margitfalvi, *Reac. Kinet. Catal. Lett.* 93 (2008) 119.
- [181] L. Bugyi, A. Berkó, L. Óvári, Anna M. Kiss, J. Kiss, *Surf. Sci.* 602 (2008) 1650.
- [182] Z. Ma, S.H. Overbury, S. Dai, *J. Molec. Catal. A.* (2007) 186.
- [183] P. Naknam, A. Luengnaruemitchai , S.Wongkasemjit, *Int. J.Hydr. En.* 34 (2009) 9838.
- [184] J.C. Fierro-Gonzales, B. C. Gates, *Catal. Tod.*, 122 (2007) 201.
- [185] J.C. Fierro-Gonzales, B. C. Gates *Chem. Soc. Rew.* 37 (2008) 2127.
- [186] M. Manzoli,G. Avgouropoulos, T. Tabakova, J. Papavasiliou, T. Ioannides, F. Boccuzzi, *J. Catal.* 256 (2008) 237.

3. EXPERIMENTAL

3.1 Catalysts preparation

3.1.1 TiO₂ and CeO₂supported catalysts

Gold-iron catalysts with different content of Au and Fe, have been prepared by impregnation of the bimetallic carbonyl cluster salts [NEt₄]₄[Au₄Fe₄(CO)₁₆] [1] and [NEt₄][AuFe₄(CO)₁₆] [2] (see Figure 3.1) on commercial TiO₂ (Millennium Chemicals DT51) and CeO₂ (VP AdNANO Ceria90 - Evonik).

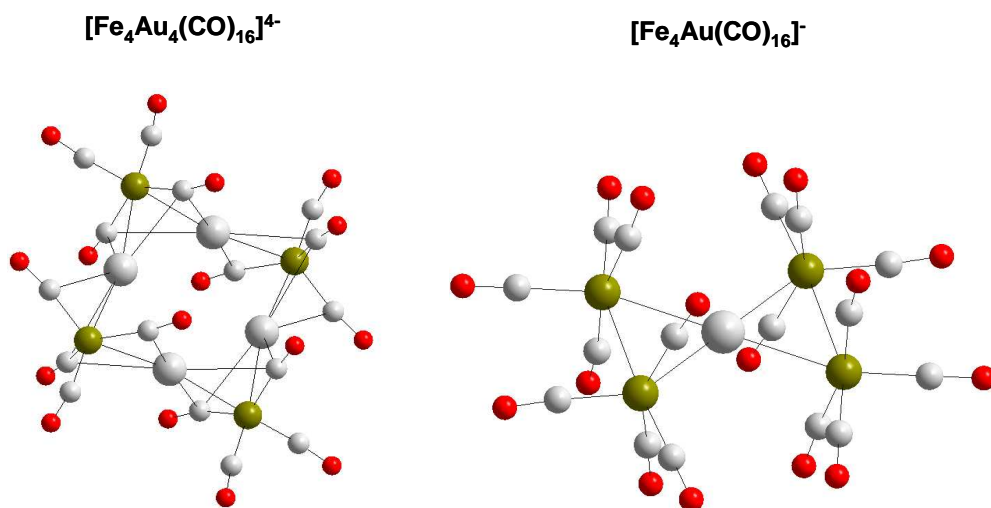


Figure 3.1: Structure of [Au₄Fe₄(CO)₁₆]⁴⁻ and [AuFe₄(CO)₁₆]⁻.

In a typical experiment, the required amount of the carbonyl cluster was dissolved in degassed acetone (20-40 mL) under nitrogen and added dropwise over a period of 1 hour to an acetone suspension of the support (10-15 g), previously degassed and stored under nitrogen. The resulting suspension was allowed to stir overnight, then the solvent was removed in vacuum at room temperature. Finally, the prepared

samples were stored in air at ambient temperature, dried at 100°C for 2 hr in air and usually thermal treated at 400°C in flowing N₂. During this last treatment, the temperature was ramped at a rate of 10°C/min from room temperature to 400°C in nitrogen, in order to fully decompose the carbonyl cluster and the ammonium cations but also control the Au crystal growth. In fact, the rapid oxidation of iron that takes place in air can lead to uncontrolled temperature rise and gold nanoparticles dimension increase as observed during a study conducted on thermal treatment conditions.

For comparison, titania and ceria supported catalysts containing only Fe were prepared following a similar procedure by employing the homo-metallic [NEt₄][HFe₃(CO)₁₁] cluster [2] (see Figure 3.2)

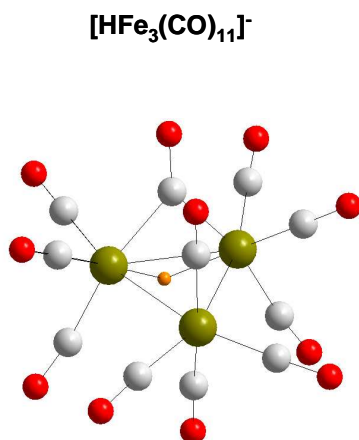


Figure 3.2: Structure of [HFe₃(CO)₁₁]⁻.

In this case the catalysts were dried at 100°C for 2 hr and calcined at 400°C in air, in fact, in this case, the atmosphere utilized during calcination do not influence catalytic properties. Prepared samples will be indicated hereafter as Fe_x and Fe_xAu_y, where the numbers x and y refer to the theoretical iron and gold content in the materials (i.e., Fe_{2.3}Au₂ indicates sample prepared with 2.3 wt. % iron and 2 wt.% gold).

3.2 Catalysts characterization

FTIR spectroscopy

In order to follow the decomposition process of the carbonyl clusters in contact with supports, the impregnation process was monitored by FTIR in the $\nu(\text{CO})$ region at different stages: starting cluster solution; acetone solution in contact with TiO_2 ; nujol mull of the dried powders before and after thermal treatment. IR spectra were recorded with a PerkinElmer SpectrumOne interferometer in CaF_2 cells.

TGA/DSC

Thermogravimetric analyses were performed on a TGA 2050 TA Instruments in the range 25-400°C, with heating rate of 5°C/min while calorimetrics data were recorded by a DSC 2920 Modulated DSC TA instrument in the range 25-250°C.

ICP-AES

The real metal content on the catalysts was determined by ICP-AES analysis with a Fision 3410+ instrument.

Specific surface area

Surface areas were measured by N_2 physisorption apparatus (Sorpty 1750 CE instruments) and single point BET analysis methods, samples were pre-treated under vacuum at 200°C.

X-Ray diffraction

XRD measurements were carried out at room temperature with a Bragg/Brentano diffractometer (X'pertPro Panalytical) equipped with a fast X'Celerator detector, using Cu anode as X-ray source ($K\alpha$, $\lambda=1.5418 \text{ \AA}$). For all samples the complete diffractogram was collected in the 2θ range 10-85°, counting 20 sec each 0.05° step while a second acquisition were made for Au crystal size evaluation counting 400 sec each 0.03 step. The latter acquisition was performed in the 2θ range 40-50° for titania samples and 36-42 for ceria ones. In fact the coherent length of the Au crystalline domains on ceria was evaluated through single line profile fitting of the reflection at $2\theta 38^\circ$, while for titania samples the reflection at $2\theta 44.3^\circ$ has been

used, since at this angle no overlap with the anatase pattern of the support was observed.

Crystal size values were calculated from the widths at half maximum intensity using the Scherrer equation.

H₂-TPR

The reduction behaviour of different samples was studied by means of Temperature Programmed Reduction using a Termoquest TPDRO instrument under 5 % H₂/Ar flow (20 mL·min⁻¹). The temperature was raised from 60 to 700°C with a heating rate of 10°C min⁻¹.

XPS

XPS analyses were performed on a Kratos Axis Ultra spectrometer (Kratos Analytical – Manchester – UK) equipped with a monochromatized aluminium X-ray source (powered at 10 mA and 15 kV). The pressure in the analysis chamber was about 10⁻⁶ Pa. The analysed area was 700 μm x 300 μm. The pass energy was set at 160 eV for the wide scan and 40 eV for narrow scans. Charge stabilisation was achieved by using the Kratos Axis device. The following sequence of spectra was recorded: survey spectrum, C 1s, O 1s, Au 4f, Fe 2p, Ti 2p and C1s again to check for charge stability as a function of time and the absence of degradation of the sample during the analyses. The C-(C, H) component of the C1s peak of carbon has been fixed to 284.8 eV to set the binding energy scale. Molar fractions [%] were calculated using peak areas normalized on the basis of acquisition parameters after a linear background subtraction, experimental sensitivity factors, and transmission factors provided by the manufacturer. Spectra were decomposed with the CasaXPS program (Casa Software Ltd., UK) with a Gaussian/Lorentzian (70:30) product function. The real metal content on the catalysts was determined by ICP-AES analysis with a Fison 3410+ instrument.

TEM

Transmission Electron Microscopy (TEM) observations have been carried out with a Fei Tecnai F20 TEM with a Schottky emitter and operating at 200 keV. The instrument is equipped with a Fischione High Angle Annular Dark Field Detector (HAADF) for Scanning Transmission Electron Microscopy (STEM) observations and

with an Edax EDS PV9761N SUTW Energy Dispersive X-Ray Spectrometer (EDX) for X-rays microanalysis. The samples were grinded in a mortar and treated with ultrasound in isopropyl alcohol to reduce the grain dimensions to a minimum. A drop of the resulting finely dispersed suspension was evaporated at room temperature and atmospheric pressure on a copper grid with a holey carbon film for the analyses.

3.3 Catalytic activity measurements

3.3.1 Toluene combustion

Catalytic experiments were carried out in a fixed bed glass reactor at atmospheric pressure. The scheme of the laboratory plant is reported in Figure 3.3.

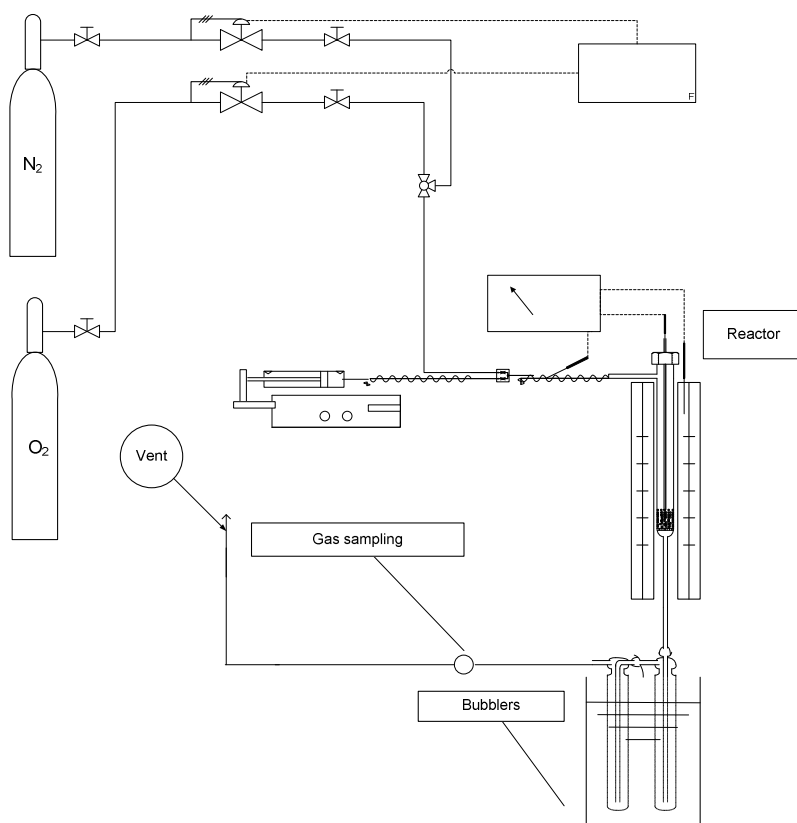


Figure 3.3: Scheme of the laboratory plant used to perform toluene combustion tests.

For each run approximately 350 mg of catalyst in the form of 30–60 mesh (250–595 μm) particles were used, mixed with 1120 mg of corundum grains of similar size for better temperature control. The total volumetric flow through the catalyst bed was held constant at 140 ml/min, 10 vol. % oxygen, 90 vol. % nitrogen and 1400 ppm of toluene. Analysis of reactants and products were carried out as follows: the

products in the outlet stream were scrubbed in cold acetone maintained at -25°C by a F32 Julabo Thermostat. The amounts of reagent and products condensed during a reaction period of 15 min at steady state conditions were analyzed with a GC (Clarus 500 Perkin Elmer) equipped with a Elite FFAP column (30m x 0.32 mm) and a FID. CO and CO₂ formed were separated on a capillary column Elite Plot Q (30 m x 0.32 mm), attached to a methanizer and analyzed with a flame ionization detector (FID). Particular care was devoted to determination of the C balance, calculated as the comparison between converted VOC and the sum of the product yields.

3.3.2 Methanol combustion

Catalytic activity tests were performed in a continuous-flow fixed-bed microreactor. The scheme of the laboratory plant is reported in Figure 3.4.

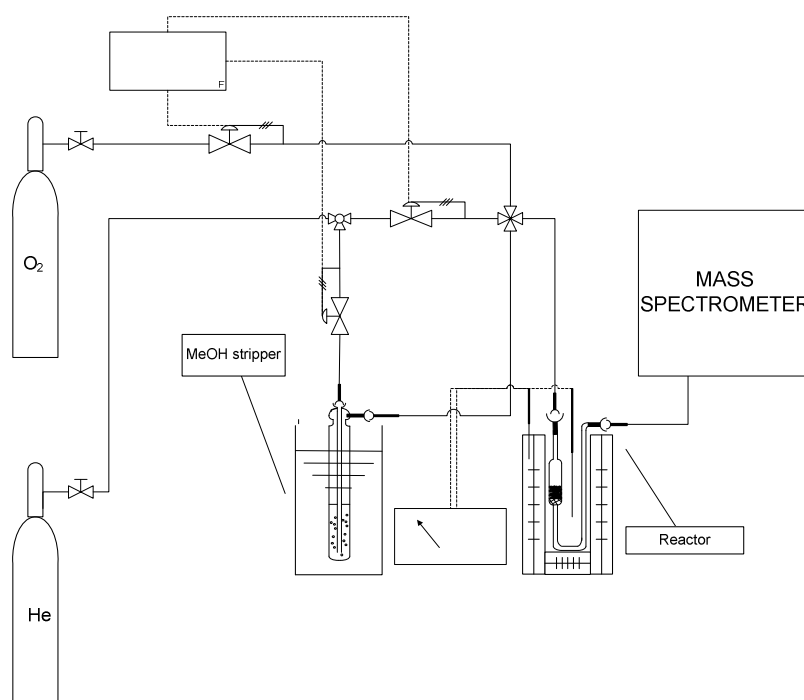


Figure 3.4: Scheme of the laboratory plant used to perform methanol combustion tests.

Each test was carried out loading 0.1 g of catalyst (80–140 mesh) diluted with an inert glass powder. The reactant mixture was fed to the reactor by flowing a part of

the He stream through a saturator containing methanol and then mixing with O₂ and He before reaching the catalyst. The reactant mixture was 0.7 vol.% methanol and 10 vol.% O₂, the remainder being helium (total flow 45 ml/min). A space velocity (GHSV) of $7.6 \cdot 10^{-3} \text{ mol h}^{-1} \text{ g cat}^{-1}$ was always used. The effluent gases were analysed on-line by a gas chromatograph, equipped with a packed column with 10% FFAP on ChromosorbW and FID detector, and by a quadrupole mass spectrometer (VG quadrupoles).

3.3.3 PROX reaction

Catalytic activity tests were carried out in the gas phase at atmospheric pressure in a continuous-flow microreactor. The laboratory plant is schematized in Figure 3.5.

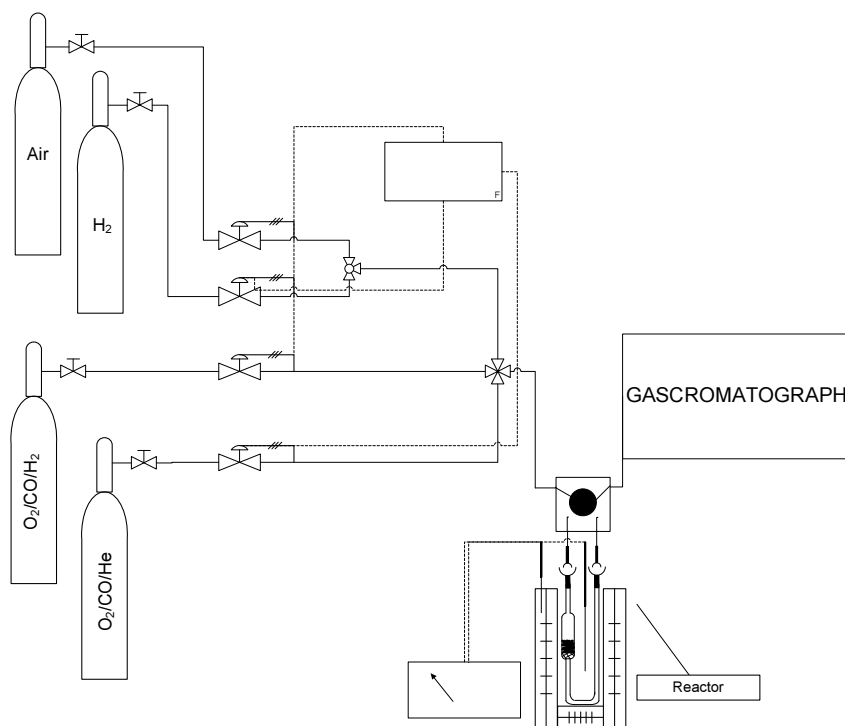


Figure 3.5: Scheme of the laboratory plant used to perform CO PROX catalytic tests.

The microreactor was filled with catalyst (0.015–0.05 g, 80–140 mesh) diluted with an inert glass powder. The gas composition (total flow rate: 80 ml/min) was 1% of

CO, 1% of O₂, the rest being H₂. Before activity tests, catalysts were reduced in H₂ at 200°C. The effluent gases were analyzed by a online gas chromatograph with a packed column (Carboxen1000) and a TCD.

3.4 References

- [1] V.G. Albano, F. Calderoni, M. C. Iapalucci, G. Longoni, M. Monari, Chem. Commun., (1995) 433.
- [2] V.G. Albano, R. Aureli, M.C. Iapalucci, F. Laschi, G. Longoni, M. Monari, P. Zanello, Chem. Commun. (1993) 1501.

4. TITANIA CATALYSTS

4.1 Introduction

Two series of supported Au/FeO_x-TiO₂ catalysts were prepared following the procedure described in the experimental chapter (Chapter 2) starting from bi-metallic carbonyl clusters with the intention of anchoring Au nanoparticles on the support via an iron layer. Two bi-metallic clusters having different Fe/Au molar ratio have been used, i. e. [NEt₄]₄[Au₄Fe₄(CO)₁₆] (Fe/Au=1) and [NEt₄][AuFe₄(CO)₁₆] (Fe/Au=4). For comparison, catalysts containing only Fe were prepared by employing the homometallic [NEt₄][HFe₃(CO)₁₁] cluster.

Each preparation step was monitored by FTIR spectroscopy in the ν(CO) region in order to understand the physical interaction between cluster and support and detect the occurrence of chemical reactions between them at any stage of the preparation. Clusters decomposition was investigated by thermal analyses in order to better understand how this process can be influenced by temperature and atmosphere composition.

Then, the conditions for the thermal treatment of the samples were optimized in order to set the parameters and basically avoid or minimize Au sintering.

All thermally treated samples were fully characterized and tested in the total combustion of toluene and methanol and in the PROX reaction.

4.2 Catalysts preparation and characterization

4.2.1 Synthesis of Au/FeO_x and FeO_x catalysts

Two series of bi-metallic catalysts supported on TiO₂ were prepared starting from the carbonyl clusters salts [NEt₄]₄[Au₄Fe₄(CO)₁₆] and [NEt₄][AuFe₄(CO)₁₆], respectively. The proper amount of each cluster was added to the support in order to obtain catalysts containing 2, 4 and 6% in weight of gold. In this way, keeping

constant the amount of gold for both series of catalysts, it was possible to investigate the effect of different Fe/Au molar ratio.

The code and nominal composition for all prepared Au/FeO_x-Ti catalyst are listed in Table 4.1

Catalyst	Carbonyl salt precursor	Fe content (wt. %)	Au content (wt. %)
Fe _{0.6} Au ₂ -Ti	[NEt ₄] ₄ [Au ₄ Fe ₄ (CO) ₁₆]	0.6	2.0
Fe _{1.2} Au ₄ -Ti		1.2	4.0
Fe _{1.8} Au ₆ -Ti		1.8	6.0
Fe _{2.3} Au ₂ -Ti	[NEt ₄][AuFe ₄ (CO) ₁₆]	2.3	2.0
Fe _{4.5} Au ₄ -Ti		4.5	4.0
Fe _{6.8} Au ₆ -Ti		6.8	6.0

Table 4.1: Code and nominal composition of the bi-metallic Au/FeO_x catalysts supported on TiO₂ employed in this study.

Fe-containing catalysts were prepared by employing the homo-metallic [NEt₄][HFe₃(CO)₁₁] cluster. In this case the amount of cluster deposited on the support for each catalyst was the one necessary to obtain the same nominal iron loading of the two bi-metallic catalysts series. Prepared iron catalysts are reported in Table 4.2.

Catalyst	Carbonyl salt precursor	Fe content (wt. %)
Fe _{0.6} -Ti	[NEt ₄][HFe ₃ (CO) ₁₁]	0.6
Fe _{1.2} -Ti		1.2
Fe _{1.8} -Ti		1.8
Fe _{2.3} -Ti		2.3
Fe _{4.5} -Ti		4.5
Fe _{6.8} -Ti		6.8

Table 4.2: Code and nominal composition of Fe catalysts supported on TiO₂ employed in this study.

4.2.2 IR study during TiO₂ catalysts preparation

TiO₂ impregnation process with the three different cluster solutions utilized to prepare the catalysts was monitored by FTIR in order to observe the clusters behaviour in contact with the support and their transformation after thermal treatment. In the Figure 4.1 are reported the IR spectra recorded in the $\nu(\text{CO})$ region at different stages of the preparation for each cluster which has been used. Namely starting cluster solution, impregnated powder after removal in vacuum of the solvent and dried powder after thermal treatment.

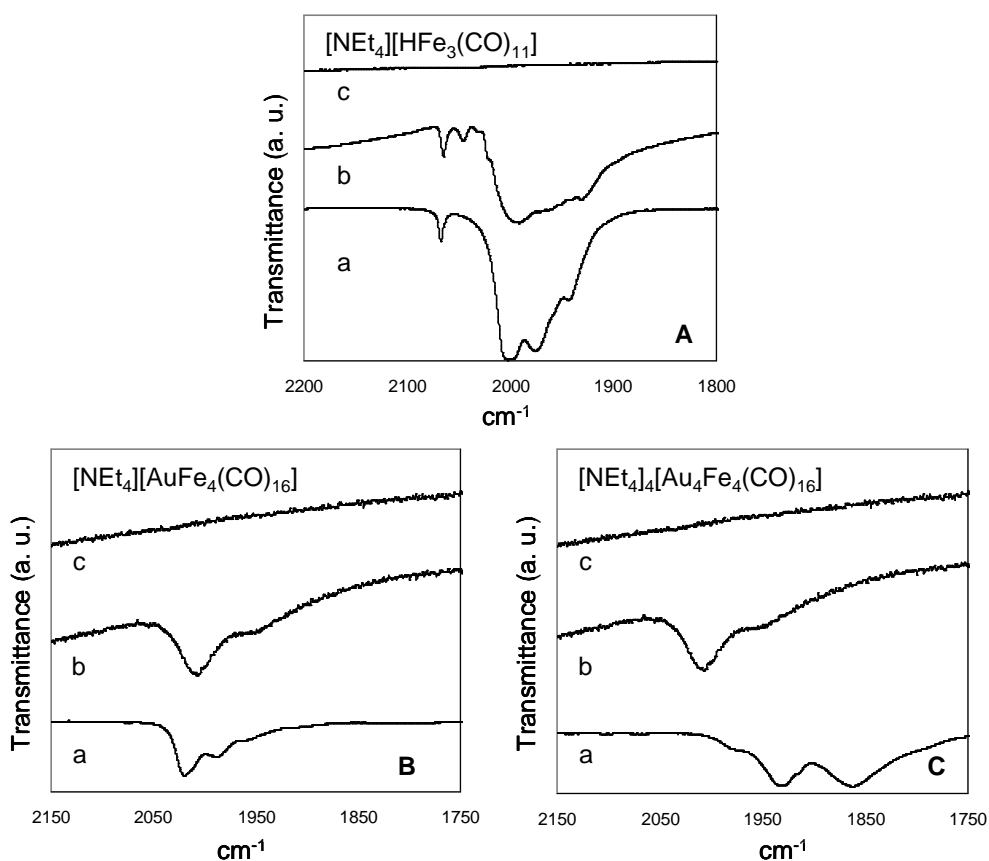


Figure 4.1: FTIR spectra in the $\nu(\text{CO})$ region obtained during the preparation of the FeO_x and Au/FeO_x catalysts on TiO₂ from (A) $[\text{NEt}_4][\text{HFe}_3(\text{CO})_{11}]$, (B) $[\text{NEt}_4][\text{AuFe}_4(\text{CO})_{16}]$ and (C) $[\text{NEt}_4]_4[\text{Au}_4\text{Fe}_4(\text{CO})_{16}]$: (a) cluster in acetone; (b) Nujol mull spectrum of the impregnated powder after removal in vacuum of the solvent; (c) Nujol mull spectrum of the powder after thermal treatment

FT-IR studies pointed out that the cluster $[\text{NEt}_4][\text{HFe}_3(\text{CO})_{11}]$ is absorbed on the support without the occurrence of any reaction as well as $[\text{NEt}_4][\text{AuFe}_4(\text{CO})_{16}]$ $[\nu(\text{CO}) 2018(\text{s}) \text{ cm}^{-1}]$ while significant differences have been observed during the adsorption of $[\text{NEt}_4]_4[\text{Au}_4\text{Fe}_4(\text{CO})_{16}]$ $[\nu(\text{CO}) 1931(\text{s}) \text{ and } 1861(\text{s}) \text{ cm}^{-1}]$. For all systems the carbonyl cluster is totally decomposed after thermal treatment since no $\nu(\text{CO})$ band is present in the final spectra. From this preliminary study it is clear that the two bi-metallic clusters not only have a different Au: Fe composition but, quite interestingly, have a different chemical behaviour. Thus, whereas $[\text{NEt}_4][\text{AuFe}_4(\text{CO})_{16}]$ is quite stable and non reactive, $[\text{NEt}_4]_4[\text{Au}_4\text{Fe}_4(\text{CO})_{16}]$ is very reactive, being easily oxidised as indicated by the increased $\nu(\text{CO})$ wavenumbers, yielding other Au–Fe carbonyl species. Moreover, the final product of its oxidation is $[\text{NEt}_4][\text{AuFe}_4(\text{CO})_{16}]$ making the two species close in relationship.

Several other Au–Fe carbonyl clusters exist between these two species, and among these $[\text{Au}_5\text{Fe}_4(\text{CO})_{16}]^{3-}$ $[\nu(\text{CO}) 1945(\text{s}) \text{ and } 1861(\text{s}) \text{ cm}^{-1}]$, $[\text{Au}_{21}\text{Fe}_{10}(\text{CO})_{40}]^{6-}$ $[\nu(\text{CO}) 1982(\text{s}), 1937(\text{sh}), 1889(\text{sh}) \text{ cm}^{-1}]$, $[\text{Au}_{22}\text{Fe}_{12}(\text{CO})_{48}]^{6-}$ $[\nu(\text{CO}) 1980(\text{s}), 1925(\text{sh}), 1880(\text{sh}) \text{ cm}^{-1}]$, $[\text{Au}_{28}\text{Fe}_{14}(\text{CO})_{52}]^{8-}$ $[\nu(\text{CO}) 1985(\text{s}), 1927(\text{sh}), 1887(\text{sh}) \text{ cm}^{-1}]$ and $[\text{Au}_{34}\text{Fe}_{14}(\text{CO})_{50}]^{10-}$ $[\nu(\text{CO}) 1990(\text{s}), 1932(\text{sh}), 1900(\text{sh}) \text{ cm}^{-1}]$ have been recently structurally characterized [1]. Overall, these brown species represent intermediates in the oxidation in solution of $[\text{Au}_4\text{Fe}_4(\text{CO})_{16}]^{4-}$ eventually to give $[\text{AuFe}_4(\text{CO})_{16}]^-$. All these information can be helpfully used in order to fully understand the fate of $[\text{Au}_4\text{Fe}_4(\text{CO})_{16}]^{4-}$ during impregnation on TiO_2 .

IR studies indicate that the oxidation process of $[\text{Au}_4\text{Fe}_4(\text{CO})_{16}]^{4-}$ occurs in two different moments during catalyst preparation, as can be inferred from Figure 4.2, where it is reported the comparison of the FTIR spectra in the $\nu(\text{CO})$ region of: (1) $[\text{NEt}_4]_4[\text{Au}_4\text{Fe}_4(\text{CO})_{16}]$ in acetone $[\nu(\text{CO}) 1931(\text{s}) \text{ and } 1861(\text{s}) \text{ cm}^{-1}]$; (2) the acetone solution after being in contact with TiO_2 $[\nu(\text{CO}) 1982(\text{s}), 1940(\text{m}), 1913(\text{w}) \text{ and } 1881(\text{s}) \text{ cm}^{-1}]$; (3) the powder (in nujol mull) after removal in vacuum of the solvent $[\nu(\text{CO}) 2000(\text{sh}), 1978(\text{s}) \text{ and } 1917(\text{m}) \text{ cm}^{-1}]$; (4) the CH_3CN extraction from the (3) dried powder $[\nu(\text{CO}) 2000(\text{sh}), 1986(\text{s}) \text{ and } 1914(\text{m}) \text{ cm}^{-1}]$. (final composition 4%wt Au).

Similar experiments have been carried out with different cluster loadings, showing the dependence of oxidation on the cluster : TiO_2 ratio.

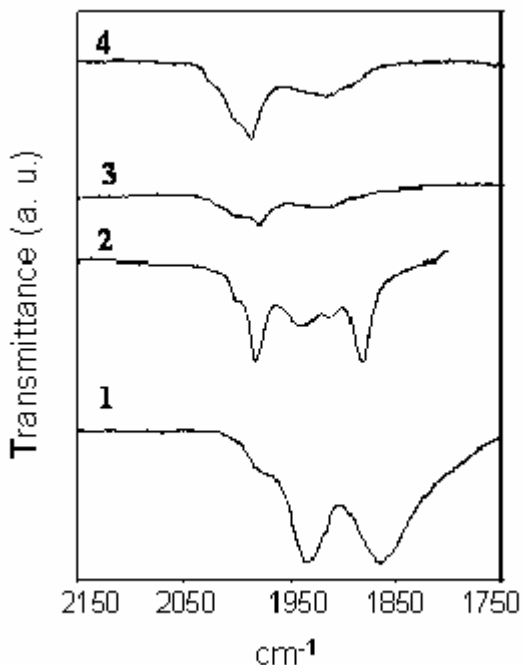


Figure 4.2: FTIR spectra in the $\nu(\text{CO})$ region obtained during the impregnation on TiO_2 of $[\text{NEt}_4]_4[\text{Au}_4\text{Fe}_4(\text{CO})_{16}]$ (4% wt Au): (1) $[\text{NEt}_4]_4[\text{Au}_4\text{Fe}_4(\text{CO})_{16}]$ in acetone; (2) the acetone solution after being in contact with TiO_2 ; (3) the powder (in nujol mull) after removal in vacuum of the solvent; (4) the CH_3CN extraction from the dried powder.

Figure 3.2 indicates that as soon as the acetone solution of $[\text{Au}_4\text{Fe}_4(\text{CO})_{16}]^{4-}$ gets in contact with TiO_2 , the cluster reacts giving more oxidised species such as $[\text{Au}_5\text{Fe}_4(\text{CO})_{16}]^{3-}$ or mixtures of the above mentioned brown compounds, depending on the cluster : TiO_2 ratio; the more cluster is added, the less oxidation is observed. The latter species contain an Au : Fe ratio higher than the precursor $[\text{Au}_4\text{Fe}_4(\text{CO})_{16}]^{4-}$ and the excess iron is released in the form of $[\text{HFe}(\text{CO})_4]^-$ as indicated by the $\nu(\text{CO})$ at 1881 cm^{-1} in FTIR spectra of the acetone solution [Figure 4.2(2)]. The oxidant is likely to be TiO_2 and, therefore, Ti(IV) is partially reduced, as indicated by the fact that the solid turns from white to grey. This is also in agreement with the fact that the degree of oxidation of the cluster increases by increasing the amount of TiO_2 (lower Au % wt). Further reaction, then, occurs when the carbonyl species are forced to get in closer contact with TiO_2 by removal in vacuum of the solvent, as indicated by the change in the FTIR spectrum [Figure 4.2(3)].

The carbonyl species present at this point on the solid support can be, then, extracted with a polar solvent such as CH_3CN and this makes easier to compare their IR features with the ones reported for the Au-Fe carbonyl clusters studied in solution [Figure 4.2(4)]. This analysis confirms that the species present on the solid supports at the end of the deposition process are oxidised clusters such as brown $[\text{Au}_{21}\text{Fe}_{10}(\text{CO})_{40}]^{6-}$, $[\text{Au}_{22}\text{Fe}_{12}(\text{CO})_{48}]^{6-}$, $[\text{Au}_{28}\text{Fe}_{14}(\text{CO})_{52}]^{8-}$, $[\text{Au}_{34}\text{Fe}_{14}(\text{CO})_{50}]^{10-}$ and green $[\text{AuFe}_4(\text{CO})_{16}]^-$; the brown species are favoured by a high load of cluster (4-6% wt Au), whereas the latter increases by lowering the amount of cluster (1-2% wt Au). Oxidation of $[\text{HFe}(\text{CO})_4]^-$ is observed, too, yielding mainly $[\text{HFe}_3(\text{CO})_{11}]^-$ [$\nu(\text{CO})$ 2000(s) cm^{-1}] as also confirmed by independent experiments where $[\text{HFe}(\text{CO})_4]^-$ has been directly deposited on TiO_2 following the same procedure.

On the contrary, it was observed that no chemical reaction occurs during any phase of the impregnation process of $[\text{NET}_4][\text{AuFe}_4(\text{CO})_{16}]$ as demonstrated by more accurate FT-IR studies carried out also during the deposition of this cluster on TiO_2 . Figure 4.3 reports FT-IR spectra in $\nu(\text{CO})$ region recorded at different stages of the catalyst preparation and show that no significant changes occur to the cluster.

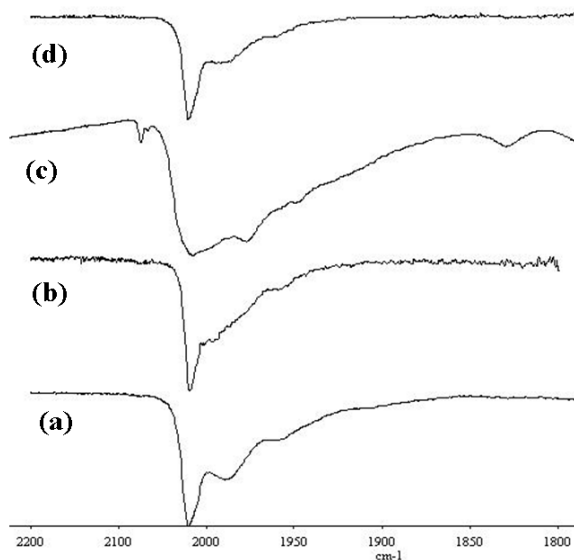


Figure 4.3: FTIR spectra in the $\nu(\text{CO})$ region obtained during the impregnation on TiO_2 of $[\text{NET}_4][\text{AuFe}_4(\text{CO})_{16}]$ for $\text{Fe}_{4.5}\text{Au}_4$ sample: (a) $[\text{NET}_4][\text{AuFe}_4(\text{CO})_{16}]$ in acetone, (b) the acetone solution after being in contact with TiO_2 ; (c) the powder (in nujol mull) after removal in vacuum of the solvent, (d) the CH_3CN extraction from the dried powder.

The $[\text{NEt}_4][\text{AuFe}_4(\text{CO})_{16}]$ salt displays a strong $\nu(\text{CO})$ peak in acetone at 2018 cm^{-1} [Figure 4.3 (a)], which is maintained also after adsorption on TiO_2 both in solution and in the solid state [Figure 4.3 (b) and (c)] [Broadening of the spectra in nujol mull is usually observed, see Figure 4.3 (c)]. Moreover, the intact starting $[\text{NEt}_4][\text{AuFe}_4(\text{CO})_{16}]$ salt can be recovered from the solid by extraction with a polar solvent such as CH_3CN [Figure 4.3 (d)]. Similar results have been also obtained with different cluster loadings on support.

Nonetheless, a careful inspection of the FT-IR spectra of supported $[\text{NEt}_4][\text{AuFe}_4(\text{CO})_{16}]$ before decomposition, beside minor changes on the terminal $\nu(\text{CO})$ region, indicates the presence in the solid state of edge-bridging carbonyls with typical absorption at 1826 and 1778 cm^{-1} , which were negligible in CH_3CN solution. This difference can be accounted by the following equilibrium (1) between the two structural isomers $[\text{AuFe}_4(\text{CO})_{16}]^-$ (all terminal CO) and $[\text{AuFe}_4(\text{CO})_{14}(\mu\text{-CO})_2]^-$ (two bridging CO).



Both these isomers have been structurally characterized and an equilibrium constant $K \sim 10^{-2}$ in solution was established [2]. In the present case, interaction with the TiO_2 support likely shifts the equilibrium toward the $[\text{AuFe}_4(\text{CO})_{14}(\mu\text{-CO})_2]^-$ isomer after deposition.

FT-IR investigation was also carried out during preparation of Fe- TiO_2 catalysts employing $[\text{NEt}_4][\text{HFe}_3(\text{CO})_{11}]$ as precursor of iron species. Following a similar procedure, IR spectra were recorded during cluster impregnation: also in this case no reaction between carbonyl iron cluster and support was observed, as it is shown in Figure 4.4.

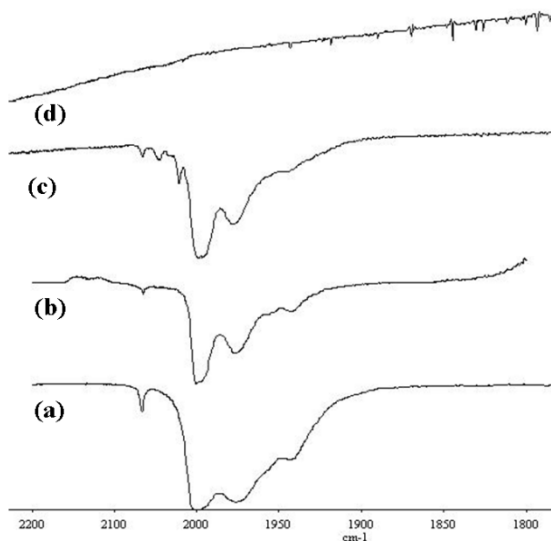


Figure 4.4: FTIR spectra in the $\nu(\text{CO})$ region for $\text{Fe}_{4.5}$ sample obtained during the impregnation of $[\text{NEt}_4][\text{HFe}_3(\text{CO})_{11}]$ on TiO_2 : (a) $[\text{NEt}_4][\text{HFe}_3(\text{CO})_{11}]$ in acetone, (b) the acetone solution after being in contact with TiO_2 ; (c) the powder (in nujol mull) after removal in vacuum of the solvent, (d) the powder (in nujol mull) after thermal decomposition of the cluster.

4.2.3 Thermal study on cluster decomposition

In order to verify the cluster decomposition processes and then understand which were the best conditions for catalyst thermal treatment, a thermal study was carried out on bulk clusters by means of TGA and DSC analyses. The information obtained, about the extent of the weight losses and the temperatures at which they occur, can help to understand how the clusters decompose under the effect of the temperature and which are the products arising from their decomposition. Performing the analyses in air and in nitrogen it leads also to the understanding of the effect of the gas atmosphere composition.

The TGA analyses of $[\text{NEt}_4][\text{HFe}_3(\text{CO})_{11}]$ (Figure 4.5) show that the decomposition process seems to take place in a single step in air, while two different processes can be distinguished under nitrogen. In both cases the results agree with quantitative formation of iron oxides. The experimental constant weight obtained after heating, in fact, is ca. 35 % of the original, which should be compared with the following calculated values for the formation of different species: Fe metal 27.6 %, Fe_2O_3 35.7 %, Fe_3O_4 38.8 %, FeO 41.9 %.

Fe_2O_3 39.5 %, Fe_3O_4 38.1 %. XRD analyses on bulk samples decomposed under similar experimental conditions indicate Fe_3O_4 as the more likely product.

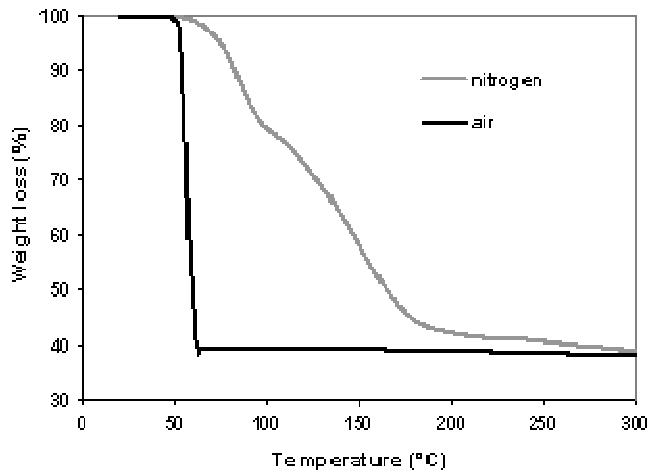


Figure 4.5: TGA analyses of $[\text{NEt}_4][\text{HFe}_3(\text{CO})_{11}]$ (bulk samples) in air and under nitrogen.

Nonetheless, for this cluster salt, the temperature at which a constant weight is reached depends on whether the TGA is performed in air (ca. 60 °C) or under nitrogen (ca. 275 °C). It is well known, in fact, that when iron is in a very disperse form, as in this case, it is highly pyrophoric, then the decomposition/oxidation of the iron carbonyl cluster in air is very fast. Thus, the combustion of the iron cluster salt in air seems to be more efficient than its thermal decomposition under nitrogen.

The same analyses were performed for the bi-metallic cluster $[\text{NEt}_4]_4[\text{Au}_4\text{Fe}_4(\text{CO})_{16}]$. In the Figure 4.6 it is possible to observe as the weight loss is similar in air and under nitrogen, and the decomposition occurs at ca. 150 °C in a single step. In this case, the final weight is 55% of the initial one; this value is lower than expected if the bi-metallic cluster decomposes to $\text{Au} + \text{Fe}_2\text{O}_3$ (67%) or $\text{Au} + \text{Fe}_3\text{O}_4$ (66%). Since it is extremely difficult that the observed discrepancy is due to a gold loss from the bulk, probably some iron is lost in the form of the volatile $\text{Fe}(\text{CO})_5$.

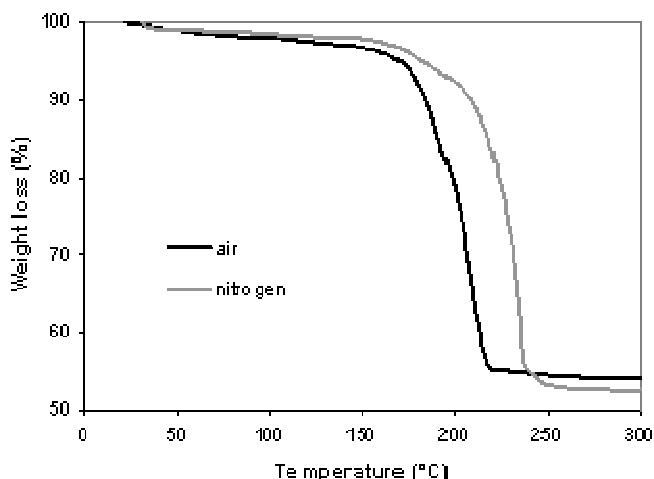


Figure 4.6: TGA analyses of [NEt₄]₄[Au₄Fe₄(CO)₁₆] (bulk samples) in air and under nitrogen

Different results have been obtained for [NEt₄][AuFe₄(CO)₁₆] decomposition. In fact for this cluster the molar ratio Fe/Au is higher than in [NEt₄]₄[Au₄Fe₄(CO)₁₆] and the oxidation state of Au is different; both these factors influence the reactivity of the cluster and its decomposition. In the Figure 4.7 are reported the TG profiles obtained under nitrogen and in air for this cluster.

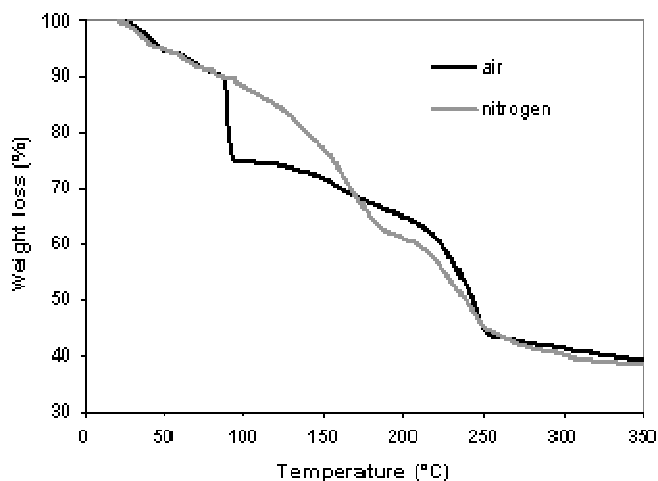


Figure 4.7: TGA analyses of [NEt₄][AuFe₄(CO)₁₆] (bulk samples) in air and under nitrogen.

The samples in air as well as under nitrogen reach a constant weight which is ca. 35 % of the starting one just above 350 °C. Conversely, the TGA profiles at lower temperatures are rather different, since under nitrogen the weight is lost in a nearly continuum way, with only a slight change of slope at ca. 175 °C, whereas two different processes are present in air. In all cases, above 280°C the two profiles become coincident. $[\text{NEt}_4][\text{AuFe}_4(\text{CO})_{16}]$ contains 19.7 % Au and 22.4 % Fe in weight. Therefore, if the sample decomposed to the metals, it would reach a weight 42.1 % of the original. The more likely formation of Au-metal and iron oxides would give a residual weight of 51.3 % ($\text{Au} + \text{Fe}_2\text{O}_3$) or 50.3 % ($\text{Au} + \text{Fe}_3\text{O}_4$). Also in this case some iron, in the form of $\text{Fe}(\text{CO})_5$, must be lost in order to justify the final weight.

Regarding the TGA profile obtained in air, it is rather likely that the first process occurring at ca. 100 °C is the decarbonylation of the cluster, followed by the thermal combustion of the organic cation and iron oxidation.

Calorimetric data reported in Figure 4.8 confirmed this hypothesis, indicating that a strong exothermic phenomenon occurs in air at temperature higher than 120°C while only rather feeble endothermic processes occur under nitrogen at ~100°C, 150°C and 200°C.

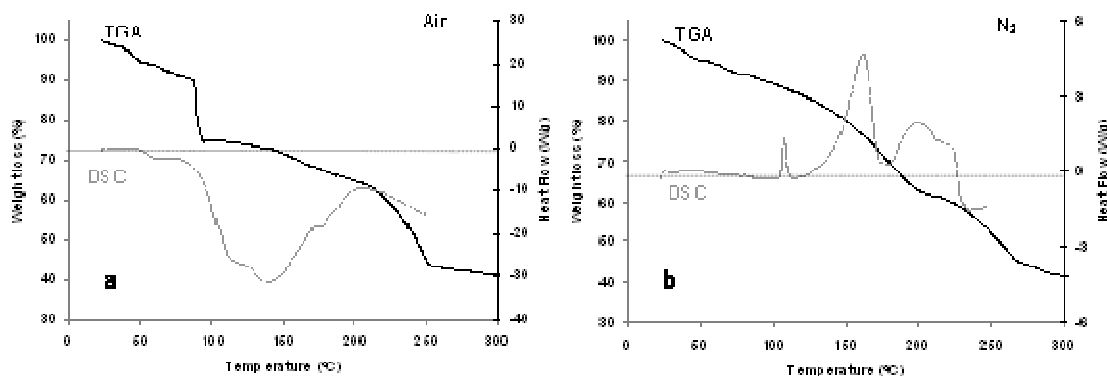


Figure 4.8: TGA and DSC analysis of bulk $[\text{NEt}_4][\text{AuFe}_4(\text{CO})_{16}]$ carbonyl clusters utilized for catalyst preparation; (a) $[\text{NEt}_4][\text{AuFe}_4(\text{CO})_{16}]$ under air; (b) $[\text{NEt}_4][\text{AuFe}_4(\text{CO})_{16}]$ under nitrogen.

Since the exothermic behaviour observed in air could lead to uncontrolled decomposition of the cluster salts, with fast temperature rise causing gold nanoparticles sintering, the supported bi-metallic clusters were thermally

decomposed under nitrogen, ramping the temperature up to 400 °C, in order to obtain the final active catalysts. Fe catalysts were instead calcined in air at 400 °C because in this case the atmosphere used to decompose the cluster does not influence their structural and catalytic properties as it was observed in a preliminary study.

4.2.4 ICP analyses

Because of the non stoichiometric weight loss observed for bi-metallic clusters during TGA experiments and of the reactivity of $[\text{NET}_4]_4[\text{Au}_4\text{Fe}_4(\text{CO})_{16}]$ in contact with titania observed during catalysts preparation, we checked the real metal content of all thermally treated catalysts by ICP analyses. The results are reported in Table 4.3.

Catalyst	Fe loading (wt. %)		Au loading ICP (wt. %)	
	Nominal	Measured	Nominal	Measured
$\text{Fe}_{0.6}\text{Au}_2\text{-Ti}$	0.6	0.4	2.0	1.1
$\text{Fe}_{1.2}\text{Au}_4\text{-Ti}$	1.2	1.2	4.0	4.3
$\text{Fe}_{1.8}\text{Au}_6\text{-Ti}$	1.8	1.6	6.0	6.0
$\text{Fe}_{2.3}\text{Au}_2\text{-Ti}$	2.3	1.1	2.0	2.0
$\text{Fe}_{4.5}\text{Au}_4\text{-Ti}$	4.5	2.9	4.0	4.8
$\text{Fe}_{6.8}\text{Au}_6\text{-Ti}$	6.8	5.4	6.0	6.6
$\text{Fe}_{0.6}\text{-Ti}$	0.6	0.5	0	0
$\text{Fe}_{1.2}\text{-Ti}$	1.2	0.6	0	0
$\text{Fe}_{1.8}\text{-Ti}$	1.8	0.9	0	0
$\text{Fe}_{2.3}\text{-Ti}$	2.3	1.4	0	0
$\text{Fe}_{4.5}\text{-Ti}$	4.5	2.5	0	0
$\text{Fe}_{6.8}\text{-Ti}$	6.8	5.3	0	0

Table 4.3: ICP analyses of studied catalysts.

ICP analyses on the catalysts prepared from both bi-metallic clusters and $[\text{NET}_4][\text{HFe}_3(\text{CO})_{11}]$ indicate that the real metal content significantly differs from the nominal one based on the amount of cluster loading. In particular, the actual Fe

loading is minor than the nominal one for all catalysts, whereas the gold content in the bi-metallic samples is almost as expected.

More in details, a substantial Fe weight loss was observed for catalysts prepared from $[\text{NEt}_4][\text{HFe}_3(\text{CO})_{11}]$ and $[\text{NEt}_4][\text{AuFe}_4(\text{CO})_{16}]$, whereas only very small differences between the actual and the nominal Fe content were observed starting from $[\text{NEt}_4]_4[\text{Au}_4\text{Fe}_4(\text{CO})_{16}]$ (Figure 4.9).

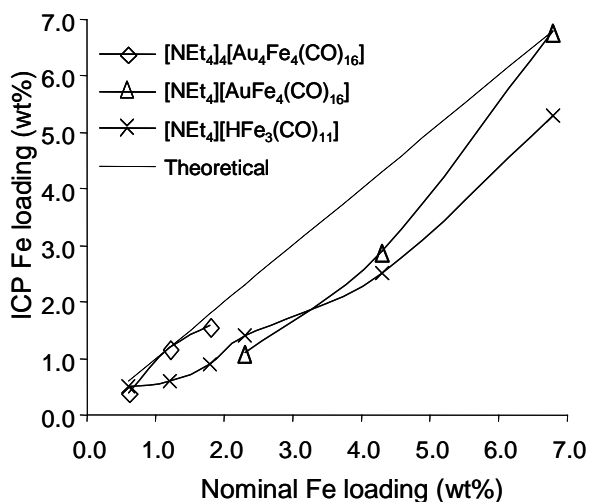


Figure 4.9: ICP Fe loading vs nominal Fe content for all titania catalysts.

Interestingly, $[\text{NEt}_4]_4[\text{Au}_4\text{Fe}_4(\text{CO})_{16}]$ reacts with the support during impregnation, whereas the other two species are not reactive. This indicates that reaction with the support is not the cause of Fe-loss. Therefore, Fe must be lost during thermal treatment, probably in the form of the volatile $\text{Fe}(\text{CO})_5$. Under the same conditions no Au-volatile species is formed and, thus, Au content is almost as expected.

For $[\text{NEt}_4][\text{HFe}_3(\text{CO})_{11}]$ there seems to be a discrepancy between TGA results on the unsupported salt and the ICP analyses on the cluster salt decomposed on TiO_2 support. In particular, no Fe is loss in the former case, whereas a significant amount has disappeared from the supported sample. This might be due to the fact that in the latter case the cluster salt precursor is highly dispersed on a support possessing high porosity, which may entrap the CO liberated from the decarbonylation of the cluster, locally building-up a CO rich atmosphere and eventually favouring the formation of the volatile $\text{Fe}(\text{CO})_5$.

The hypothesis concerning the Fe loss by releasing of $\text{Fe}(\text{CO})_5$ during thermal treatment is corroborated by the presence of an endothermic process at ca. 110°C in the DSC diagram of $[\text{NEt}_4][\text{AuFe}_4(\text{CO})_{16}]$ registered under nitrogen that is in fair agreement with $\text{Fe}(\text{CO})_5$ evaporation (b.p. 103 °C). Moreover, evolution of $\text{Fe}(\text{CO})_5$ during thermal treatment of the as-prepared catalysts has been confirmed experimentally by condensation of the gases evolved in a cold trap and their consequent analyses by FT-IR, fully corroborating our hypothesis.

4.3 Catalysts characterization

All thermally treated catalysts have been characterized by means of BET, XRD, TEM, XPS and TPR analyses in order to investigate their structural and redox properties.

4.3.1 Specific surface area and XRD

Samples surface areas were measured by N₂ physisorption and single point BET analysis methods while the complete XRD diffractogram was collected in the 2θ range 10-85°. A second, more careful, XRD acquisition in the 2θ range 40-50° was performed for bi-metallic catalysts to evaluate Au crystal size. In Table 4.4 are listed the surface areas for Au/FeO_x and FeO_x catalysts and average Au crystals size for bi-metallic systems.

Catalyst	Carbonyl salt precursor	Surface Area (m ² /g)	Au particle size (nm)
Support (TiO ₂)	-	80	-
Fe _{0.6} Au ₂ -Ti	[NEt ₄] ₄ [Au ₄ Fe ₄ (CO) ₁₆]	80	6.0
Fe _{1.2} Au ₄ -Ti		79	6.6
Fe _{1.8} Au ₆ -Ti		71	7.4
Fe _{2.3} Au ₂ -Ti	[NEt ₄][AuFe ₄ (CO) ₁₆]	78	< 3.0
Fe _{4.5} Au ₄ -Ti		67	6.9
Fe _{6.8} Au ₆ -Ti		69	7.0
Fe _{0.6} -Ti	[NEt ₄][HFe ₃ (CO) ₁₁]	80	-
Fe _{1.2} -Ti		76	-
Fe _{1.8} -Ti		76	-
Fe _{2.3} -Ti		79	-
Fe _{4.5} -Ti		78	-
Fe _{6.8} -Ti		78	-

Table 4.4: BET specific surface area and average crystallite size of Au for all studied catalysts

Similar surface areas, from 80 to 76 m²/g, were obtained in the case of iron supported catalysts, indicating that iron cluster deposition did not result in a significant change in the total porosity. On the contrary, the impregnation with the

bimetallic cluster determines a more significant decrease of surface area. However, the effect of active phase content on this parameter is limited and it is not linearly correlated with the gold content but could indicate that, in some cases, there is a moderate blockage of the titania pores due to the gold presence.

Figure 4.10 reports the XRD patterns for the gold/iron catalysts series prepared starting from $[\text{NEt}_4]_4[\text{Au}_4\text{Fe}_4(\text{CO})_{16}]$ and thermally treated under nitrogen with increasing content of gold.

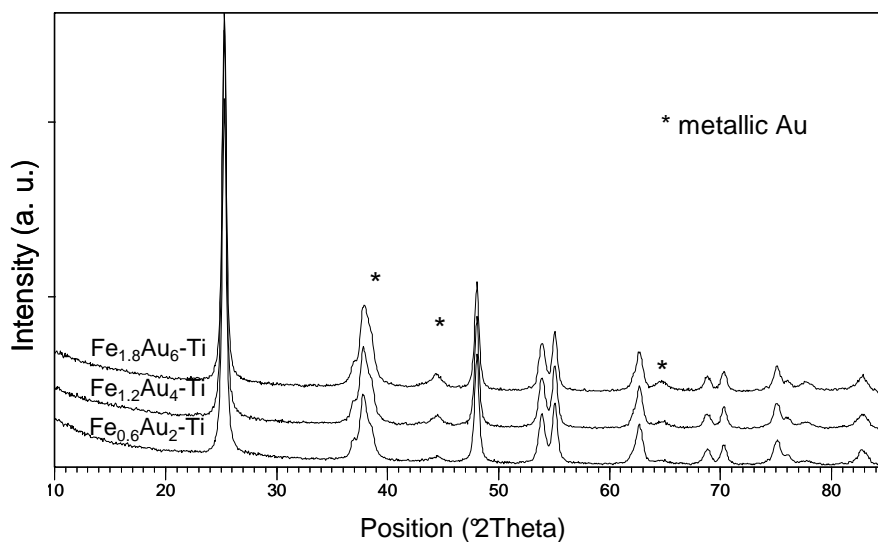


Figure 4.10: XRD patterns of bi-metallic catalysts prepared from $[\text{NEt}_4]_4[\text{Au}_4\text{Fe}_4(\text{CO})_{16}]$.

For all samples the XRD patterns present, besides the characteristic peaks of the TiO_2 support (anatase phase), weak reflections due to the presence of gold while no diffraction peaks of metallic iron or FeO_x compounds were observed.

The intensities of gold peaks slightly increased with the gold loading; in fact, the mean gold particle size, determined from XRD reflection at $2\theta=44.3^\circ$ and reported in Table 4.4 are very similar (6-7 nm) even if the Au loading increases from 2 to 6 wt.

A good dispersion of iron species was also achieved, since no diffraction peaks of metallic iron or FeO_x compounds were observed.

Similar results have been obtained for $\text{Au}/\text{FeO}_x\text{-Ti}$ catalysts prepared starting from $[\text{NEt}_4][\text{AuFe}_4(\text{CO})_{16}]$. Gold and iron species dispersion resulted to be as good as in the other cited samples: in the corresponding XRD patterns reported in Figure 4.11

only weak reflections due to metallic gold were detected and, despite the higher Fe loading on these catalysts, no reflection corresponding to iron species were observed. For these samples the average Au crystal size increases from 3 to 7 nm (see Table 4.4) increasing Au loading on the support.

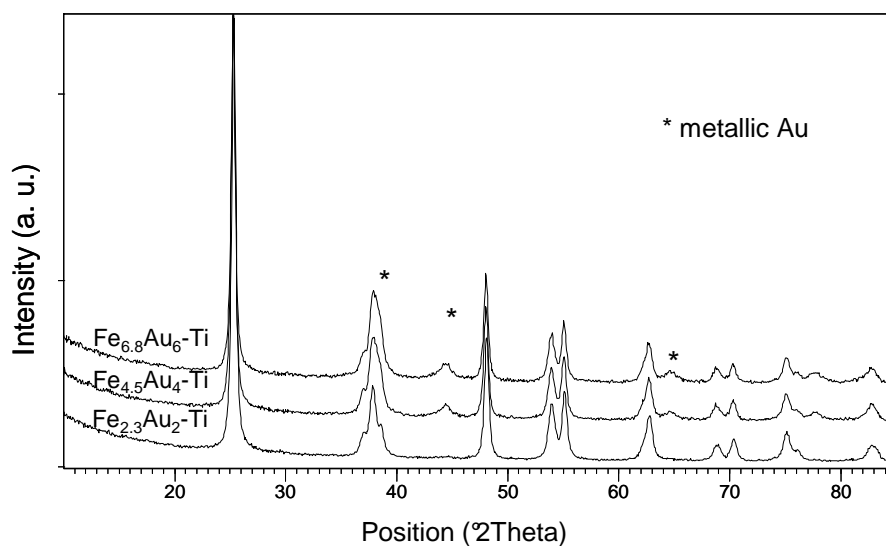


Figure 4.11: XRD patterns of bi-metallic catalysts prepared from $[\text{NET}_4][\text{AuFe}_4(\text{CO})_{16}]$.

Also in the case of iron supported materials a very good dispersion of iron was obtained, since no detectable crystallite formation of any kind of ferric oxide or hydroxide was observed in all diffraction patterns, even at the highest Fe loading (see Figure 4.12).

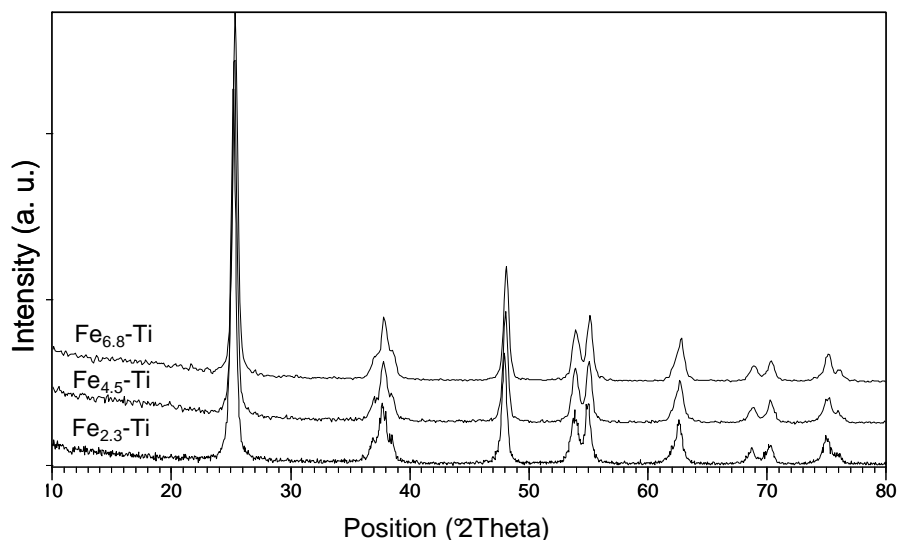


Figure 4.12: XRD patterns of Fe-Ti catalysts at highest metal content.

4.3.2 Study of catalysts thermal treatment

In order to optimize thermal treatment conditions of bi-metallic catalysts one sample of $[\text{NEt}_4]_4[\text{Au}_4\text{Fe}_4(\text{CO})_{16}]$ supported on titania, $\text{Fe}_{0.6}\text{Au}_2\text{-Ti}$, was thermally treated ramping the temperature up to 400°C respectively under three different gas atmospheres: air, nitrogen and hydrogen.

XRD analyses were carried out to observe if there was any effect of the gas atmosphere on the dispersion of gold over the support. Au crystallites were found to significantly sinter during the calcination in air but did not greatly change after thermal treatment under N_2 and H_2 . The average Au particles sizes for these samples, as determined from XRD line broadening, are given in Table 4.5.

Catalyst	Pretreatment conditions	Au particle size (nm)
Fe _{0.6} Au ₂ -Ti	Not calcined	3.4
Fe _{0.6} Au ₂ -Ti-O ₂	Air at 400°C	23.1
Fe _{0.6} Au ₂ -Ti-N ₂	N ₂ at 400°C	6.0
Fe _{0.6} Au ₂ -Ti-H ₂	H ₂ at 400°C	5.2

Table 4.5: Effect of the thermal treatment conditions on Au particles size Fe_{0.6}Au₂-Ti.

These results indicate an appreciable agglomeration of gold particles upon calcination in air, confirming the hypothesis that the cluster transformation in the presence of an oxidising atmosphere could lead to uncontrolled decomposition with fast temperature rise causing gold nanoparticles sintering, but underline the possibility to direct the size of gold particles by controlling cluster oxidation/decomposition.

Thus, the supported bi-metallic catalysts were thermally treated under nitrogen while the iron catalysts were calcined in air because the performances of the latter materials are not affected by a similar treatment, as it was experimentally observed in a preliminary study on this systems.

4.3.3 TEM study

In order to obtain more information on the distribution of gold and iron on titania samples, TEM analyses were also performed.

Scanning transmission electron microscopy studies on the Fe_{4.5}Au₄-Ti catalyst were carried out. An overall, preliminary panoramic view of the sample, showed aggregates of TiO₂ decorated by nanoparticles of what turned out to be metallic gold and iron oxide. Detailed selected area diffraction (SAD) studies confirmed the predominant presence of the TiO₂ anatase and revealed some occurrence of crystalline hematite Fe₂O₃, the latter only for the fresh catalyst. Crystalline Au was found and properly identified by combining SAD with HAADF STEM (High Angle Annular Dark Field Scanning Transmission Electron Microscopy) studies. A clear image of gold nanoparticles is shown in Figure 4.13.

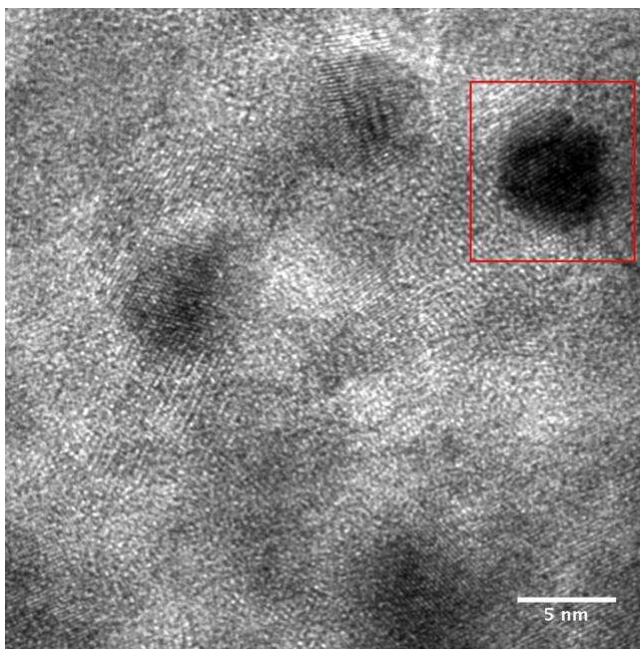


Figure 4.13: High Resolution TEM image of the Fe_{0.5}Au₄-Ti fresh sample, showing the presence of a gold nanoparticle of about 5 nm in diameter (square box).

HAADF STEM, in fact, proves to be ideal for compositional reconstruction as it generates strong contrast that has a fully monotonic relationship with density (mass) and thickness. The assigned indexed reflections of crystalline anatase, hematite and Au for the fresh catalyst are shown in Table 4.6.

	TiO ₂ anatase	Fe ₂ O ₃	Au
Exp. Reflections	H K L	H K L	H K L
3.52	1 0 1 (1.0)		
2.7		1 0 4 (1.0)	
2.53		1 1 0 (0.73)	
2.36	0 0 4 (0.20)		1 1 1 (1.0)
2.05			2 0 0 (0.47)
1.89	2 0 0 (0.28)		
1.69	1 0 5 (0.18)	1 1 6 (0.45)	
1.49	2 0 4 (0.13)	2 1 4 (0.30)	
1.43		3 0 0 (0.29)	2 2 0 (0.28)
1.34	2 2 0 (0.06)		
1.27	2 1 5 (0.10)		
1.22			3 1 1 (0.31)
1.17			

Table 4.6: Assigned indexed reflections of crystalline anatase, hematite and Au for the fresh Fe_{4.5}Au₄-Ti catalyst. The expected relative intensity of the reflection is indicated in brackets

Unfortunately, the presence of metallic iron on the catalysts could not be unambiguously identified by SAD because of the overlapping of its reflections with those of crystalline gold.

However, with EDX mapping it was possible to observe the distribution, hence the presence, of even the non-crystalline Fe species, which appeared to be evenly dispersed all over the TiO₂ support. As shown in Figure 4.14 for Fe_{4.5}Au₄-Ti catalyst, iron species are finely and homogeneously distributed on the TiO₂ matrix, while gold is more aggregated in small particles. These TEM results are in agreement with the findings of the XRD studies and suggest that iron oxide is diffused and not segregated in clusters.

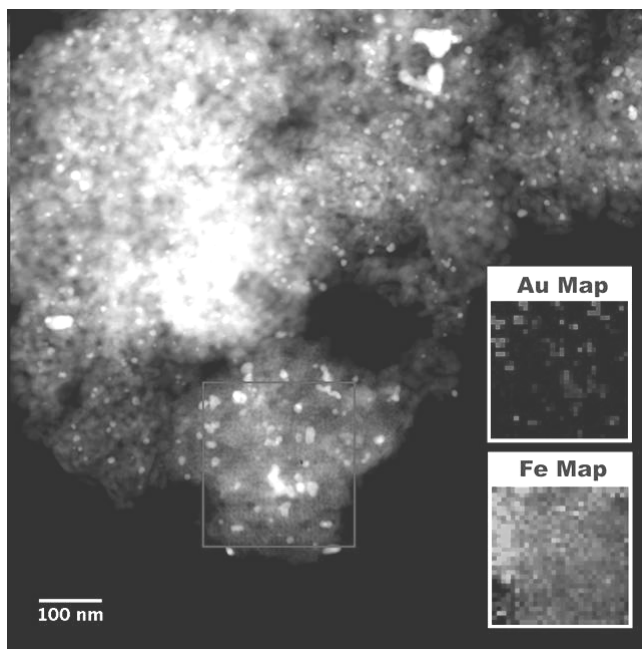


Figure 4.14: STEM image of the fresh $\text{Fe}_{4.5}\text{Au}_4\text{-Ti}$ catalyst. The insets report the EDX maps for Au and Fe of the region inside the square.

Size distribution was evaluated by ImageJ program [3]. Au particles average size is around 7-8 nm in diameter, with a distribution within the range 2-15 nm (see Figure 4.15).

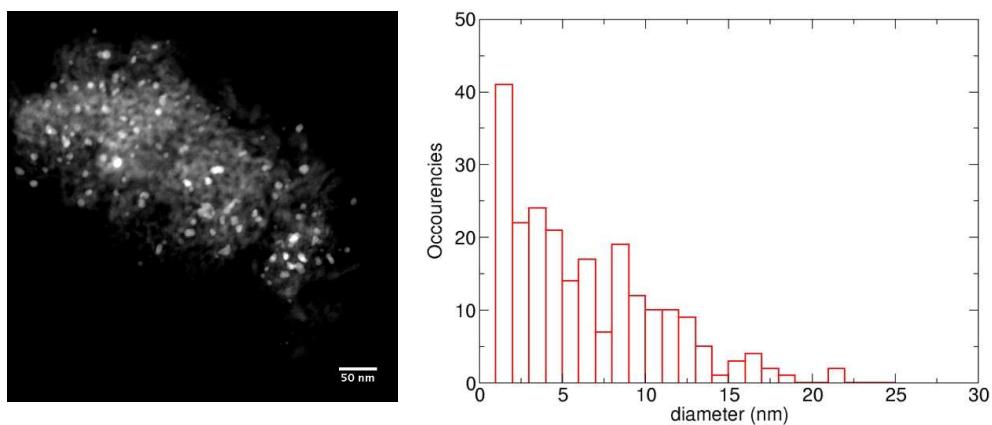


Figure 4.15:STEM image at higher magnification of a smaller TiO_2 cluster in the fresh $\text{Fe}_{4.5}\text{Au}_4\text{-Ti}$ catalyst, with evidences of metallic gold (details with brighter contrast and size distribution of the Au nanoparticles).

Also in this case TEM results are in fair agreement with the average Au-crystalline particle dimensions calculated from XRD data; in fact mean Au crystal size for Fe_{4.5}Au₄-Ti sample were found to be 6.9 nanometer.

4.3.4 XPS studies

The surface composition and the oxidation state of some selected catalysts were characterized by XPS.

These data were first analyzed in term of atomic concentration ratios, reported in Table 4.7.

Catalysts	Atomic concentration ratios				Binding Energy (eV)	
	Au/Ti XPS	Fe/Ti XPS	Au/Fe XPS	Au/Fe ICP	Au 4f	Fe 2p
Fe _{2.3} Au ₂ -Ti	0.003	0.02	0.12	0.52	83.9	710.5
Fe _{4.5} Au ₄ -Ti	0.014	0.19	0.07	0.47	84.0	710.6
Fe _{4.5} -Ti	/	0.15	/	/	/	710.6

Table 4.7: Atomic concentration ratios and binding energy of gold and iron in the catalysts.

Increases of the Au/Ti and Fe/Ti ratios can be correlated with the increase of the loading of these elements in the catalysts. However, the Au/Fe ratio is systematically under the bulk ratio determined by ICP. This result suggests that the atoms of iron or FeO_x species cover the atoms of gold. Indeed, in this kind of configuration, atoms of gold will be less available for XPS analyses and will thus take less part in the signal/spectra.

Figure 4.16 shows the Au 4f core level spectra and Fe 2p_{3/2} spectra Fe_{4.5}Au₄-Ti.

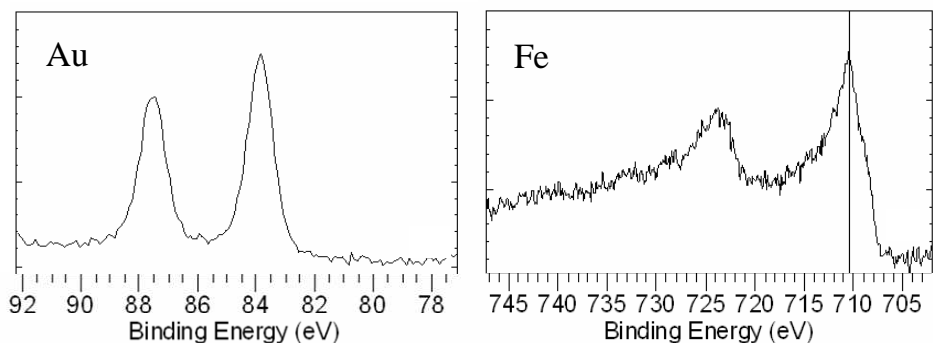


Figure 4.16: XPS Au 4f core level spectra (left) and XPS Fe 2p spectra (right) of $\text{Fe}_{4.5}\text{Au}_4\text{-Ti}$.

Concerning the oxidation state, the binding energy of gold corresponds clearly to the metallic state (Au^0) in each catalyst.

The Fe $2p_{3/2}$ peak and the iron binding energy (Table 4.7) are similar in the presence and in the absence of gold in the catalyst as can be observed in Figure 4.17, where the spectra recorded for a Fe-Ti and a $\text{Au/FeO}_x\text{-Ti}$ sample are compared.

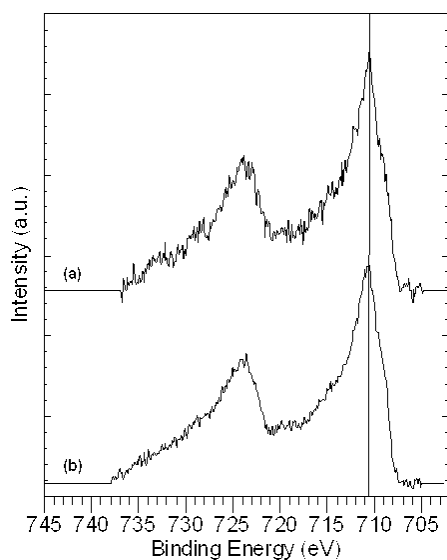


Figure 4.17: Fe 2p XPS spectra of (a) $\text{Fe}_{4.5}\text{Au}_4\text{-Ti}$; and (b) $\text{Fe}_{4.5}\text{-Ti}$

This peak exhibits a shoulder at about 710 eV and can be fitted with two peaks which, according to their binding energy, are attributed to Fe^{3+} (711 eV) and Fe^{2+}

(709.8 eV) species [4]. Thus, the iron oxide layer appears to be composed of a mixture of Fe_2O_3 and FeO or Fe_3O_4 .

4.3.5 Temperature programmed reduction (TPR)

TPR analyses were performed in order to understand the redox behaviour of prepared catalysts.

In the scientific literature a considerable effort has been devoted to the study of the reduction of unsupported and supported iron oxides [5], nevertheless the nature of the total process is extremely complex and may vary with the physicochemical characteristics of the iron oxide or with the conditions of its reduction [6]. Figure 4.18 reports the TPR profiles of the $\text{FeO}_x\text{-Ti}$ catalysts at increasing iron loadings. The thermal treatment of these samples at 400 °C was conducted in air since it was not necessary to work under nitrogen as it was useful for gold containing materials [7].

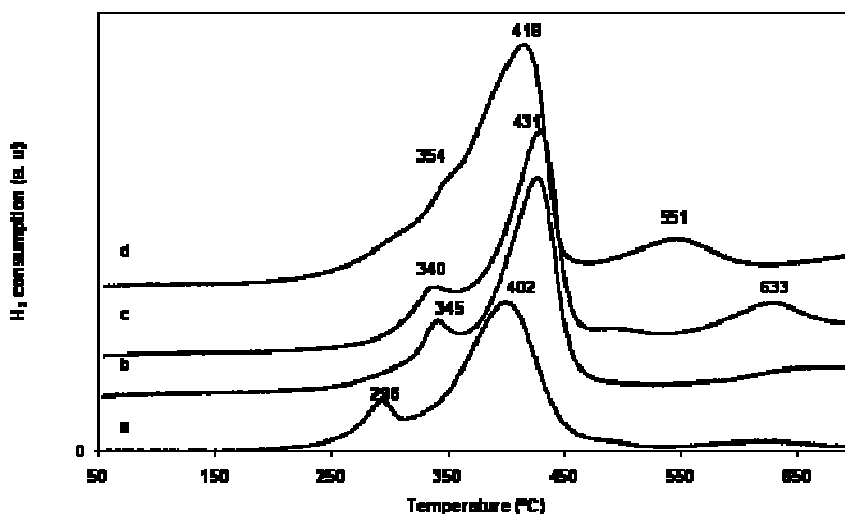


Figure 4.18: H_2 -TPR analysis of $\text{FeO}_x\text{-Ti}$ catalysts. (a) Fe=0.9 wt. %, (b) Fe=1.4 wt. %, (c) Fe=2.5 wt. %, (d) Fe=5.3 wt. %.

In all profiles, two main reduction peaks were present, with a maximum at 290–360 °C (P1) and at about 420 °C (P2). According to the literature the P1 peak can be attributed to the reduction of the hydroxylated iron oxide species and the P2 to the reduction of hematite to Fe_3O_4 . Addition of increasing amounts of iron shifts both P1 and P2 peaks to higher temperature.

The area under the reduction peaks was used to calculate the hydrogen uptake during the analyses, reported in Table 4.8.

Catalyst	Fe loading (wt.%) ICP analysis	Fe loading $\mu\text{mol/g}$ sample	H ₂ uptake $\mu\text{mol H}_2/\text{g}$ sample	Portion of metal reduced (%)
Fe _{0.6} -Ti	0.5	87	615	468
Fe _{1.2} -Ti	0.6	111	471	283
Fe _{1.8} -Ti	0.9	164	449	182
Fe _{2.3} -Ti	1.4	241	533	147
Fe _{4.5} -Ti	2.5	451	534	79
Fe _{6.8} -Ti	5.3	954	764	53

Table 4.8: Characterization of redox properties of iron in the FeO_x-Ti samples according to TPR data.

The hydrogen consumption was found to be significantly greater than the stoichiometric amount necessary for the reduction especially for catalysts at low iron content. It can be suggested that some reduction associated to the TiO₂ support could overlap that of iron oxides. It is, in fact, known [8][9] that the presence of metals can influence the reduction of oxygen species in TiO₂.

The presence of gold in the bi-metallic systems was expected to increase iron reducibility; in fact from the literature it is well known that gold enhances iron oxide reducibility [10] [11]. Conversely, TPR profile of FeO_x-Au catalyst were found to be very similar to the ones obtained for Fe-Ti samples. Gold effect on iron species reducibility is not evident on samples thermally treated at 400 °C “as prepared” because the nitrogen treatment, utilized for the preparation of these samples to control Au crystal growth, causes the reduction of those very reducible species, but can be observed for pre-oxidized samples.

In the Figure 4.19 are compared the reduction profile of the “as prepared” Fe_{4.5}Au₄-Ti catalyst and the one obtained for the same sample after an oxidation treatment in air at low temperature (200°C).

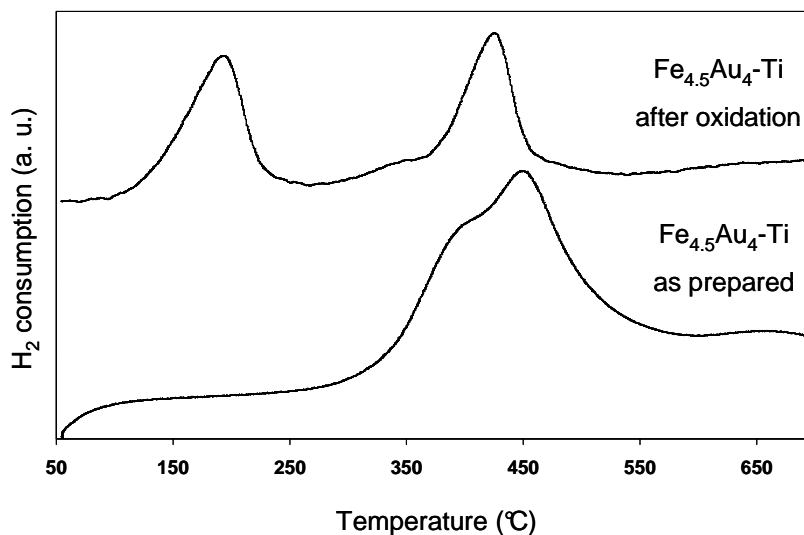


Figure 4.19: H₂-TPR analysis Fe_{4.5}Au₄-Ti catalyst after different treatment: as prepared and after an oxidation treatment.

In the reduction profile obtained for the oxidized sample a peak at 180-190°C appears, confirming that the preparation of Au/FeO_x-Ti catalysts by utilizing the gold/iron carbonyl clusters leads to the formation of highly reducible iron species. This effect was observed for both series of bi-metallic catalysts, in which reduction profiles an intense peak at 140-190 °C appears when the samples were oxidized before performing TPR analyses.

The shift of the Fe₂O₃ to Fe₃O₄ reduction peak to lower temperatures in presence of Au is a well documented phenomenon [11] and it is generally explained by the weakening of the Fe–O bonds of the species located near gold, leading to higher lattice oxygen mobility and thus availability at the catalysts surface. Similar results have been reported by Minico` et al. [10]. The fact that the peaks at around 430 °C, albeit less intense, are still present in the Fe_{4.5}Au₄-Ti TPR profiles recorded after oxidation, seems to indicate that some fractions of the iron oxides species supported on TiO₂ are preferably bonded to the support itself rather than to Au. Nevertheless, the support reduction, promoted by iron and gold, could also overlap with iron oxide bands.

4.4 Catalytic activity

Au/FeO_x-Ti and FeO_x-Ti catalysts were tested in total oxidation of toluene and methanol and in the PROX reaction. Even if Pd and Pt based catalysts are the most efficient systems used for total oxidation of volatile organic compounds, cheaper catalytic materials are under investigation in order to find an alternative for this kind of applications.

In the literature there are several studies concerning the use of gold-based catalyst for environmental applications and good results are reported for the catalytic oxidation of different molecules such as alcohols, acetone and toluene [10]. Moreover, it was proven that the addition of iron to supported gold catalysts leads to improved activity and stability during CO oxidation, thus these catalysts were also tested in the PROX reaction.

4.4.1 Toluene combustion

Toluene combustion catalytic tests were performed in a laboratory plant as described in the experimental chapter (Chapter 2) ramping the temperature from 250 to 400 °C .

In Figure 4.20 is reported the toluene conversion trend depending on the reaction temperature for the FeO_x-Ti supported samples at different iron content.

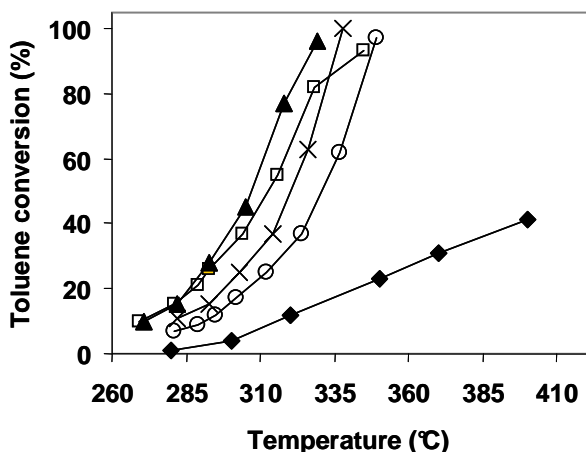


Figure 4.20: Toluene conversion as a function of reaction temperature for FeO_x-Ti catalysts at different content of active phase. Symbols: TiO₂ (♦), Fe=0.5 wt. % (○), Fe=0.9 wt. % (×), Fe=2.5 wt. % (▲), Fe=5.3 wt. % (□)

These data indicate that iron species dispersed on titania are active component for the oxidation of toluene and the catalytic activity is significantly enhanced as the iron content increases up to 2.5 wt. %. CO₂, CO and water were the only determined products and the selectivity to total oxidation (CO₂) was higher for the catalysts containing the highest amount of iron as it is shown Figure 4.21.

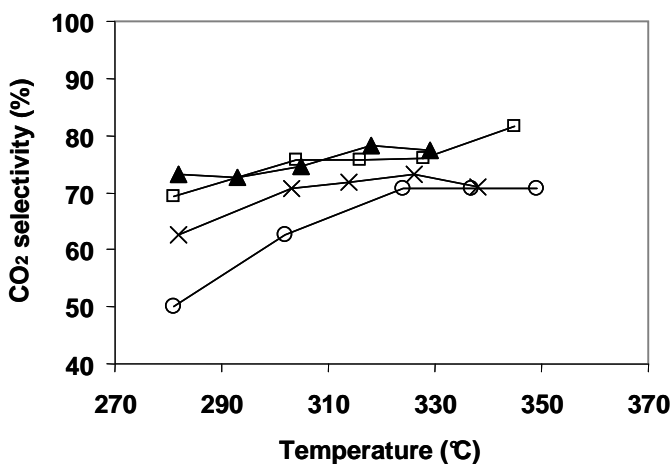


Figure 4.21: CO₂ selectivity as a function of reaction temperature for FeO_x/Ti catalysts at different content of active phase. Symbols: Fe=0.5 wt. % (○), Fe=0.9 wt. % (×), Fe=2.5 wt. % (▲), Fe=5.3 wt. % (□)

The presence of gold was found to moderately improve the catalytic activity of FeO_x-Ti toward the combustion of toluene but only for the catalysts with higher gold content. In Figure 4.22 are reported the results obtained for the two series of

Au/FeO_x-Ti catalysts; it can be observed that better catalytic performances can be achieved at higher gold and iron loading.

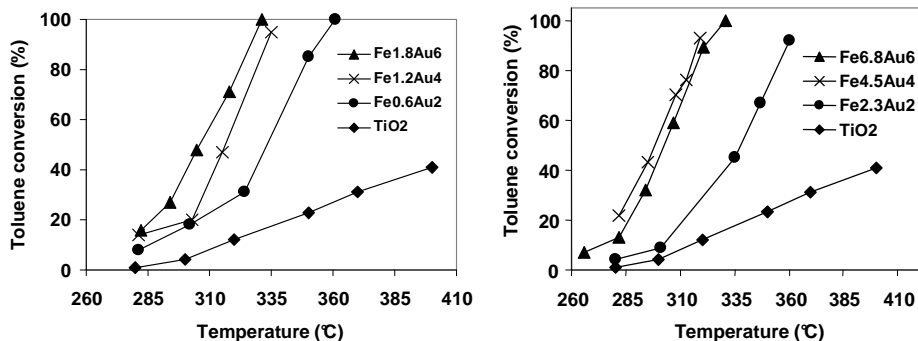


Figure 4.22: Toluene conversion as a function of reaction temperature for Au/FeO_x-TiO₂ catalysts prepared with [NEt₄]₄[Au₄Fe₄(CO)₁₆] (left) and [NEt₄][AuFe₄(CO)₁₆] (right) at different content of active phase.

In order to understand the effect on toluene combustion activity of different Fe/Au ratios on the two Au-FeO_x-Ti series, these data were compared in terms of the temperature required to have 50% of toluene conversion, as a function of measured gold content (Figure 4.23).

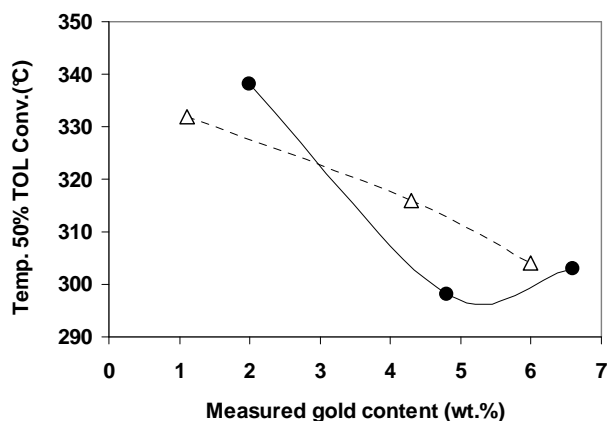


Figure 4.23: Temperature of 50% of toluene conversion as a function of the gold content for Au/FeO_x-Ti samples. Symbols: (Δ) cluster precursor [NEt₄]₄[Au₄Fe₄(CO)₁₆], (●) Cluster precursors [NEt₄][AuFe₄(CO)₁₆].

It is clear that there is a trend in catalytic activity depending on the gold content and on the Au/Fe ratio in the bi-metallic system. The higher Fe content introduced by meaning of $[\text{NEt}_4][\text{AuFe}_4(\text{CO})_{16}]$, taking constant the amount of gold, leads to higher efficiency of these catalysts in toluene oxidation, mainly for $\text{Fe}_{4.5}\text{Au}_4\text{-Ti}$ catalyst.

Despite the moderate effect due to the presence of Au on $\text{FeO}_x\text{-Ti}$ systems, a significant influence on product distribution was observed; in fact, on bi-metallic catalysts, CO_2 is the only detected product at high toluene conversion (see Figure 4.24)

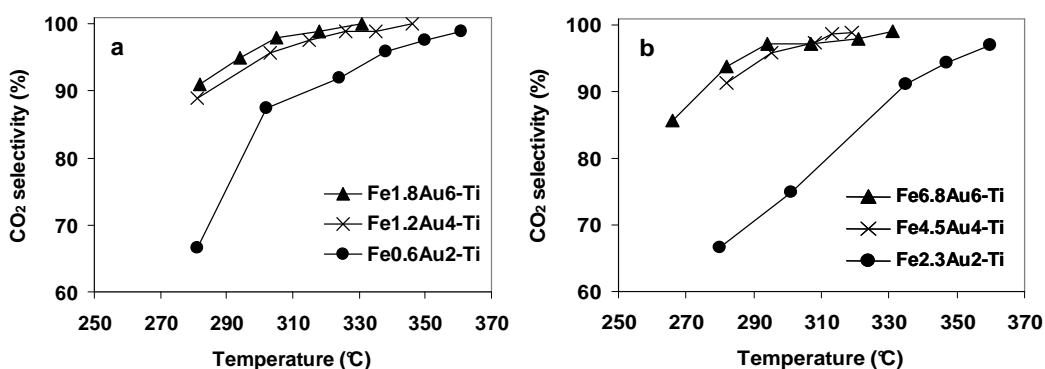


Figure 4.24: CO_2 selectivity as a function of reaction temperature for Au/FeO_x-Ti catalysts prepared with $[\text{NEt}_4]_4[\text{Au}_4\text{Fe}_4(\text{CO})_{16}]$ (a) and $[\text{NEt}_4][\text{AuFe}_4(\text{CO})_{16}]$ (b) at different content of active phase.

At this point, even if it is difficult to discriminate between the contribution of gold and iron because their content varied simultaneously, it has been observed that the toluene combustion activity, measured in terms of the temperature required to have 50% of toluene conversion, passes through a maximum for catalysts having an iron content of 2-3 wt. % (see Figure 4.25)

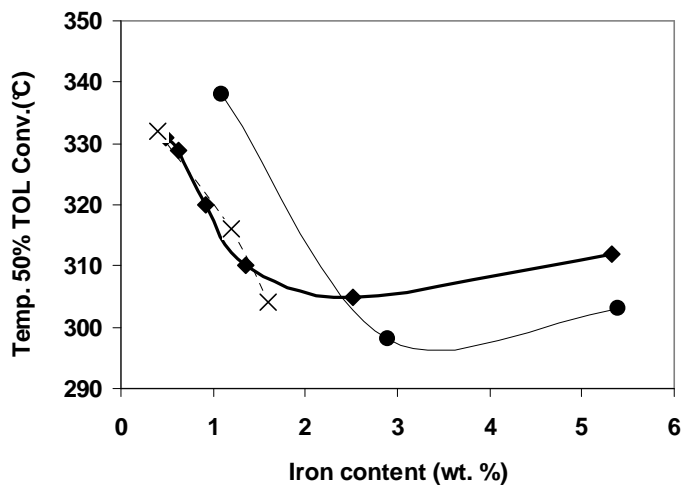


Figure 4.25: Temperature of 50% of toluene conversion as a function of the iron content for the FeO_x-Ti and the Au/FeO_x-Ti samples Symbols: (-♦-) FeO_x-Ti catalysts, (-●-) Au/FeO_x-Ti catalysts. (Fe:Au= 4), (-x-) Au/FeO_x-Ti catalysts. (Fe:Au= 1).

In conclusion, these data seem to indicate that the catalytic performances of these materials in total oxidation of toluene depend on both iron and gold content. Moreover, in spite of the fact that Fe and Au contents varied simultaneously, making difficult to discriminate between the contribution of each one, the presence of gold significantly increases the efficiency of the total oxidation reaction, leading to complete conversion of toluene to CO₂. (see Figure 3.26)

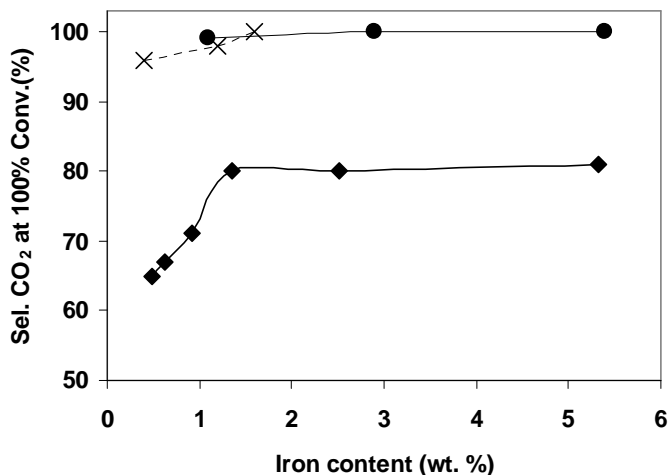


Figure 4.26: CO₂ selectivity at 100% of toluene conversion as a function of the iron content for the FeO_x-Ti and the Au/FeO_x-Ti samples Symbols: (-♦-) FeO_x-Ti catalysts, (-•-) Au/FeO_x-Ti catalysts. (Fe:Au= 4), (-x-) Au/FeO_x-Ti catalysts. (Fe:Au= 1).

The stability of gold/iron catalysts was also investigated. All tested catalysts showed an excellent stability under catalytic conditions in toluene total oxidation, as reported in Figure 4.27. In fact, after a short period of activation, during the first 2 h of run, the Fe_{4.5}Au₄-Ti catalyst remained perfectly stable for further 80 h, both regarding toluene conversion and CO₂ selectivity.

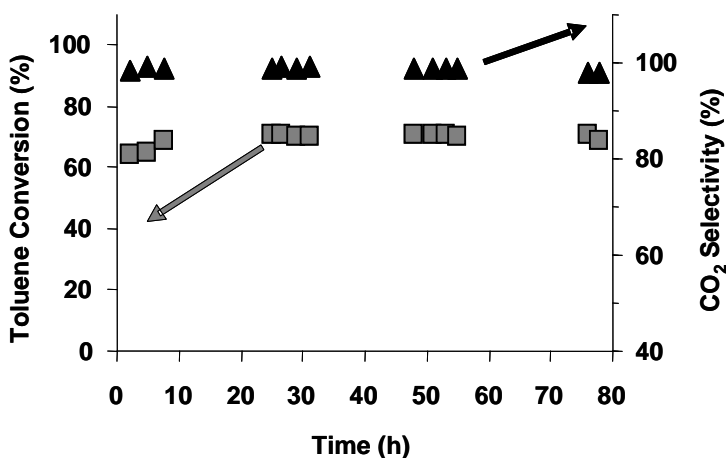


Figure 4.27: Long-term activity test on Fe_{4.5}Au₄-Ti sample. Toluene conversion (■) and CO₂ selectivity (▲) at 308°C as a function of time.

4.4.2 Characterization of spent catalysts after toluene combustion reaction

A detailed study was carried out in order to verify if and how catalysts chemical and physical properties were changed after catalytic measurement tests in toluene oxidation.

Gold catalysts are usually very unstable if gold particles are present in a very disperse form because they tend to sinter, thus it is very important to understand if any change occurs to the catalysts during their utilization.

Au/FeO_x-Ti catalysts were found to be very stable under reaction conditions for more than 80 hours, in fact data regarding gold dispersion after catalytic operations confirmed that only minor changes can be observed comparing spent catalysts to the corresponding as-prepared samples.

In fact, observing XRD patterns of freshly prepared and spent catalysts reported in Figure 4.28 it is clear that there are no significant changes in terms of gold dispersion on the support.

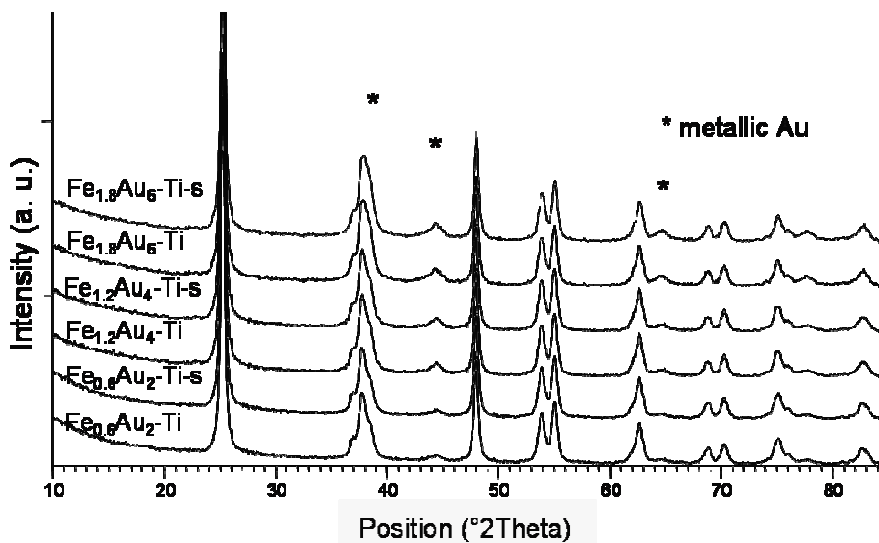


Figure 4.28: XRD patterns of the fresh and spent Au/FeO_x-Ti catalysts (Fe/Au = 1) after catalytic tests in complete oxidation of toluene.

As in the patterns related to fresh catalysts, beside anatase reflections, only broad peaks due to metallic gold are observed and their intensities slightly increase in the patterns related to spent samples. Similar results have been obtained for all bi-metallic catalysts, as it is confirmed looking at Au crystal size reported in Table 4.9.

Catalyst	Au particle size	
	Fresh (nm)	Spent (nm)
Fe _{0.6} Au ₂ -Ti	6.0	6.0
Fe _{1.2} Au ₄ -Ti	6.6	6.7
Fe _{1.8} Au ₆ -Ti	7.4	7.6
Fe _{2.3} Au ₂ -Ti	< 3.0	3.7
Fe _{4.5} Au ₄ -Ti	6.9	8.7
Fe _{6.8} Au ₆ -Ti	7.0	7.3

Table 4.9: Au particle size for fresh and spent Au-FeOx-Ti catalysts.

A more detailed investigation was carried out on Fe_{4.5}Au₄-Ti spent catalyst, for which a little bigger particle size were calculated from XRD profile and for which the highest catalytic activity was observed.

TEM results obtained for spent Fe_{4.5}Au₄-Ti indicate that the sample does not show drastic changes compared with the fresh catalyst. Only minor differences were noticed by selected area diffraction data, that revealed no evidence of crystalline hematite Fe₂O₃ in the spent sample. In this case, in fact, it was possible to assigned indexed reflections only to crystalline anatase and Au (Table 4.10).

	TiO ₂ anatase	Au
Exp. Reflections	H K L	H K L
3.51	1 0 1 (1.0)	
2.36	0 0 4 (0.20)	
2.34		1 1 1 (1.0)
2.05		2 0 0 (0.47)
1.88	2 0 0 (0.28)	
1.70	1 0 5 (0.18)	
1.47	2 0 4 (0.13)	
1.43		2 2 0 (0.28)
1.34	2 2 0 (0.06)	
1.24	2 1 5 (0.10)	3 1 1 (0.31)
1.16		

Table 4.10: Assigned indexed reflections of crystalline anatase and Au for spent Fe_{4.5}Au₄-Ti catalysts. The expected relative intensity of the reflection is indicated in brackets

The metal dispersion was found to be very similar to the fresh sample and the size distribution of gold nanoparticles was basically the same as it can be seen in Figure 4.29.

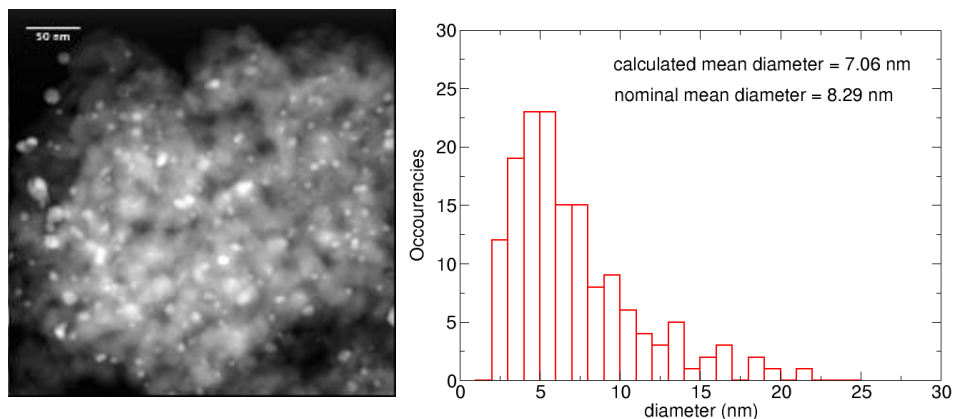


Figure 4.29: STEM image at higher magnification of a smaller TiO_2 cluster in spent $\text{Fe}_{4.5}\text{Au}_4\text{-Ti}$ catalyst, with evidences of metallic gold (details with brighter contrast) and size distribution of the Au nanoparticles.

Since no structural changes were observed for spent catalysts after working in toluene combustion, the oxidation state of catalysts was investigated by means of XPS and TPR analyses.

In Table 4.11 are compared XPS results obtained for fresh and spent catalysts in terms of atomic concentration ratios. These data show that the catalytic tests do not have a significant influence on the surface content and on the dispersion of iron and gold species, confirming the information already suggested by the measurement of the average Au crystallite sizes of spent catalysts.

Catalysts	Atomic concentration ratios				Binding Energy (eV)	
	Au/Ti XPS	Fe/Ti XPS	Au/Fe XPS	Au/Fe ICP	Au 4f	Fe 2p
$\text{Fe}_{2.3}\text{Au}_2\text{-Ti}$	0.003	0.02	0.12	0.52	83.9	710.5
$\text{Fe}_{2.3}\text{Au}_2\text{-Ti s}$	0.004	0.02	0.16	0.52	83.6	710.2
$\text{Fe}_{4.5}\text{Au}_4\text{-Ti}$	0.014	0.19	0.07	0.47	84.0	710.6
$\text{Fe}_{4.5}\text{Au}_4\text{-Ti s}$	0.014	0.19	0.07	0.47	83.9	710.3

Table 4.11: Atomic concentration ratios and binding energy of gold and iron in fresh and spent catalysts.

Concerning the oxidation state, the binding energies of gold and iron in spent catalysts are the same observed in the fresh samples and correspond clearly to the metallic state for gold and a mixture of Fe^{3+} and Fe^{2+} for iron layer in each catalyst. No differences were in fact observed in the spent catalysts spectra, compared to the ones registered for fresh samples (see Figure 4.30).

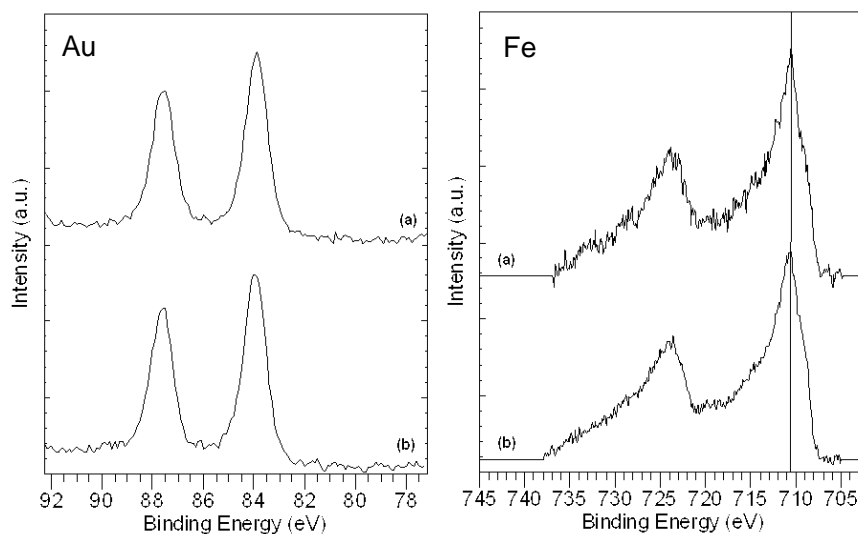


Figure 4.30: XPS Au 4f core level spectra (left) and XPS Fe 2p spectra (right) of (a) $\text{Fe}_{4.5}\text{Au}_4\text{-Ti}$ catalyst in the initial state and (b) $\text{Fe}_{4.5}\text{Au}_4\text{-Ti}$ sample after the catalytic reaction.

Further investigations on the redox properties of spent catalysts were carried out by TPR measurements. Figure 4.31 reports the H_2 -TPR analysis of $\text{Au/FeO}_x\text{-Ti}$ catalysts with higher iron loading at different content of active phase after catalytic tests

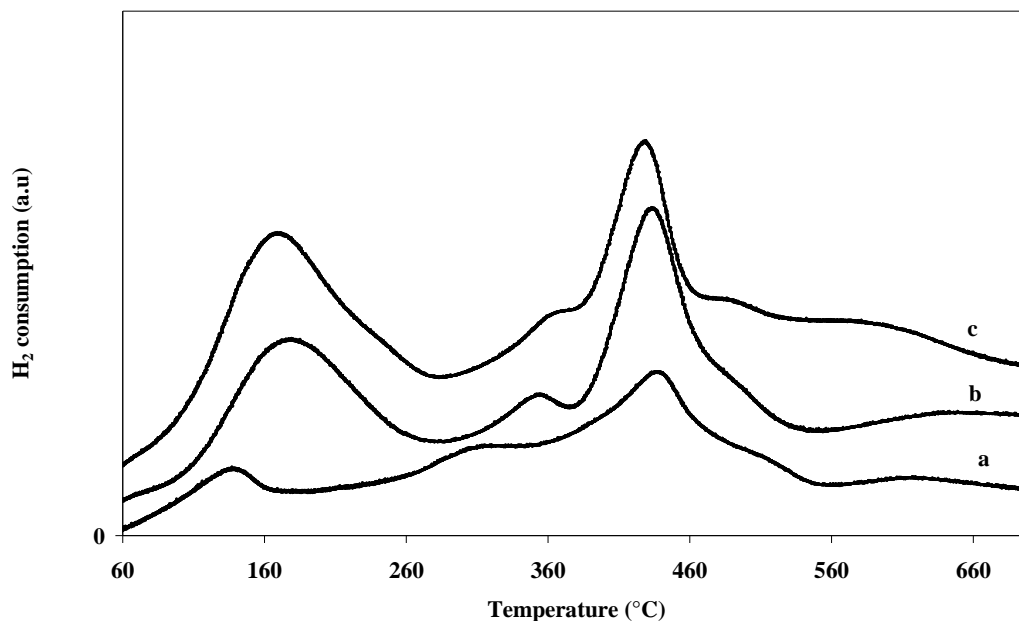


Figure 4.31: H_2 -TPR analysis of Au/ FeO_x -Ti catalysts after catalytic tests. (a) $\text{Fe}_{2.3}\text{Au}_2$, (b) $\text{Fe}_{4.5}\text{Au}_4$, (c) $\text{Fe}_{6.8}\text{Au}_6$.

Differently from the fresh catalysts, on spent samples the iron reduction peak at low temperature is already evident because during activity measurements the catalysts are exposed to an oxidising atmosphere and the iron species reduced under the thermal treatment under nitrogen are easily oxidized. The temperature of this peak is very similar for all prepared catalysts irrespective of the gold content, thus indicating that all cluster-derived systems present similar species distribution while the peak intensities increase on increasing the Au and Fe loadings.

In conclusion we can say that the catalytic test does not seem to have an influence on the dispersion and on the oxidation state of gold and iron species in the studied catalysts.

4.4.3 Methanol combustion

Since the results obtained in toluene combustion demonstrated that Au has a little influence on toluene conversion, because of the scarce adsorption of toluene on gold catalysts [10] methanol combustion reaction was also investigated.

In fact, it was proven that alcohols strongly adsorb on Au based catalysts, probably with formation of oxygenates species [12].

Methanol total oxidation activity measurements were carried out in a laboratory plant, as described in the experimental chapter. In Figure 4.20 is reported the methanol conversion evolution depending on the temperature for the $\text{FeO}_x\text{-Ti}$ and $\text{Au/FeO}_x\text{-TiO}_2$ supported samples that showed highest catalytic activity in toluene combustion.

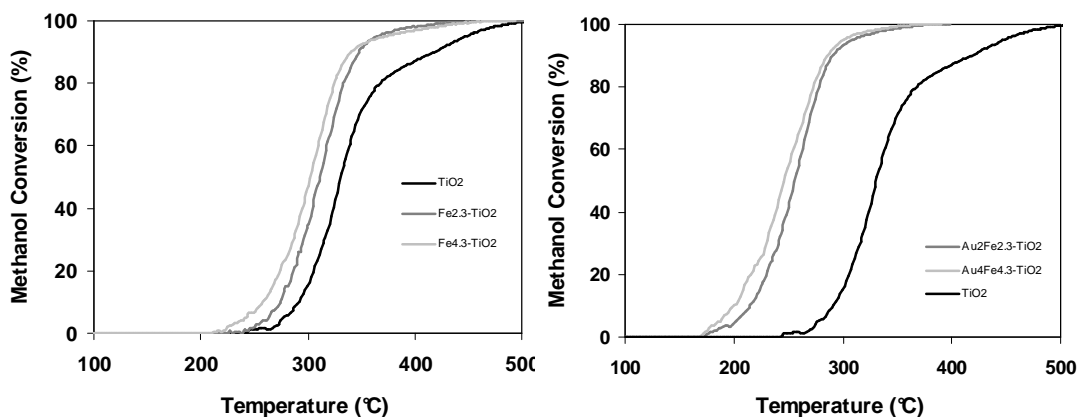


Figure 4.32: Methanol conversion as a function of reaction temperature for $\text{FeO}_x\text{-Ti}$ (left) and $\text{Au/FeO}_x\text{-Ti}$ (right) catalysts at different content of active phase.

From these data it is clear that Au strongly affect $\text{FeO}_x\text{-Ti}$ catalysts performances during methanol oxidation while a moderate effect of iron species on titania were observed. Light off temperatures for bi-metallic systems are much lower than iron catalysts while the selectivity towards combustion reactions is higher than 90% even at low methanol conversion for both kind of systems.

No big differences were observed in methanol oxidation rate increasing the amount of active phase on the support. These results can be justified looking at XPS data regarding the metal atomic ratio at the catalysts surface: even if on $\text{Fe}_{4.5}\text{Au}_4\text{-Ti}$ the Au/Ti atomic ratio is obviously higher than $\text{Fe}_{2.3}\text{Au}_2\text{-Ti}$ (0.014 vs 0.003), due to the fact that a higher amount of cluster was employed, the Au/Fe ratio is lower for the first sample (0.07 vs 0.12). Thus, XPS results suggested that iron atoms probably cover gold particles making them less accessible for organic substrate adsorption.

Despite the scarce intermediates formation, since just small amounts of formaldehyde were detected at low conversion, no significant differences towards

their selectivity were noticed for all tested samples. In Figure 4.33 are reported intermediates selectivity trends and it can be seen that they are very similar for all catalysts.

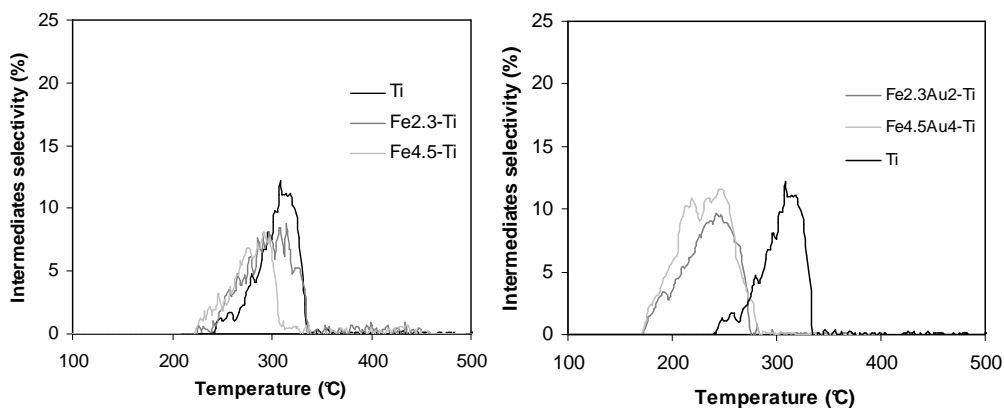


Figure 4.33: Intermediates selectivity for $\text{FeO}_x\text{-Ti}$ (left) and $\text{Au/FeO}_x\text{-Ti}$ catalysts at different content of active phase.

4.4.4 PROX reaction

Preferential CO oxidation in H_2 -rich gas stream is one of the most promising reaction to reduce CO concentration in H_2 stream for its application in PEM fuel cells for energy production.

In the literature there are many studies demonstrating the beneficial effect due to the addition of an iron component to gold supported catalysts in terms of enhanced activity, selectivity, resistance to deactivation and then prolonged lifetime of the material. Both higher activity and improved stability are linked to the ability of FeO_x phase to provide hydroxyl groups that are needed for the catalytic cycle and to form anion vacancies [13]. Moreover, it has been demonstrated that the addition of iron in the preparation lowered the rate of deactivation during CO oxidation when TiO_2 is used as support.

Actually $\text{Au/FeO}_x\text{-Ti}$ catalysts prepared starting from bi-metallic carbonyl clusters should be particularly suitable for this kind of application. The aim of this preparation method using carbonyl Fe-Au clusters with a well defined structure was, in fact, to anchor gold nanoparticles to the support via an iron layer. In this way we tried to stabilize gold particles and, at the same time, exploit the beneficial effect of gold on

iron oxide since it is well known that gold enhances iron oxide reducibility promoting the formation of anionic vacancies where oxygen can chemisorb.

Figure 4.34 reports catalytic activity results in terms of CO conversion and selectivity towards CO oxidation over two selected Au/FeO_x-Ti samples.

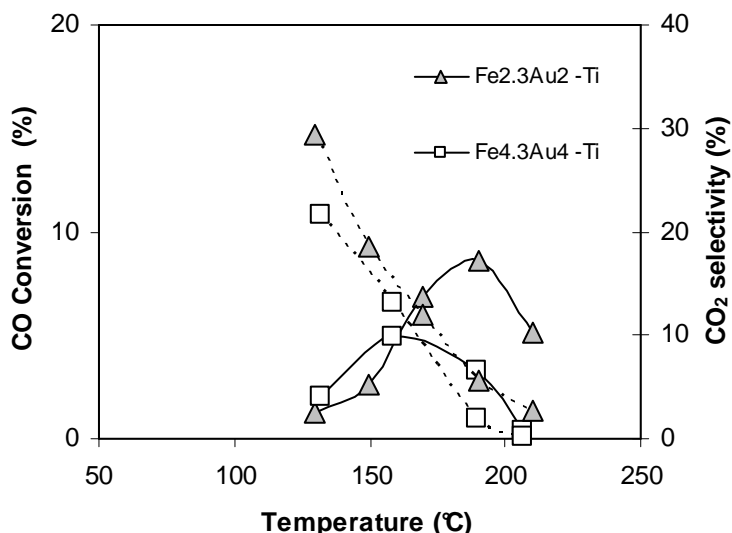


Figure 4.34: CO conversion (full lines) and CO selectivity (dotted lines) as function of reaction temperature over Au/FeO_x-Ti catalysts.

No significant CO conversion was observed for these catalysts, which performances resulted to be very similar in terms of CO conversion but also selectivity in CO oxidation.

For each tested sample it can be noticed that CO conversion increases with increasing temperature reaching a maximum and then decreasing at higher temperature. Also selectivity is strongly influenced by the reaction temperature; the higher temperature the lower selectivity was observed. These data are in agreement with literature results: in fact the activation energy of hydrogen oxidation is higher than CO oxidation and at higher temperature the CO/H ratio surface coverage on gold nanoparticles strongly decreases.

Moreover, the poor activity in PROX reaction of Au/FeO_x-Ti prepared catalysts can be attributed to the low Au/Fe surface ratio determined by XPS (as reported in Table 4.11) and the relatively large dimensions of gold nanoparticles (around 7-8 nm). It is, in fact, widely accepted that CO activation occurs only on very small gold

nanoparticles < 5 nm and when their dimensions increase the activation of CO on gold becomes more difficult and at a certain point can be the rate determining step in the CO oxidation.

4.5 References

- [1] C. Femoni, M. C. Iapalucci, G. Longoni, C. Tiozzo, S. Zacchini, *Angew. Chem. Int Ed.* 2008, 47, 6666 C.
- [2] C. Femoni, M. C. Iapalucci, G. Longoni, C. Tiozzo, J. Wolowska, S. Zacchini, E. Zazzaroni, *Chem. Eur. J.* 13 (2007) 654.
- [3] T.J. Collins, *BioTechniques* 43 (2007) 25.
- [4] L. Guzzi, K. Frey, A. Beck, G. Peto, C. S. Daroczi, N. Kruse, S. Chnakin *Appl. Catal. A* 291 (2005) 116.
- [5] G. Munteanu, L. Ilieva, D. Andreeva, *Thermochim. Acta* 291 (1997) 171.
- [6] Jozwiak, E. Kaczmarek, T.P. Maniecki, W. Ignaczak, W. Maniukiewicz *Appl. Catal. A* 326 (2007) 17. W.K.
- [7] S. Albonetti, R. Bonelli, J. Epoupa Mengou, C. Femoni, C. Tiozzo, S. Zacchini, F. Trifirò *Catal. Today* 137 (2008) 483.
- [8] C. Gennequin, M. Lamallem, R. Cousin, S. Siffert, F. Aissi, A. Aboukais, *Catal. Today* 122 (2007) 301.
- [9] S. Albonetti, J. Epoupa Mengou, F. Trifirò *Catal. Today* 119 (2007) 295.
- [10] S. Minicò, S. Scirè, C. Crisafulli, R. Maggiore, S. Galvagno *Appl. Catal. B* (2000) 245.
- [11] G. Neri, A.M. Visco, S. Galvagno, A. Donato, M. Panzalorto *Thermochim. Acta* 329 (1999) 39.
- [12] M. Baldi, E. Finocchio, F. Milella, G. Busca, *Appl. Catal. B environ.* 16, (1998) 43.
- [13] S. Carrettin, Y. Hao, V. Aguilar-Guerrero, B. C. Gates, S. Trasobares, J. J. Calvino, A. Corma, *Chem. Eur. J.* 13 (2007) 7771.

5. CERIA CATALYSTS

5.1 Introduction

Au/FeO_x and FeO_x catalysts supported on ceria were prepared employing the same procedure described for analogous titania supported catalysts. In this case only a single series of bi-metallic catalysts was prepared starting from [NEt₄][AuFe₄(CO)₁₆] salt (Fe/Au=4), while FeO_x samples were obtained by employing the homometallic [NEt₄][HFe₃(CO)₁₁] cluster.

Also in this case each preparation step was monitored by FTIR spectroscopy in the $\nu(\text{CO})$ region in order to observe the interaction between the clusters and CeO₂ during the impregnation process.

All thermally treated samples were fully characterized and tested in total combustion of toluene and methanol and in the PROX reaction in order to compare their activity to the titania based catalysts.

5.2 Catalysts preparation and characterization

5.2.1 Synthesis of Au/FeO_x and FeO_x ceria catalysts

A series of bi-metallic catalysts supported on CeO₂ was prepared starting from the carbonyl cluster salt [NEt₄][AuFe₄(CO)₁₆]. The amount of cluster used for impregnating ceria was dosed in order to obtain a gold loading of 1, 2 and 4 % in weight on support. In Table 4.1 are listed the code and nominal composition of all prepared Au/FeO_x-Ce catalysts.

Catalyst	Carbonyl salt precursor	Fe content (wt. %)	Au content (wt. %)
Fe _{1.2} Au ₁ -Ce	[NEt ₄][AuFe ₄ (CO) ₁₆]	1.2	1.0
Fe _{2.3} Au ₂ -Ce		2.3	2.0
Fe _{4.5} Au ₄ -Ce		4.5	4.0

Table 5.1: Code and nominal composition of prepared Au/FeO_x-Ce catalysts.

FeO_x-Ce were prepared by employing the homo-metallic [NEt₄][HFe₃(CO)₁₁] cluster, impregnating ceria with the amount of cluster necessary to obtain the same nominal iron loading of the Au/FeO_x-Ce catalysts. Prepared iron catalysts are listed in Table 4.2.

Catalyst	Carbonyl salt precursor	Fe content (wt. %)
Fe _{1.2} -Ce	[NEt ₄][HFe ₃ (CO) ₁₁]	1.2
Fe _{2.3} -Ce		2.3
Fe _{4.5} -Ce		4.5

Table 5.2: Code and nominal composition of FeO_x-Ce catalysts.

5.2.2 IR study during CeO₂ catalysts preparation

A detailed IR study was carried out during the impregnation process of ceria with the two cluster solutions in order to observe if there was any change in the clusters chemical behaviour in contact with a different kind of support. In the Figure 5.1 are reported the IR spectra recorded in the $\nu(\text{CO})$ region at different stages of the preparation of Au/FeO_x-Ce catalysts.

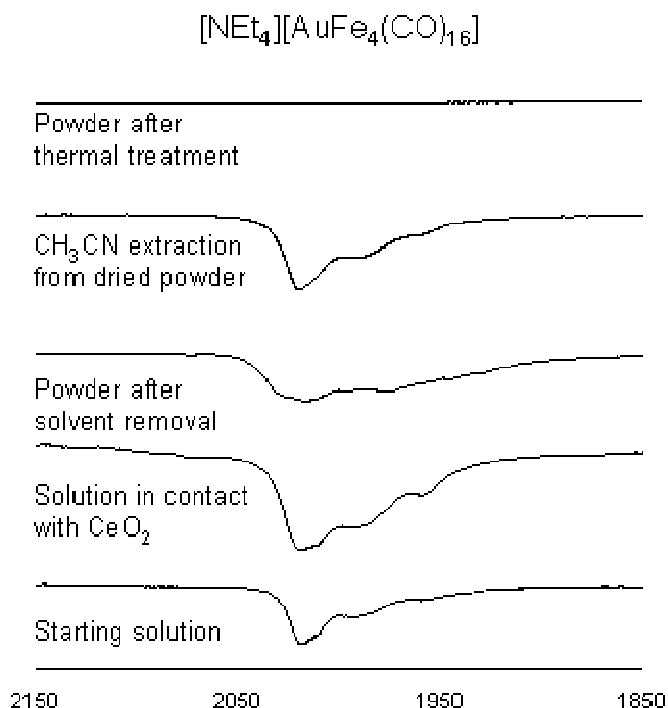


Figure 5.1: FTIR spectra in the $\nu(\text{CO})$ region obtained during the impregnation on CeO_2 of $[\text{NEt}_4][\text{AuFe}_4(\text{CO})_{16}]$

FT-IR studies pointed out that the cluster $[\text{NEt}_4][\text{AuFe}_4(\text{CO})_{16}]$ is absorbed on ceria without the occurrence of any reaction as it was observed during titania impregnation. This carbonyl cluster resulted to be quite stable and non reactive also during its deposition on CeO_2 and no significant changes were observed in the spectra recorded in the CO region at any preparation stage.

FTIR analysis indicates that $[\text{NEt}_4][\text{AuFe}_4(\text{CO})_{16}]$ salt displays a strong $\nu(\text{CO})$ peak in acetone at 2018 cm^{-1} which is maintained after adsorption on CeO_2 both in solution and in the solid state after solvent removal in vacuum. To confirm that this cluster does not react with support the extraction of the powder with CH_3CN was also carried out, and the intact starting $[\text{NEt}_4][\text{AuFe}_4(\text{CO})_{16}]$ was again identified. After thermal treatment at 400°C the cluster resulted totally decomposed as no bands in the CO region can be detected.

Following a similar procedure, an FT-IR investigation was also carried out during $[\text{NEt}_4][\text{HFe}_3(\text{CO})_{11}]$ impregnation on CeO_2 to obtain $\text{FeO}_x\text{-Ce}$ catalysts. IR spectra

were recorded in the CO region at same stages as Au/FeO_x-Ce preparation during cluster deposition, as it is shown in Figure 4.4.

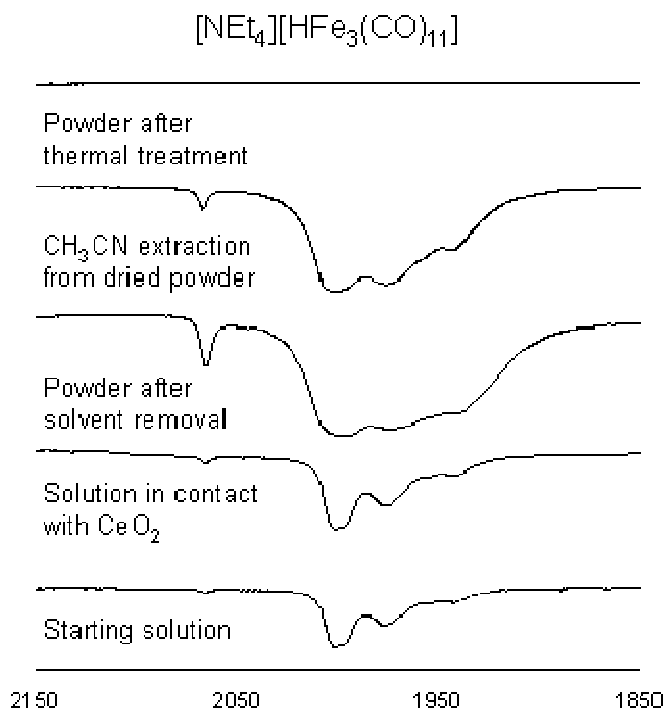


Figure 5.2: FTIR spectra in the $\nu(\text{CO})$ region obtained during the impregnation of $[\text{NEt}_4][\text{HFe}_3(\text{CO})_{11}]$ on CeO_2

Also in this case no reaction occurs between the carbonyl iron cluster and ceria as it was observed during titania impregnation.

Intact $[\text{NEt}_4][\text{HFe}_3(\text{CO})_{11}]$ can be, in fact, clearly identified also analyzing the solution in contact with CeO_2 and the nujol mull of the powder after solvent removal in vacuum. Then the cluster can be perfectly recovered by CH_3CN extraction of the powder and, as expected, it is fully decomposed under thermal treatment conditions.

5.2.3 ICP analyses of ceria catalysts

After the reported IR study, which pointed out the similarity in the chemical reactivity between the employed carbonyl clusters in contact with ceria and titania, it was

decided to exploit the know-how we experienced during titania catalysts preparation.

Ceria catalysts, bi-metallic and iron based samples, were thermally treated respectively under nitrogen (to avoid gold sintering) and in air .

As in the case of titania samples, we expected a metal weight loss for both series of catalysts, thus we checked the real metal content in all thermally treated ceria samples by meaning of ICP analyses.

The results are reported in Table 4.3.

Catalyst	Fe loading (wt. %)		Au loading ICP (wt. %)	
	Nominal	Measured	Nominal	Measured
Fe _{1.2} Au ₁ -Ce	1.2	0.7	1.0	1.0
Fe _{2.3} Au ₂ -Ce	2.3	1.6	2.0	2.2
Fe _{4.5} Au ₄ -Ce	4.3	3.2	4.0	2.7
Fe _{1.2} -Ce	1.2	0.9	-	-
Fe _{2.3} -Ce	2.3	1.7	-	-
Fe _{4.5} -Ce	4.3	2.6	-	-

Table 5.3: ICP analyses of prepared ceria catalysts.

ICP analyses on Au/FeO_x and FeO_x ceria catalysts indicate that the real metal content differs from the nominal one based on the amount of cluster deposited on support. The real Fe loading is minor than the nominal one for all catalysts and some differences are also noticed between the nominal and the real gold content in the bi-metallic sample at highest metal loading.

Evolution of Fe(CO)₅ has been verified by FT-IR analyses of condensated gases evolved during thermal treatment of the as-prepared catalysts, whereas we are not able to explain the observed gold weight loss for bi-metallic catalysts.

5.3 Catalysts characterization

In order to better understand the influence of the support on physical-chemical and catalytic properties of Au/FeO_x and FeO_x catalysts supported on titania and ceria we followed the characterization program carried out for titania samples: all thermally treated ceria catalysts have been characterized by means of BET, XRD, TEM, XPS and TPR analyses.

5.3.1 Specific surface area and XRD

For all ceria samples, surface area was measured by N₂ physisorption and single point BET analysis methods. The complete diffractograms were collected in the 2θ range 10-85°. A second, more careful, acquisition in the range 36-42 2θ° was made for Au crystal size evaluation in bi-metallic catalysts.

Surface areas and average Au crystals size for Au/FeO_x-Ce catalysts are listed in Table 4.4.

Catalyst	Carbonyl salt precursor	Surface Area (m ² /g)	Au particle size (nm)
Support (CeO ₂)	-	78	-
Fe _{1.2} Au ₁ -Ce	[NEt ₄][AuFe ₄ (CO) ₁₆]	78	<3
Fe _{2.3} Au ₂ -Ce		73	4.8
Fe _{4.5} Au ₄ -Ce		65	9.0
Fe _{1.2} -Ce	[NEt ₄][HFe ₃ (CO) ₁₁]	83	-
Fe _{2.3} -Ce		76	-
Fe _{4.5} -Ce		72	-

Table 5.4: BET specific surface area and average crystallite size of Au for studied Au/FeO_x-Ce catalysts.

BET surface area results obtained for all Au/FeO_x-Ce prepared catalysts evidence that gold/iron deposition has a little influence on the ceria porosity. Nevertheless, the material at highest cluster loading show a more significant area decrease, thus indicating that in this case Au and FeO_x particles can partially block the pores of the support. In the case of FeO_x-Ce samples, surface area values similar to the bare support were obtained, indicating that iron cluster deposition did not result in a significant change in the total porosity. The same trend was previously observed

also for titania samples [1] for which impregnation with the bimetallic cluster $[\text{NEt}_4][\text{AuFe}_4(\text{CO})_{16}]$ determined a more significant decrease of surface area while the deposition of iron carbonyl cluster did not affect this parameter.

Metal dispersion and crystal phases in ceria samples were investigated by XRD.

Figure 4.10 reports the XRD patterns for the gold/iron catalysts thermally treated under nitrogen.

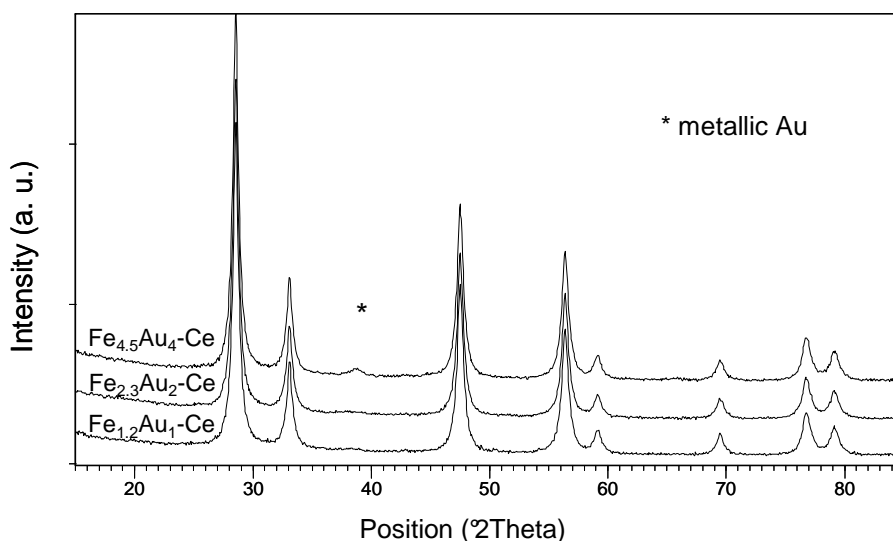


Figure 5.3: XRD patterns of bi-metallic ceria catalysts prepared with $[\text{NEt}_4][\text{AuFe}_4(\text{CO})_{16}]$.

For samples with lowest metal loading, $\text{Fe}_{1.2}\text{Au}_1\text{-Ce}$, a high metal dispersion was observed since in the related XRD patterns only characteristic reflections of CeO_2 (cubic structure) are present.

In the pattern collected for higher metal loading catalysts, besides ceria reflections, only a weak and broad peak corresponding to the most intense reflection of metallic gold was detected at $38^\circ 2\theta$ (see Table 4.4). A good dispersion on iron species was also achieved, because no diffraction peaks of metallic iron or FeO_x compounds were observed.

Similar results have been obtained for $\text{FeO}_x\text{-Ce}$ systems, for which iron species dispersion resulted to be as good as in the bi-metallic samples: in the corresponding XRD patterns reported in Figure 4.12 the cubic CeO_2 reflections were only detected

and, even at highest Fe loading on support, no reflection corresponding to iron species was observed

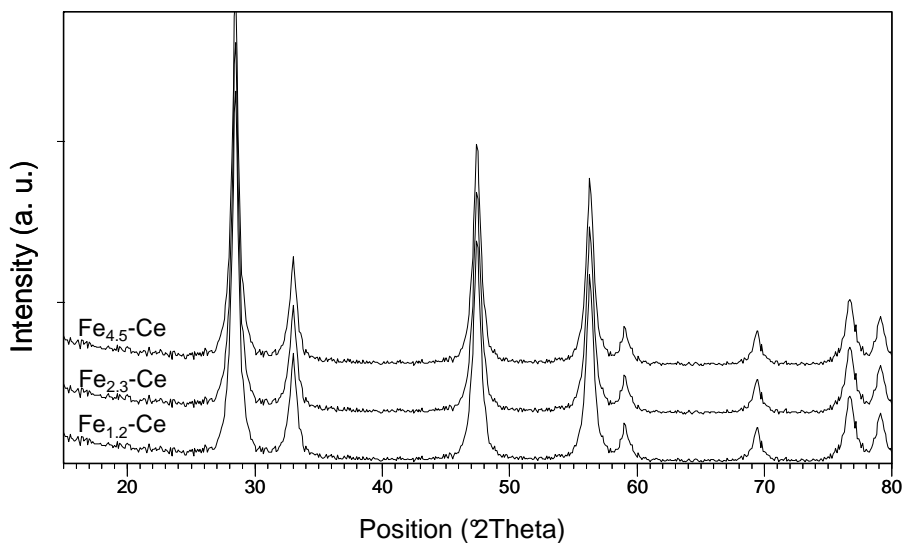


Figure 5.4: XRD patterns of FeO_x-Ce catalysts at highest metal content.

5.3.2 TEM study

The distribution of gold and iron on ceria samples was also determined by TEM. A preliminary study on the Fe_{2.3}Au₂-Ce catalyst was carried out. A typical STEM HAADF image of collected for this sample, combining also EDX analysis to observe the elemental distribution on the sample, is reported in Figure 5.5.

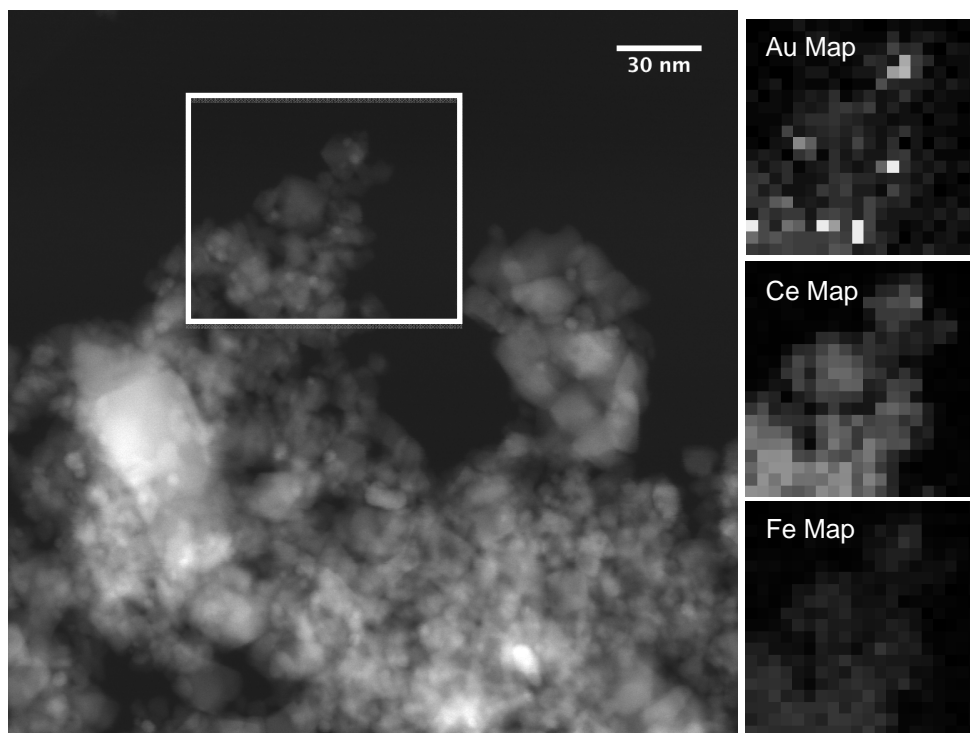


Figure 5.5: STEM image of the fresh $\text{Fe}_{2.3}\text{Au}_2\text{-Ce}$ catalyst. On the right are reported the EDX maps for Au, Ce and and Fe for the region inside the white square.

Gold appears to be aggregated in small nanoparticles over ceria surface, while iron seems to be homogeneously dispersed all over the sample.

Thus, gold and iron dispersion degrees on ceria seems to be very similar to titania catalyst.

Moreover, from HAADF images, Au particles size distribution was evaluated by ImageJ program [2] (see Figure 5.6).

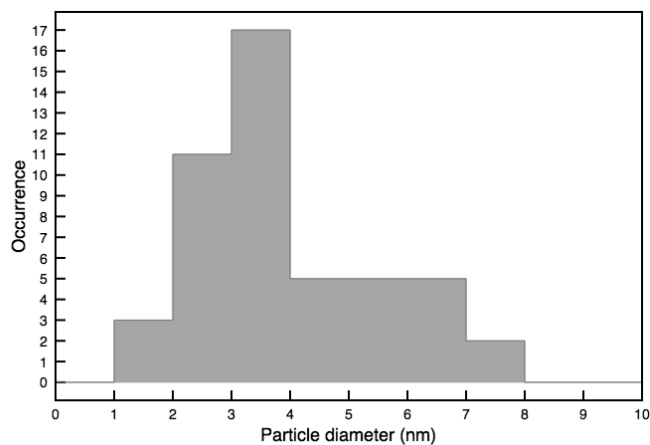


Figure 5.6: Size distribution of Au nanoparticles for $\text{Fe}_{2.3}\text{Au}_2\text{-Ce}$ catalyst.

The Au particles size is around 3-4 nm in diameter, with a distribution within the range 1-8 nm.

These data are perfectly in agreement with XRD results, concerning the metal dispersion and the evaluation of gold crystal size; moreover they suggest that a high gold and iron dispersion degree was achieved by depositing bi-metallic carbonyl clusters on ceria. These data confirm the previous results obtained depositing gold-iron carbonyl cluster on TiO_2 [3].

5.3.3 XPS studies

In order to verify the support influence on gold and iron species dispersed on ceria and make a comparison with the corresponding titania catalysts, XPS analyses were also carried out on $\text{Au/FeO}_x\text{-Ce}$ systems.

The results, in terms of Au and Fe oxidation state and surface composition are reported in Table 4.7.

Catalysts	Atomic concentration ratios				Binding Energy (eV)	
	Au/Ce XPS	Fe/Ce XPS	Au/Fe XPS	Au/Fe ICP	Au 4f	Fe 2p
Fe _{1.2} Au ₁ -Ce	0.006	0.29	0.03	0.40	83.9	710.6
Fe _{2.3} Au ₂ -Ce	0.012	0.38	0.04	0.30	83.8	710.4
Fe _{4.5} Au ₄ -Ce	0.006	0.49	0.03	0.24	83.8	710.4

Table 5.5: Atomic concentration ratios and binding energy of gold and iron in ceria catalysts.

As it was found for titania catalysts, the binding energies of gold and iron correspond respectively to metallic Au and a mixture of Fe³⁺ and Fe²⁺ species. Thus, the iron oxide layer appears to be composed of a mixture of Fe₂O₃ and FeO or Fe₃O₄ also on ceria systems.

Concerning the ceria oxidation state, there were evidences for Ce³⁺ presence; moreover Ce³⁺/Ce⁴⁺ ratio was found to be 25%/75% for all Au/FeO_x-Ce catalysts. However, it should be considered that a partial reduction of Ce⁴⁺ to Ce³⁺ could occur under analysis conditions.

Fe/Ce atomic ratio is correlated to the iron loading while Au/Ce ratio is very low in all materials and the trend does not agree with ICP results.

Au/Fe surface ratio is always under the bulk ratio; thus, a partial coverage of gold by iron atoms seems to be obtained depositing [NEt₄][AuFe₄(CO)₁₆] on ceria as previously observed on TiO₂ probably explaining also the low Au/Ce ratio observed above.

5.3.4 Temperature programmed reduction analysis

Ceria catalysts reduction profiles were recorded in order to investigate the redox interaction between the species dispersed on the surface and on the support.

In Figure 4.18 are reported H₂-TPR profiles of the FeO_x-Ce systems.

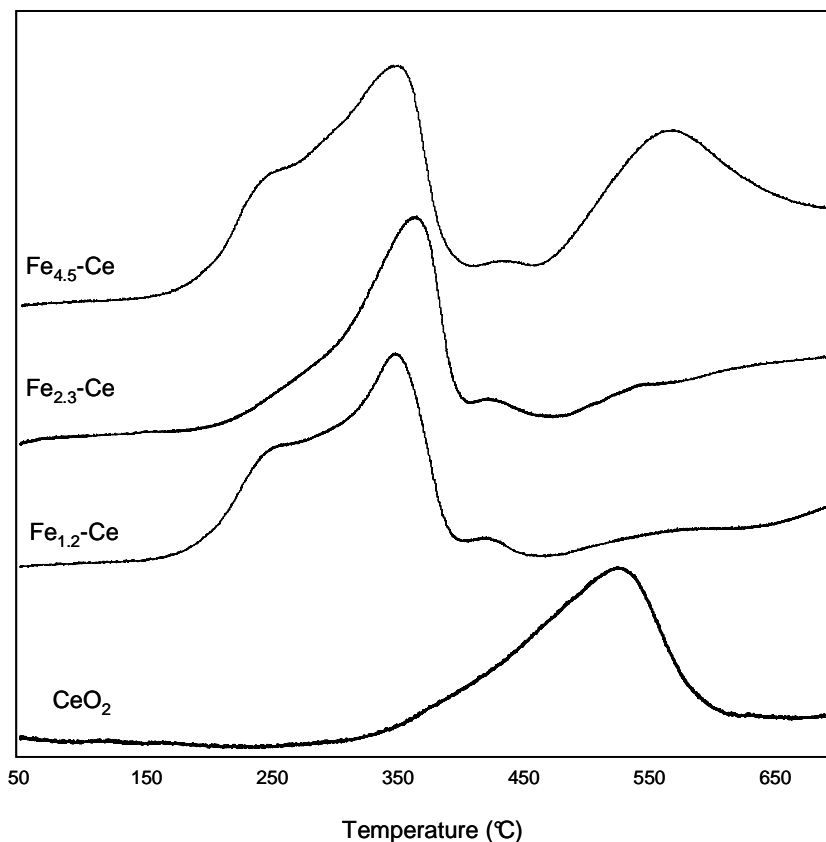


Figure 5.7: H₂-TPR analysis of FeO_x-Ce catalysts.

A reduction peak with a maximum at 340-350 °C is present in all profiles. The form of this peak is very similar for the samples at lowest and highest iron loading, in which a big shoulder at ca. 250°C can be clearly observed. Fe_{2.3}-Ce reduction profile shows instead a narrower peak at 350°C with a slight fronting. The main peak can be assigned to the reduction of Fe₂O₃ to Fe₃O₄, while the shoulder at 250°C corresponds to the reduction of hydroxylated iron oxide species, which in the case of Fe_{2.3}-Ce sample does not seem to be present. The reduction of these latter species was found to occur at lower temperature compared to titania systems and can be due to a stronger interaction between iron oxides and ceria [4]. In Fe_{4.5}-Ce reduction profile a broad peak at 550°C also appears.

The area under the reduction peak assigned to the reduction of Fe₂O₃ to Fe₃O₄ (350°C) was used to calculate the hydrogen uptake during the analyses; these data are reported in Table 4.8.

Catalyst	Fe loading (wt.%) ICP analysis	Fe loading $\mu\text{mol/g}$ sample	H ₂ uptake $\mu\text{mol H}_2/\text{g}$ sample	Portion of metal reduced (%)
Fe _{1,2} -Ce	0.9	247	642	260
Fe _{2,3} -Ce	1.7	448	664	148
Fe _{4,5} -Ce	2.6	706	517	73

Table 5.6: Characterization of redox properties of iron in the FeO_x-Ce samples according to TPR data.

As it was previously reported for FeO_x-Ti catalysts, also in this case the hydrogen consumption is greater than the stoichiometric amount necessary for iron species reduction for catalysts at low iron content. These data could indicate that CeO₂ surface oxygen reduction overlaps that of iron oxides. In fact, it is reported in literature that the addition of iron species could enhance the oxygen-release capability of CeO₂ by improving oxygen mobility [5][6]. The absence in Fe_{1,2}-Ce and Fe_{2,3}-Ce reduction profile of the peak at 550°C, typical of CeO₂ surface reduction, could thus indicate a strong interaction between iron and ceria in these two samples.

On the contrary, the hydrogen consumption detected for Fe_{4,5}-Ce catalysts was found to be much lower than the other FeO_x-Ce samples and very similar to the stoichiometric amount needed for Fe₂O₃ to Fe₃O₄ reduction. These results could confirm the hypothesis that at higher iron loading the interaction between iron species and ceria decreases, leading to lower reducibility of CeO₂. These data are confirmed by the peak at 550 °C observed in Fe_{4,5}-Ce reduction profile, attributable to ceria surface capping oxygen, which indicates that at high iron loading the interaction between iron species and ceria surface decreases.

Au/FeO_x-Ce systems reduction profile are reported in Figure 5.8. As in the case of titania bi-metallic catalysts, gold presence was expected to increase iron reducibility. Moreover, the presence of gold could also strongly influence CeO₂ reduction.

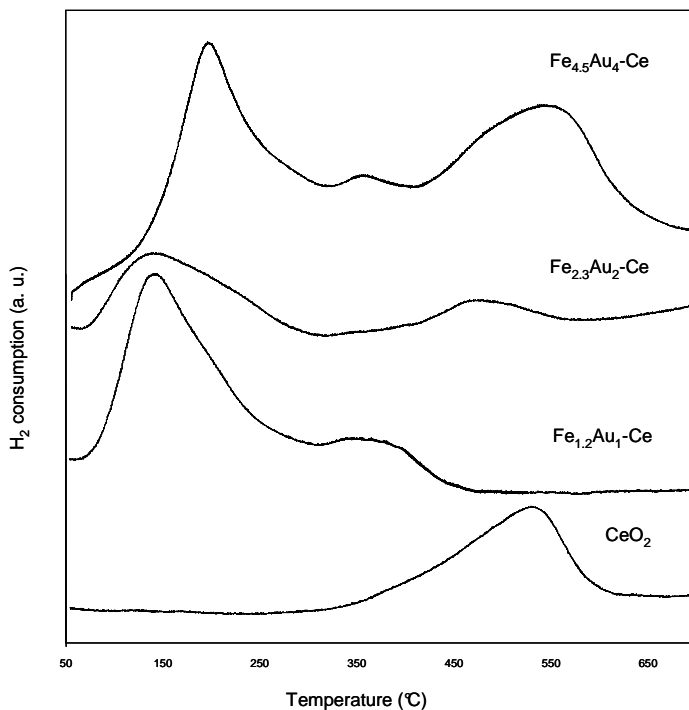


Figure 5.8: H₂-TPR analysis of Au/FeO_x-CeO₂ catalysts.

In all reduction profiles obtained for bi-metallic samples a peak at 150°C appears, confirming that gold/iron carbonyl cluster deposition on ceria leads to the formation of highly reducible iron or ceria species. In fact, it has also been reported that the presence of gold facilitates the reduction of ceria surface oxygen species [7]. Thus, in the reduction profile of Au/FeO_x-Ce catalysts it could be observed gold effect both on iron species and CeO₂ reducibility. TPR data reported in literature indicate that gold can cause a decrease in the strength of the surface Fe–O and Ce–O bonds adjacent to gold atoms, thus leading to a higher surface lattice oxygen mobility and therefore to a higher reactivity of these oxygens [7] [8] [9]. Observing the reduction profiles obtained for Au/FeO_x-Ce series, some differences can be noticed. The interaction degree between metals dispersed on the surface and ceria seems to be different. In fact, in the reduction profile of the sample prepared with the lowest cluster loading appears a single peak at low temperature followed by a broad shoulder, while for Fe_{2.3}Au₂-Ce only a weaker and broad peak appeared at low temperature. On the contrary, Fe_{4.5}Au₄-Ce reduction profile presents, beside the intense peak at low temperature, a big peak above 500 °C. The presence of this

latter peak seems to indicate the presence of a large fraction of surface ceria interacting neither with gold nor with iron. This behaviour can be clearly observed in Figure 5.9, where a comparison between the reduction profiles recorded for pure ceria, $\text{Fe}_{4.5}\text{-Ce}$ and $\text{Fe}_{4.5}\text{Au}_4\text{-Ce}$ are reported.

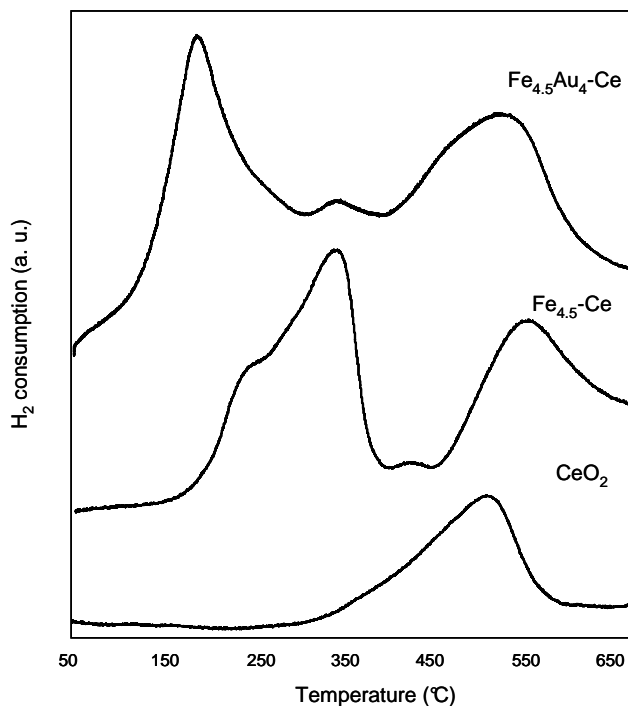


Figure 5.9: Comparison between H_2 -TPR profile of CeO_2 , $\text{Fe}_{4.5}\text{-Ce}$ and $\text{Fe}_{4.5}\text{Au}_4\text{-Ce}$.

These data, combined with the results obtained for $\text{FeO}_x\text{-Ce}$ samples, indicate that at high iron loading, the reducibility of CeO_2 surface oxygen is less influenced by iron and neither by gold.

5.4 Catalytic activity

$\text{Au/FeO}_x\text{-Ce}$ and $\text{FeO}_x\text{-Ce}$ catalysts were tested in total oxidation of toluene and methanol and in the PROX reaction

5.4.1 Toluene combustion

Toluene combustion catalytic test were performed, as described previously, ramping the temperature from 180 to 400 °C .

In Figure 4.20 is reported the toluene conversion trend depending on the temperature for FeO_x-Ce and Au/FeO_x-Ce systems

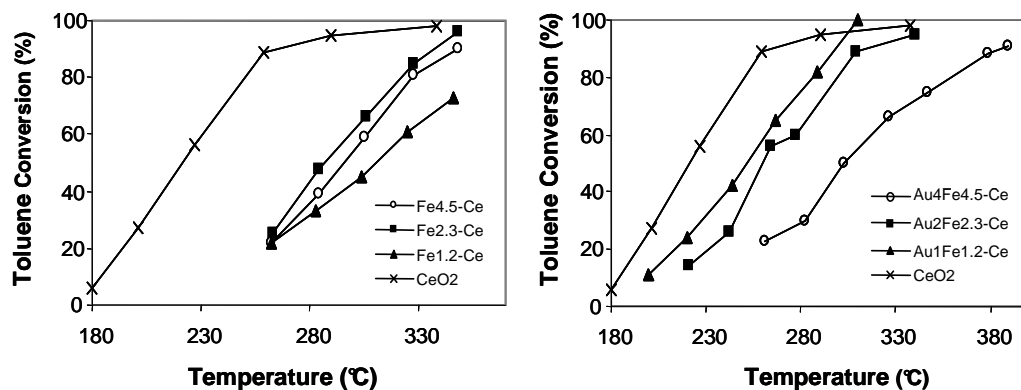


Figure 5.10: Toluene conversion as a function of reaction temperature for FeO_x-Ce (left) and Au/FeO_x-Ce (right) catalysts at different metal loading.

Surprisingly toluene total oxidation activity of ceria based catalysts strongly decreases when iron is added to the support. The same trend was also observed for bi-metallic catalysts; in this case the deactivation of ceria is depending on the cluster loading on support even if gold presence seems to mitigate this effect.

The excellent performance of CeO₂ at high surface area was also observed in toluene catalytic incineration by Wang and Lin [10]. They compared ceria performances to Pd and Pt supported catalyst and found that ceria is more active than these commonly used catalysts for VOC removal. Ceria catalytic activity is due to its ability to strongly adsorb toluene and O₂, as it has been demonstrated by TPD study conducted either on toluene and oxygen on pure CeO₂.

Moreover, it was also demonstrated that, promoted oxygen mobility is not a key catalytic parameter for toluene combustion [11]. CO₂ and water were the only determined products for all catalysts; thus, even if catalysts performances are not good in terms of toluene conversion, the efficiency toward total oxidation is maximum in all temperature reaction range.

Instead, in the case of titania systems, the presence of FeO_x species lead to an enhanced catalytic activity for toluene combustion and, even if gold had just a moderate effect on activity, it was observed that its presence was fundamental in order to increase the selectivity towards toluene complete oxidation.

5.4.2 Characterization of spent catalysts after toluene combustion reaction

In order to verify if any changes occurs on the metal dispersion of $\text{Au/FeO}_x\text{-Ce}$ samples after catalytic measurement tests in toluene oxidation, XRD analyses were performed.

Figure 4.28 reports XRD patterns of freshly prepared and spent catalysts.

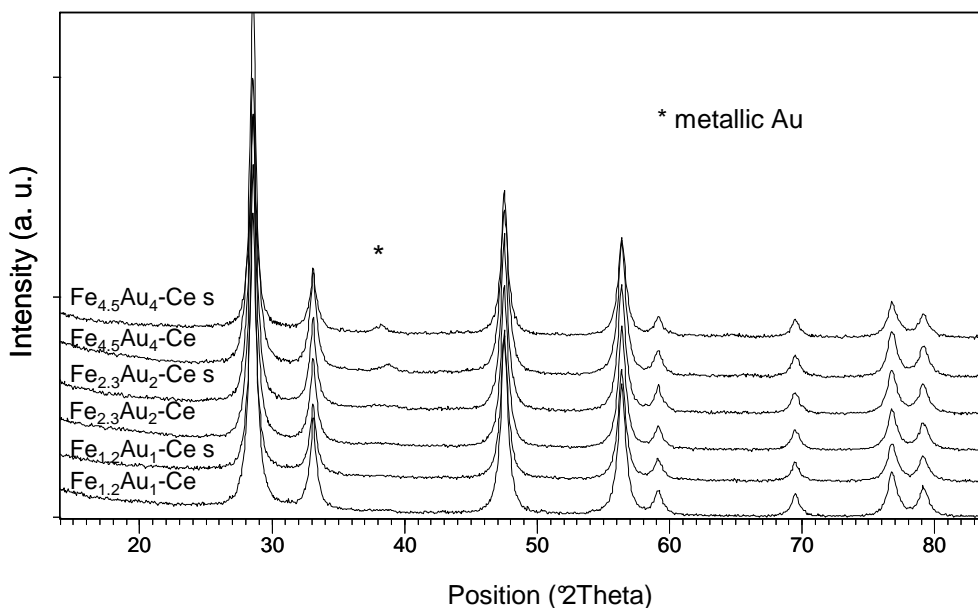


Figure 5.11: XRD patterns of the fresh and spent $\text{Au/FeO}_x\text{-Ce}$ catalysts after catalytic tests in complete oxidation of toluene.

It is clear that there are no significant changes in terms of gold dispersion on the support. As it was observed for titania catalysts, Au/FeO_x-Ce samples were found to be very stable under reaction conditions.

5.4.3 Methanol combustion

Ceria catalysts were also tested in methanol combustion. In this case better results were expected, since it is well known that methanol strongly adsorbs on gold catalysts and good results were previously obtained on Au/FeO_x-Ti catalysts.

Figure 5.12 reports light-off curves obtained for FeO_x-Ce systems.

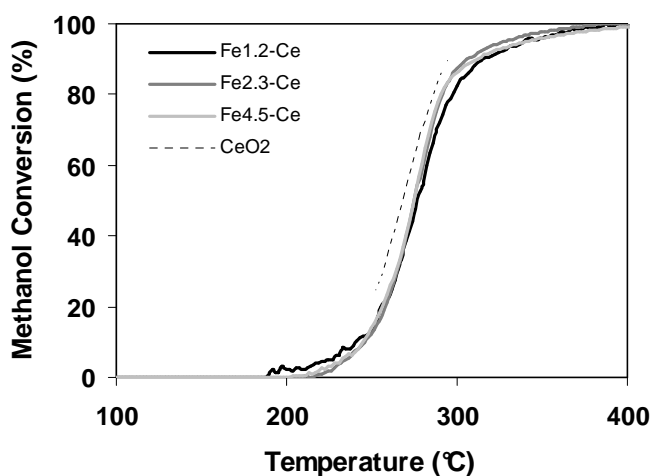


Figure 5.12: Methanol conversion as a function of reaction temperature for FeO_x-Ce catalysts at different content of active phase.

Ceria itself was found to be quite active toward methanol total oxidation; its catalytic activity is much higher than TiO₂, for which light-off curve is shifted more than 100°C to higher temperature. This effect is basically due to the extraordinary reducibility that makes ceria one of the most active materials for combustion reactions.

Anyway, it was observed that iron addition does not influence CeO₂ activity since no improvement was obtained in terms of methanol combustion at any iron loading on the support.

Catalytic tests were then performed on Au/FeO_x-ceria catalysts (see Figure 5.13).

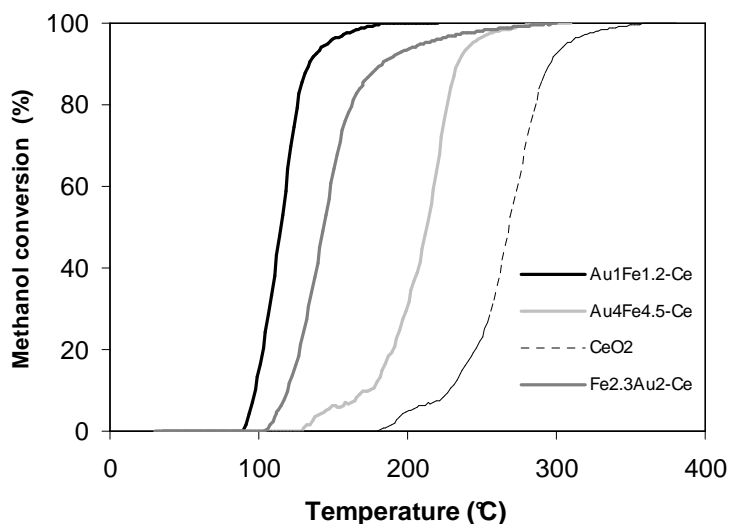


Figure 5.13: Methanol conversion as a function of reaction temperature for Au/FeO_x-Ce catalysts at different content of active phase.

From these data it is clear that Au strongly affect FeO_x-Ce catalysts performances during methanol oxidation. On the systems at lowest Au and Fe content the light-off temperature is about 100 °C lower than with just the pure ceria, while on the catalyst with the highest metal loading the shift is of about 50°C. This trend well agrees with the oxygen reducibility of catalysts evaluated by H₂-TPR. It can be suggested that there is a strong interaction between gold and surface oxide species, which increases the reactivity of the surface oxygen species, assumed to be responsible for the oxidation activity of ceria catalyst [7]. The beneficial effect of gold on FeO_x systems resulted to be significantly enhanced in the case of ceria catalysts. Also in the case of FeO_x-Ti materials the introduction of gold was found to be beneficial for methanol conversion, but gold addition to FeO_x-Ce systems leads to a much higher activity of these latter catalysts as it can be seen in Figure 5.14.

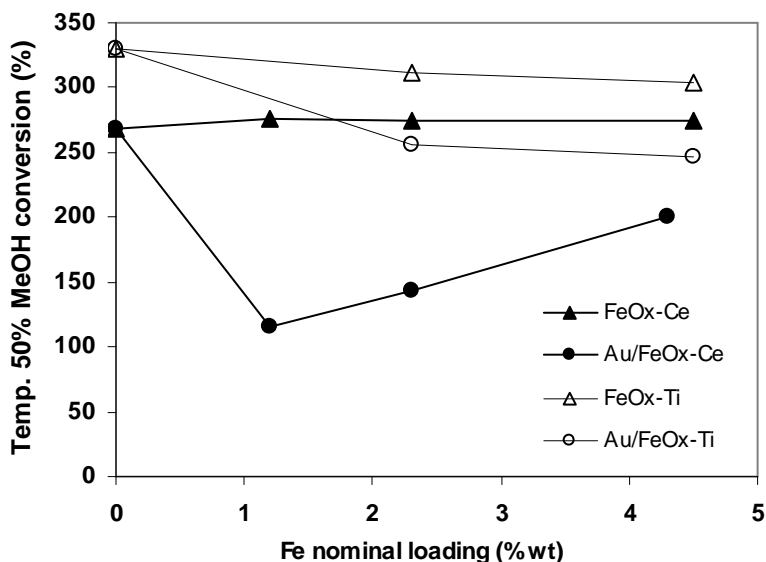


Figure 5.14: Temperature of 50% of methanol conversion as a function of the iron nominal content for titania and ceria supported FeO_x and Au/FeO_x catalysts

Observing these data it is clear that iron species dispersed on the support do not have any influence on both titania and ceria activity for methanol combustion. On the contrary, the presence of gold improved FeO_x catalysts performances, mainly in the case of ceria. In fact, T50 value is much lower for Au/FeO_x-Ce catalyst at lowest metal loading compared with the bare support.

Gold effect on surface oxygen mobility is also displayed on bi-metallic ceria catalysts selectivity towards total methanol oxidation. Figure 5.15 shows the intermediates (mainly formaldehyde) selectivity obtained for Au/FeO_x-Ce and FeO_x-Ce systems.

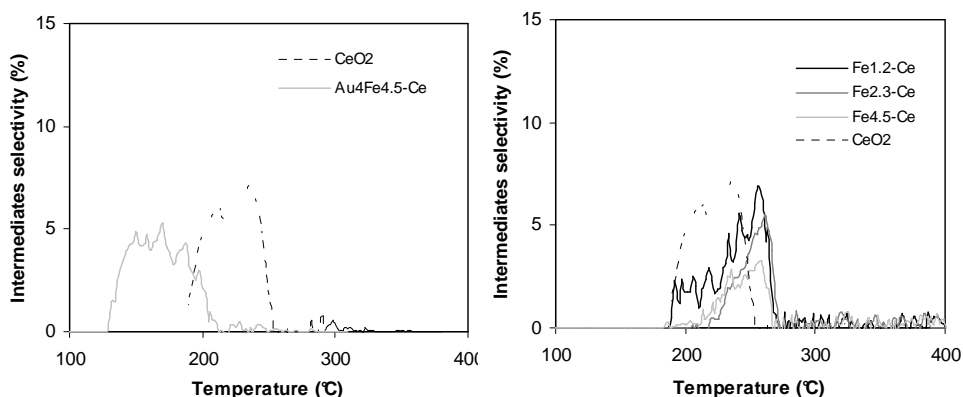


Figure 5.15: Intermediates selectivity for Au/FeO_x-Ce (left) FeO_x-Ce (right) and catalysts at different content of active phase.

The selectivity trend was the same observed for methanol conversion. In the case of bi-metallic catalysts no intermediates formation was detected for samples with lower metal loading, while a very slight effect was noticed for Fe_{4.5}Au₄-Ce sample and for FeO_x-Ce catalysts at any iron loading, compared with pure ceria performances.

5.4.4 Reaction mechanism for toluene and methanol combustion over titania and ceria catalysts

Different catalytic behaviour was observed on FeO_x and Au/FeO_x based titania and ceria catalysts, on both toluene and methanol combustion. Bigger differences were observed overall on toluene combustion.

Comparing the performances obtained on toluene total oxidation on the two different bare oxide, it was observed that ceria is much more active than titania; this difference is not only attributed to the higher and well known CeO₂ reducibility, but overall to its ability to adsorb and activate toluene. In fact it is known that oxygen mobility is not a key factor in toluene combustion, which instead strongly depend on toluene activation step.

Our results followed and confirm these reaction pathway.

VOCs combustion occurs via Mars van Krevelen mechanism, which involves adsorbed organic molecules reacting whit lattice oxygen on the catalyst surface [7] [8] [9]. In the case of titania catalysts, toluene combustion was improved due to a

higher oxygen mobility enhanced by FeO_x and Au/FeO_x species. On the contrary, FeO_x were found to decrease CeO_2 activity, even if a higher oxygen mobility was observed for these last samples. In fact, toluene activation, which is the determining factor for its oxidation [12], resulted to be more difficult due to the partial coverage of ceria sites, responsible of toluene adsorption, by FeO_x species finely dispersed on the surface.

A gold promotional effect on FeO_x -Ce was however observed, due to the furtherly improved oxygen mobility in presence of Au. In fact, as it is reported in literature [9], even if toluene does not adsorb on gold based catalyst, Au promotes toluene oxidation by enhancing oxygen mobility, probably assisting the dissociation of adsorbed oxygen on the catalyst surface.

Thus we can confirm that the determining step in toluene combustion is the toluene adsorption and activation; on the other hand a promotional effect is obtained by gold addition, due to its ability to enhance oxygen mobility of the oxide species dispersed on the catalyst surface.

In fact, even if the oxygen mobility is not a key factor in toluene combustion, it has however an important role in this reaction, being involved in the Mars van Krevelen mechanism.

Conversely, a more similar behaviour was observed for both ceria and titania catalysts on methanol total oxidation.

Methanol combustion occurs at lower temperature than toluene on both ceria and titania since alcohols oxidation is easier than aromatic compounds. In this case, performances achieved on differently supported catalysts, indicate that the oxygen mobility is the determining factor in the methanol combustion.

In fact on both TiO_2 and CeO_2 catalysts, the introduction of gold and consequently higher oxygen mobility due to the weakening of both Fe-O and Ti-O or Ce-O bonds leads to an improved methanol combustion.

It can be furtherly confirmed by our results: the catalytic activity was found to strongly depend by oxygen mobility and followed the same trend observed for catalysts reducibility.

5.4.5 PROX reaction

Au/FeO_x-Ce catalysts were also tested in the PROX reaction; in fact, both iron oxide and ceria are considered suitable supports for CO oxidation gold catalysts.

CO conversion curves obtained with these catalysts at different metal loading are reported in Figure 5.16.

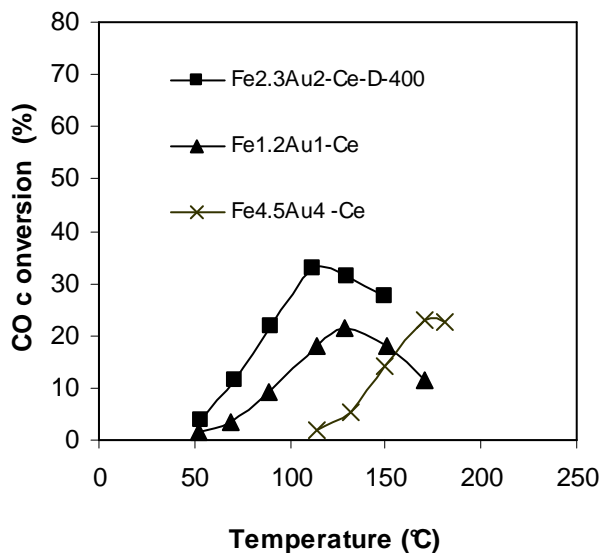


Figure 5.16 CO conversion as function of reaction temperature over Au/FeO_x-Ce catalysts.

On all catalysts CO conversion increased rising temperature, reaching a maximum which was respectively around 20-25% for Fe_{1.2}Au₁-Ce and Fe_{4.5}Au₄-Ce, and 35% for Fe_{2.3}Au₂-Ce, which was found to be the most active sample among bi-metallic ceria catalysts.

For each catalysts CO conversion follows the trend expected considering the reaction temperature; in fact all curves presented a maximum and then CO conversion decreases at higher temperatures, simultaneously to an increased H₂ activation.

These data pointed out that the CO oxidation activity of Au/FeO_x-Ce catalysts is strongly affected by metal loading on ceria, which influences metal dispersion and redox properties of the samples.

The catalytic activity in the PROX reaction observed for Au/FeO_x-Ce systems follows the order: Fe_{2.3}Au₂-Ce > Fe_{1.2}Au₁-Ce > Fe_{4.5}Au₄-Ce.

This trend can be justified in terms of catalyst metal dispersion: Fe_{4.5}Au₄-Ce showed the worst activity since the Au particles sizes are quite big for CO activation (9 nm). The difference observed between the two samples at lower metal content can be instead justified in terms of number of active sites.

Fe_{2.3}Au₂-Ce sample contains obviously more active sites than Fe_{1.2}Au₁-Ce and Au average particle size are still suitable for CO oxidation, being less than 5 nm. In addition, XPS results indicated that Au/Ce surface ratio is higher in the first sample, as well as Au/Fe atomic surface ratio.

However, the CO oxidation activity observed for these samples is not really high compared with literature data. It is probably due to the very low Au/Fe surface ratio inferred from XPS data, which was found to be much lower than bulk ratio. In fact, as it was observed for titania samples, a kind of encapsulation effect of gold by iron and FeO_x atoms can be supposed, making the active sites less accessible for CO adsorption and activation.

In this way, the positive effect that was expected to be achieved by iron addition to Au-Ce system resulted to be strongly reduced by this kind of disposition of the metal over the support.

Generally, in fact, FeO_x species are responsible to provide hydroxyl groups needed for the catalytic cycle but also oxygen defect sites at which oxygen can chemisorb[13]; moreover it has been observed that the presence of iron near to gold-TiO₂ interface enhanced oxygen activation on defects in this kind of sites that generate oxygen vacancies [14]. In addition, it has to be considered that in the presence of gold the strength of Fe-O and Ce-O bonds is weaker, thus leading to a higher lattice oxygen mobility and then improved catalyst performances [7] [8] [9]. All these considerations become important taking into account that on Au/iron oxides catalysts, PROX reaction occurs through a Mars-van Krevelen mechanism, which involves active lattice oxygen species of the support reacting with CO adsorbed on gold particles and/or at the metal-support interface [15]. Actually, the effect of gold on the reducibility of oxides species on the catalysts surface was clearly observed in all Au/FeO_x-Ce catalysts reduction patterns, mainly for the sample at lower metal content, on which higher CO oxidation was achieved.

The selectivity towards CO oxidation, defined as the ratio of O₂ consumption for the CO oxidation to the total amount of O₂ consumption, are reported in Figure 5.17.

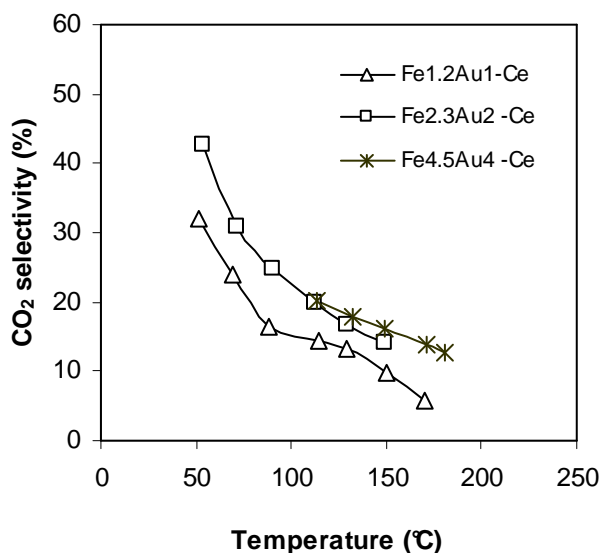


Figure 5.17: CO₂ selectivity as function of reaction temperature over Au/FeO_x-Ce catalysts.

These results follow the same trend of CO conversion observed for Au/FeO_x-Ce catalysts: CO₂ selectivity is higher for Fe_{2.3}Au₂-Ce. This samples showed then the best performances on CO PROX reaction.

5.5 Effect of catalyst thermal treatment

The effect of the thermal treatment temperature on Au/FeO_x-Ce performances was also investigated. In fact, it is known that there could be an effect on catalytic activity probably related to the changes induced in the iron oxides phase and their oxidation state by different thermal treatment conditions.

It has been reported that the activity of Au/FeO_x catalysts towards CO conversion is influenced by the treatment temperature both in oxidizing and in reducing atmosphere. In particular the higher the treatment temperature the lower the CO conversion, the detrimental effect being more evident when the temperature exceeded 300°C and preferentially when a reducing atmosphere is used [15].

This negative effect on catalytic activity can be related to the enlargement of gold particles and to the transformation of the more active hydroxylated iron oxide species into less reducible species.

In order to investigate the effect of the temperature used during the thermal treatment of Au/FeO_x-Ce catalysts on their properties, a study was carried out on Fe_{2.3}Au₂-Ce sample.

Fe_{2.3}Au₂-Ce was prepared following the same procedure used to deposit the bi-metallic cluster, as described in Chapter 2. After carbonyl cluster impregnation and solvent removal in vacuum, all samples were dried in air at 100°C. At this point, one part of the sample was treated under nitrogen at 200 °C, while the other part was characterized and used like that. These two samples were then compared with Fe_{2.3}Au₂-Ce treated at 400°C. All cited samples are listed in Table 5.7.

Catalyst	Drying conditions	Thermal treatment conditions
Fe _{2.3} Au ₂ -Ce-D	Air at 100°C	-
Fe _{2.3} Au ₂ -Ce-D-200	Air at 100°C	N ₂ at 200°C
Fe _{2.3} Au ₂ -Ce-D-400	Air at 100°C	N ₂ at 400°C

Table 5.7: Code of Fe_{2.3}Au₂-Ce samples treated at different temperature.

The metal dispersion on these samples was determined by XRD in order to verify by lowering the temperature a better gold dispersion could be achieved.

Au crystal size was evaluated from Au diffraction line at 38 2θ° for all samples. (see Table 5.8).

Catalyst	Surface Area (m ² /g)	Au particle size (nm)
Fe _{2.3} Au ₂ -Ce-D	-	7.7
Fe _{2.3} Au ₂ -Ce-D-200	64	4.6
Fe _{2.3} Au ₂ -Ce-D-400	73	4.8

Table 5.8: Surface area and Au crystal size for Fe_{2.3}Au₂-Ce samples depending on thermal treatment temperature.

Actually these results indicate that a higher dispersion was achieved for the catalyst thermally treated at 200°C and 400°C compared to the just dried sample and that, rising the temperature up to 400°C under nitrogen, do not have any detrimental

effect on gold particle size for $\text{Fe}_{2.3}\text{Au}_2\text{-Ce}$ sample. Conversely, a kind of redispersion effect is observed after thermal treatment.

Beneficial effect due to the temperature rise was observed also on surface area; it is possible that at 200°C the cationic part of the cluster salt (tetra-Ethyl ammonium) is just partially decomposed, blocking part of support porosity.

The influence of different thermal treatments on the catalytic properties of these samples was investigated both in methanol combustion and PROX reaction.

Results obtained for methanol combustion are reported in Figure 5.18.

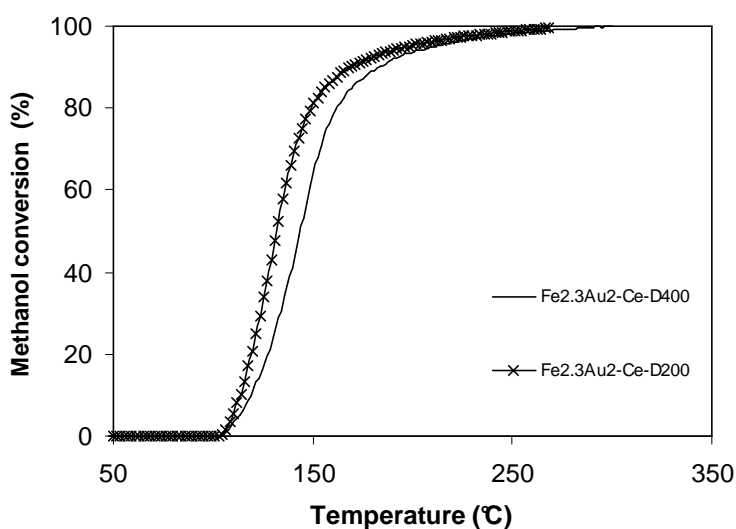


Figure 5.18: Methanol conversion on $\text{Fe}_{2.3}\text{Au}_2\text{-Ce}$ samples depending on thermal treatment temperature.

These data indicate that lowering the temperature used to treat this kind of catalyst lead to a higher activity in methanol combustion, probably due to the formation of more reducible species responsible for the higher catalytic activity.

On the contrary, the catalytic activity in preferential CO oxidation was found to be higher in the case of the samples treated at highest temperature, as it is shown in Figure 5.19.

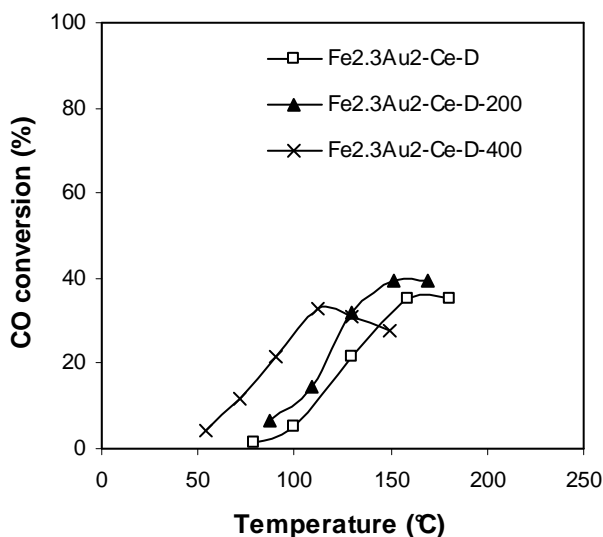


Figure 5.19: CO conversion on Fe_{2.3}Au₂-Ce samples depending on thermal treatment temperature.

The observed trend in the CO oxidation activity for Fe_{2.3}Au₂-Ce material treated in different ways depends firstly from Au dispersion on the samples. In fact, Au crystal dimensions are larger in the case of the dried catalyst (7.7 nm), which showed the lowest activity, while are almost the same in the two samples treated under nitrogen at 200°C and 400°C, respectively. Among these last two samples, even if the sample treated at 400°C is more active at lower temperature, a higher conversion can be achieved on Fe_{2.3}Au₂-D-200 (see Figure 5.20).

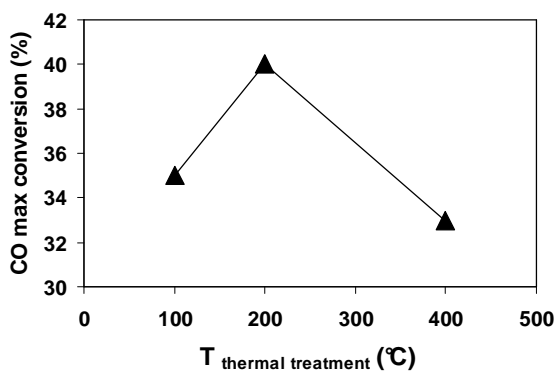


Figure 5.20: CO maximum conversion on Fe_{2.3}Au₂-Ce samples depending on thermal treatment temperature.

The same trend was also observed in terms of selectivity to CO oxidation (Figure 5.21)

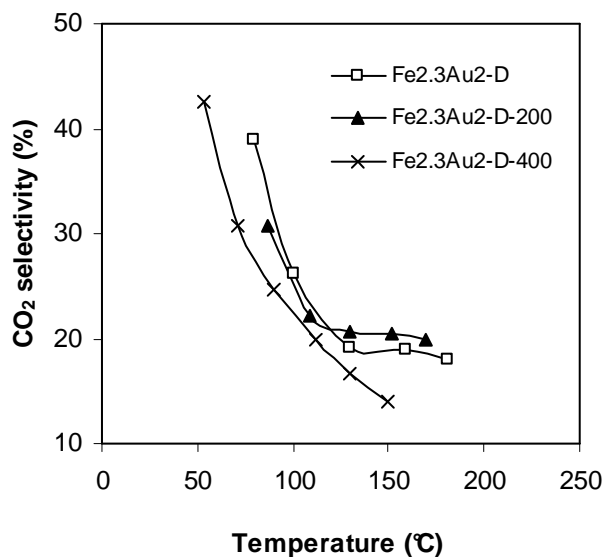


Figure 5.21: CO selectivity on Fe_{2.3}Au₂-Ce samples depending on thermal treatment temperature.

These results indicate that, among investigated Fe_{2.3}Au₂-Ce catalysts, the sample treated at 200°C is the most selective at temperature above 120°C.

This behaviour is in agreement with data reported in the literature; even if the differences in the catalytic activity are not very big, they confirm the possibility to obtain more hydroxylated iron oxide species, responsible for a higher CO oxidation activity, tuning the temperature used during catalyst thermal treatment.

5.5.1 Study on catalysts pretreatment conditions

A more detailed study was also carried out on catalyst pretreatment conditions. The aim of this study was basically to better-control the bi-metallic cluster decomposition over the support, avoiding Fe(CO)₅ loss. In fact, for both titania and ceria catalyst series, the real iron loading was always found to be lower than the theoretical one and evolution of Fe(CO)₅ has been verified during thermal treatment of as prepared catalysts.

Thus, in order to reduce the Fe loss extent, the formation of this volatile compound should be prevented or at least minimized using more suitable operative conditions. With the intention of avoiding $\text{Fe}(\text{CO})_5$ evolution during cluster decomposition, a wet air flow was used during $\text{Fe}_{2.3}\text{Au}_2\text{-Ce}$ pretreatment at 100°C , instead of dry air. In this way iron oxidation should occur simultaneously with cluster decomposition, being favoured by the presence of water, instead of escaping from the support surface in the form of $\text{Fe}(\text{CO})_5$.

Some of this “as prepared” sample was characterized and tested without performing any other treatment in order to verify if the wet air pretreatment induced any change in the catalyst properties. Moreover, part of $\text{Fe}_{2.3}\text{Au}_2\text{-Ce}$ pretreated in wet air, was also thermally treated at 400°C under nitrogen in order to compare its performances with the standard sample.

The codes of these last samples and their respective drying conditions are reported in Table 5.9.

Catalyst	Drying conditions	Thermal treatment conditions
$\text{Fe}_{2.3}\text{Au}_2\text{-Ce-D}$	Air at 100°C	-
$\text{Fe}_{2.3}\text{Au}_2\text{-Ce-D-400}$	Air at 100°C	N_2 at 400°C
$\text{Fe}_{2.3}\text{Au}_2\text{-Ce-W}$	Flowing Wet Air (10% vol H_2O)	-
$\text{Fe}_{2.3}\text{Au}_2\text{-Ce-W-400}$	Flowing Wet Air (10% vol H_2O)	N_2 at 400°C

Table 5.9: Code and their pretreatment conditions of $\text{Fe}_{2.3}\text{Au}_2\text{-Ce}$ systems.

In order to verify if the pretreatment in wet air resulted to be useful for limiting iron weight loss, iron content of these samples was measured by ICP. The results are reported in Table 5.10.

Catalyst	Fe loading (wt. %)	
	Nominal	Measured
Fe _{2.3} Au ₂ -Ce-D	2.3	1.9
Fe _{2.3} Au ₂ -Ce-D-400		1.6
Fe _{2.3} Au ₂ -Ce-DW		2.3
Fe _{2.3} Au ₂ -Ce-DW-400		2.0

Table 5.10: ICP results of Fe_{2.3}Au₂-Ce systems pretreated under different conditions.

These data clearly indicate that iron loss is smaller for samples pretreated in wet air, confirming the possibility of limiting the evolution of Fe(CO)₅ and consequently reducing the discrepancy between the theoretical and the real iron loading observed for samples treated in dry air.

Metal dispersion and crystal phases in Fe_{2.3}Au₂-Ce systems treated under different conditions were investigated by XRD.

Figure 5.22 reports the XRD results obtained for these catalysts.

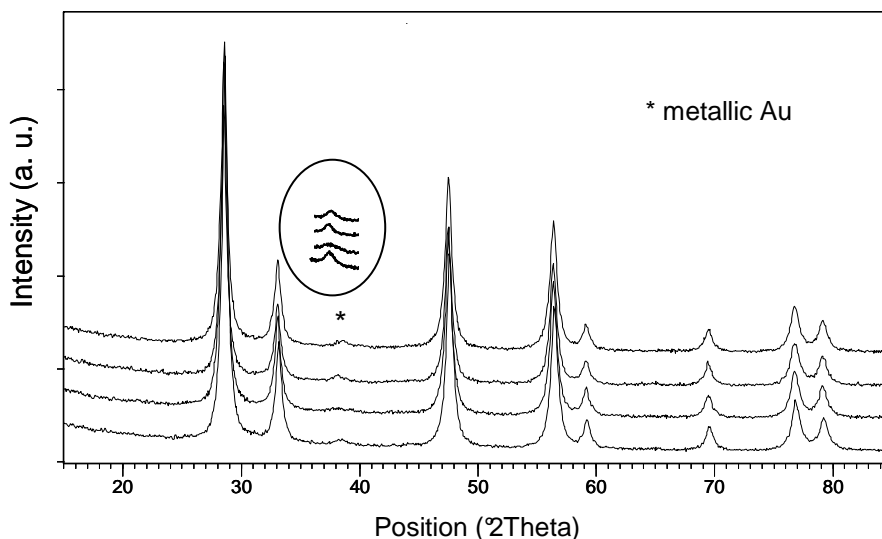


Figure 5.22: XRD patterns of Fe_{2.3}Au₂-Ce systems pretreated under different conditions.

In all patterns collected, besides ceria reflections, only a weak and broad peak corresponding to the most intense reflection of metallic gold was detected at 38.26° . No reflections due to iron oxide species were detected, indicating that wet air pretreatment does not influence iron dispersion on ceria. On the contrary, a detrimental effect on gold dispersion was observed. Au crystal size, calculated from XRD patterns are reported in Table 5.11. Gold particles present on sample $\text{Fe}_{2.3}\text{Au}_2\text{-Ce-W}$ are bigger than dispersed on sample pretreated in dry air, moreover the gold redispersion observed for this latter system after being thermal treated under nitrogen at 400°C was absent for the material pretreated in wet air.

Catalyst	Surface Area (m^2/g)	Au particle size (nm)
$\text{Fe}_{2.3}\text{Au}_2\text{-Ce-D}$	-	7.7
$\text{Fe}_{2.3}\text{Au}_2\text{-Ce-D-400}$	73	4.8
$\text{Fe}_{2.3}\text{Au}_2\text{-Ce-W}$	-	8.5
$\text{Fe}_{2.3}\text{Au}_2\text{-Ce-W-400}$	70	7.1

Table 5.11: Surface area and Au crystal size for $\text{Fe}_{2.3}\text{Au}_2\text{-Ce}$ catalyst treated under different conditions.

The worse gold dispersion could be related to the fast iron oxidation induced by water which could lead to local higher temperature, responsible of gold sintering. Thus, a careful optimization of thermal treatment in presence of steam is still necessary.

BET surface area were also measured in order to understand if this different pretreatment could affect support porosity. Data reported in Table 5.11 indicate a substantial equality in the surface area detected for samples treated under different conditions.

The prepared $\text{Fe}_{2.3}\text{Au}_2\text{-Ce}$ samples were first tested in the PROX reaction (see Figure 5.23)

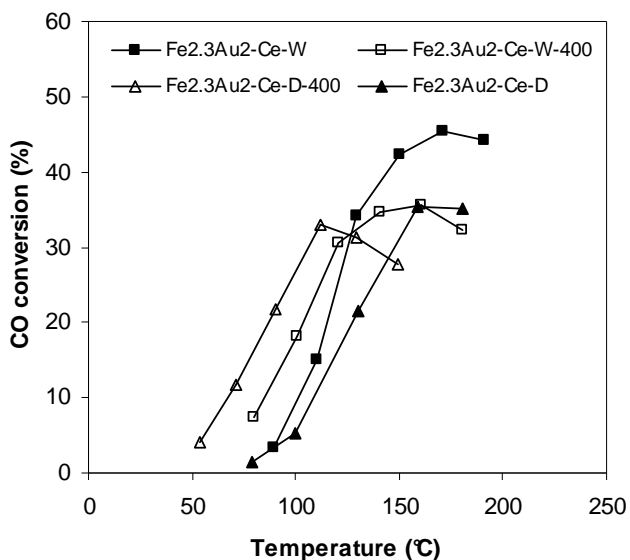


Figure 5.23: CO conversion on Fe_{2.3}Au₂-Ce catalyst treated under different conditions.

From these results it is clear that CO oxidation activity on Fe_{2.3}Au₂-Ce system is affected by the pretreatment conditions, being in the order: D-400 >W-400 >W >D. This trend can be explained on the bases of gold particle dimensions: in fact, a good correlation exists between Au crystal size and the temperature at which the maximum of CO conversion can be achieved on the corresponding catalyst (see Figure 5.24).

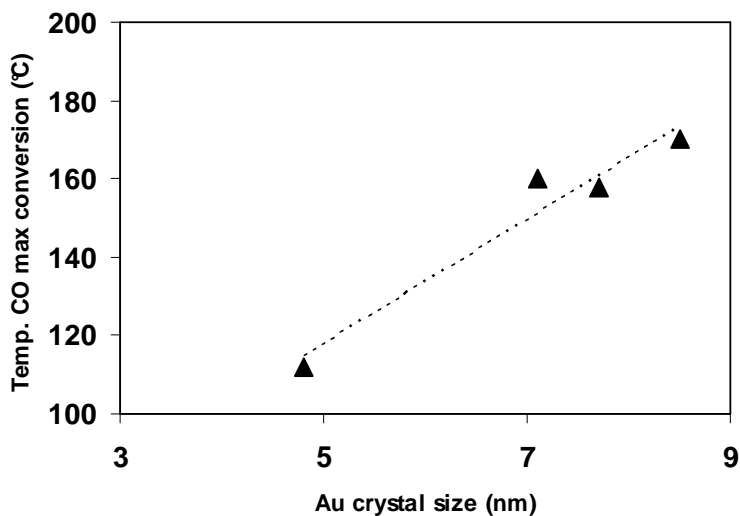


Figure 5.24: Temperature at the maximum of CO conversion depending on Au crystal size on $\text{Fe}_{2.3}\text{Au}_2\text{-Ce}$ catalyst treated under different conditions.

The sample D-400 is the most active catalyst at low temperature having the smallest gold particle size, but its activity fastly decrease rising temperature. In fact, on this catalyst the lowest selectivity toward CO oxidation was achieved, as it is shown in Figure 5.25.

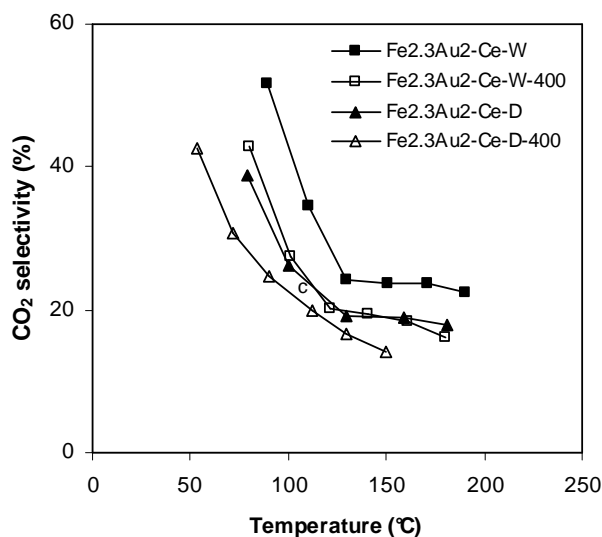


Figure 5.25: CO₂ selectivity on Fe_{2.3}Au₂-Ce catalyst treated under different conditions.

The trend observed for both activity and CO₂ selectivity can be explained considering that CO mainly adsorbs on small Au particles and on Au/oxide interface. Thus, in the presence of bigger gold particles, CO activation is more difficult depending on both Au dimensions and Au/oxide perimeter interface, the latter being shorter when gold dimensions increase. In addition it has to be considered that when gold particles are bigger, the oxygen supply, considered to enhance CO oxidation, resulted decreased, since a weaker oxygen mobility is achieved when interaction between Au and oxide species is not favoured. In this way CO oxidation occurs at higher temperature and a higher CO₂ selectivity is obtained. O₂ conversion trend obtained for this series of samples can also confirm these considerations: in fact the lower oxygen conversion observed on bigger particles could negatively affect also the hydrogen oxidation, responsible of lowering CO oxidation.

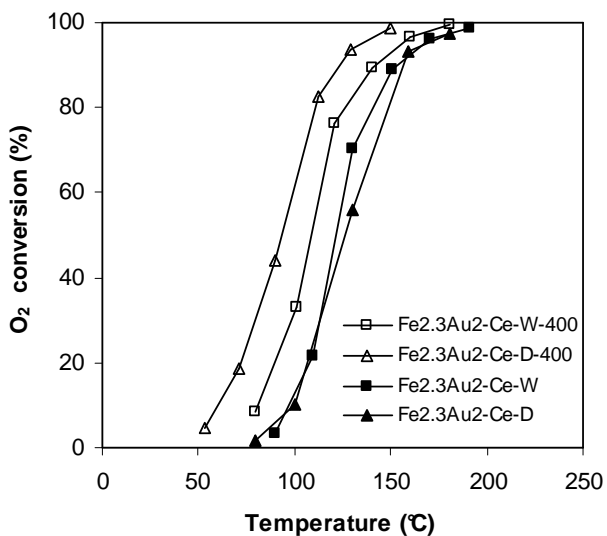


Figure 5.26: O₂ conversion on Fe_{2.3}Au₂-Ce catalysts treated under different conditions.

The samples thermal treated under nitrogen at 400°C were also tested in methanol combustion reaction (see Figure 5.27).

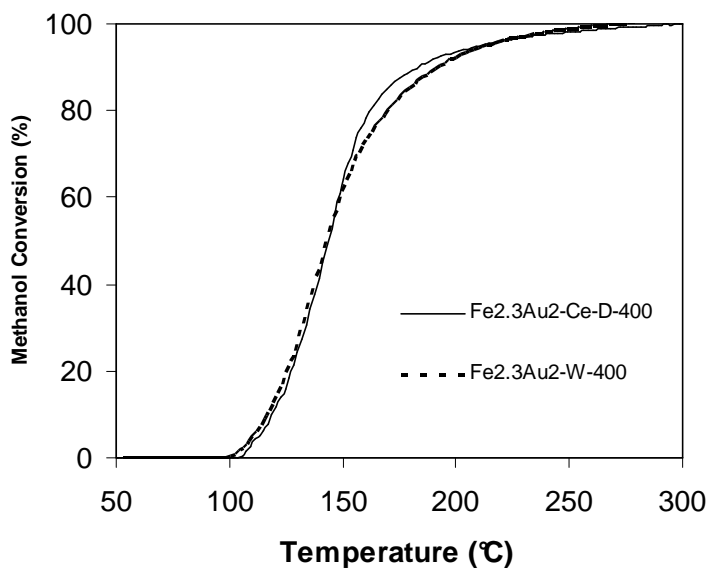


Figure 5.27: Methanol conversion depending on reaction temperature for Fe_{2.3}Au₂-Ce-D400 and Fe_{2.3}Au₂-Ce-W-400 samples.

No differences were observed in the methanol combustion performances of samples $\text{Fe}_{2.3}\text{Au}_2\text{-Ce-D}$ and $\text{Fe}_{2.3}\text{Au}_2\text{-Ce-W-400}$, indicating that the efficiency of this reaction is not depending on Au particle size.

5.6 Iron content effect

Au/ $\text{FeO}_x\text{-Ce}$ performances obtained in the PROX reaction, beside depending on Au particles dimension, are probably strongly affected by the number of surface active sites. Au/ FeO_x catalysts preparation by depositing bi-metallic carbonyl cluster on the support leads to a good metal dispersion, but very low surface Au/Fe atomic ratio. A kind of gold encapsulation effect by iron specie was hypotised, probably depending on the cluster structure and composition.

With the intent to obtain a higher Au/Fe surface atomic ratio and consequently a larger gold sites availability, the bi-metallic cluster salt $[\text{NEt}_4]_4[\text{Au}_4\text{Fe}_4(\text{CO})_{16}]$ (Fe/Au=1) was employed to prepare Au/ $\text{FeO}_x\text{-Ce}$ materials at lower iron content.

Using the method described in Chapter 2, a bi-metallic sample was prepared by impregnation of the cluster solution on ceria, dosed in order to obtain Au 2%wt. and, consequently, Fe 0.6% wt.. This sample was then pretreated following the same methods used to perform the study on the pretreatment conditions, as described in the previous section, in order to investigate on catalysts properties when a smaller amount of iron species is dispersed on the support.

The code and the treatment conditions of these samples are listed in Table 5.12.

Catalyst	Dryng conditions	Thermal treatment conditions
$\text{Fe}_{0.6}\text{Au}_2\text{-Ce-D}$	Air at 100°C	-
$\text{Fe}_{0.6}\text{Au}_2\text{-Ce-D -400}$	Air at 100°C	N_2 at 400°C
$\text{Fe}_{0.6}\text{Au}_2\text{-Ce-W}$	Flowing Wet Air (10% vol H_2O)	-
$\text{Fe}_{0.6}\text{Au}_2\text{-Ce-W-400}$	Flowing Wet Air (10% vol H_2O)	N_2 at 400°C

Table 5.12: Code and preparation conditions for $\text{Fe}_{0.6}\text{Au}_2\text{-Ce}$.

Since a detrimental effect on gold particle size was previously observed for wet air pretreated Au/FeO_x-Ce samples, metal dispersion on ceria was firstly investigated by XRD .

In the obtained diffraction patterns no reflections related to iron species were observed, indicating that iron dispersion is not affected by the thermal treatment conditions. Conversely, gold dispersion on Fe_{0.6}Au₂-Ce is slightly lower than Fe_{2.3}Au₂-Ce (Au particle size =4.8 nm) as it can be seen Table 5.13.

Catalyst	Surface Area (m ² /g)	Au particle size (nm)
Fe _{0.6} Au ₂ -Ce-D	-	6.8
Fe _{0.6} Au ₂ -Ce-D -400	78	6.9
Fe _{0.6} Au ₂ -Ce-W	-	6.8
Fe _{0.6} Au ₂ -Ce-W-400	67	7.8
Fe _{2.3} Au ₂ -Ce-D	-	7.7
Fe _{2.3} Au ₂ -Ce-D-400	73	4.8
Fe _{2.3} Au ₂ -Ce-W	-	8.5
Fe _{2.3} Au ₂ -Ce-W-400	70	7.1

Table 5.13: Surface area and Au crystal size for Fe_{0.6}Au₂-Ce catalyst treated under different conditions.

These data perfectly agree with results reported in literature, indicating that FeO_x species can stabilize small Au particles [16]. These results also indicate that, starting from [NEt₄]₄[Au₄Fe₄(CO)₁₆], a very similar metal dispersion can be achieved on both ceria and titania, as it was previously observed in the case of [NEt₄]₄[AuFe₄(CO)₁₆].

In this case, Au crystal size were found to be the same for both Fe_{0.6}Au₂-Ce-D and Fe_{0.6}Au₂-Ce-W, thus, gold dispersion was found not to be affected by the wet air pretreatment. At lower iron loading the iron oxidation should be a milder phenomenon and consequently the exothermicity extent related to the iron oxidation does not furtherly affect Au crystal size . Moreover, the gold redispersion obtained on Fe_{2.3}Au₂-Ce samples by the thermal treatment performed at 400 °C under nitrogen, was not observed in this case: in fact, a slight increase of gold particle size was

observed overall on $\text{Fe}_{0.6}\text{Au}_2\text{-Ce-W-400}$. These data furtherly confirm the stabilization effect due to FeO_x species on gold particles.

Thermally treated catalysts were first tested in methanol combustion.

Results obtained on samples pretreated in dry air, $\text{Fe}_{0.6}\text{Au}_2\text{-Ce-D-400}$, were compared to the respective sample at higher Fe content, $\text{Fe}_{2.3}\text{Au}_2\text{-Ce-D-400}$, in Figure 5.28.

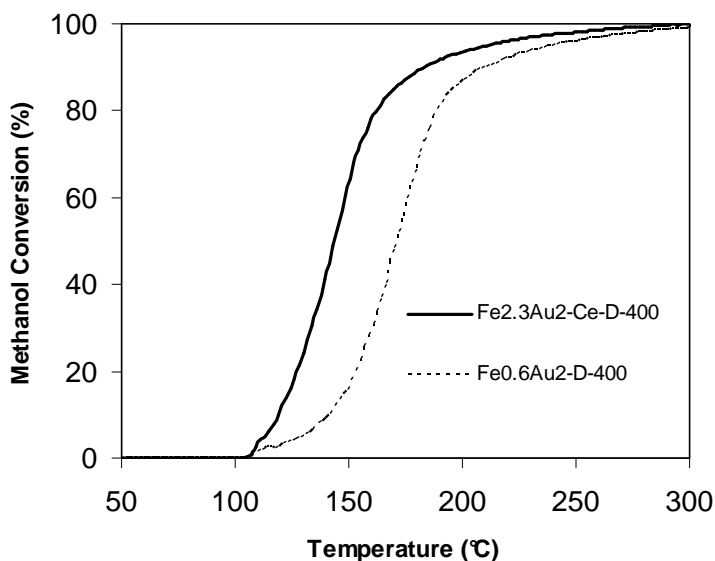


Figure 5.28: Methanol conversion over Au/ FeO_x -Ce samples at 2%Au wt. at different iron loading.

These results indicate that methanol conversion depends on iron loading: the higher metal content the higher methanol combustion rate.

This trend seems to not agree with the previously observed FeO_x -Ce behaviour: in fact FeO_x species did not show any influence on ceria catalytic performance in methanol combustion. However, the higher activity detected for $\text{Fe}_{2.3}\text{Au}_2\text{-Ce-D-400}$ could be related to higher amount of reducible species due to a stronger interaction between gold and surface oxide species.

Pretreatment conditions effect on methanol combustion activity was also investigated on sample at lower iron content (see Figure 5.29).

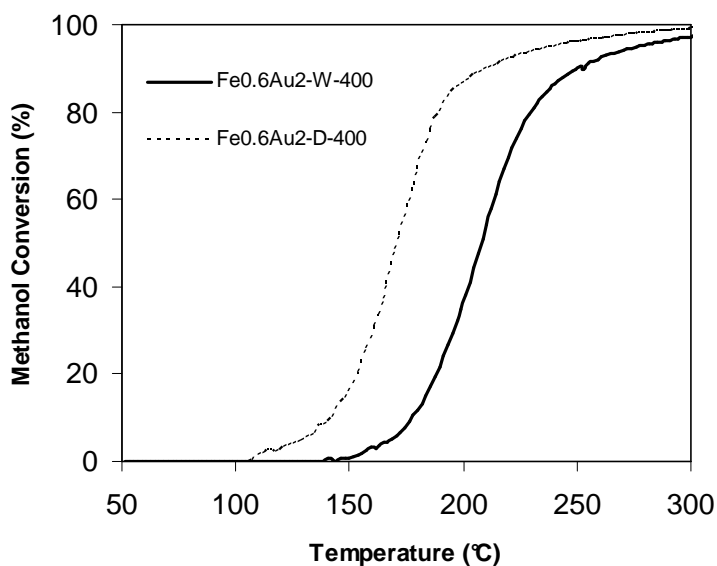


Figure 5.29: Methanol conversion over thermal treated $\text{Fe}_{0.6}\text{Au}_2\text{-Ce}$ thermal treated in different conditions.

Contrary to what it was previously observed on $\text{Fe}_{2.3}\text{Au}_2\text{-Ce}$ sample pretreated under different conditions, $\text{Fe}_{0.6}\text{Au}_2\text{-Ce}$ pretreated under wet air showed a worse activity than the respective sample pretreated in dry conditions. In Figure 5.30 are reported the catalytic performances of $\text{Au}/\text{FeO}_x\text{-Ce}$ systems in terms of T50 depending on iron loading and pretreatment conditions.

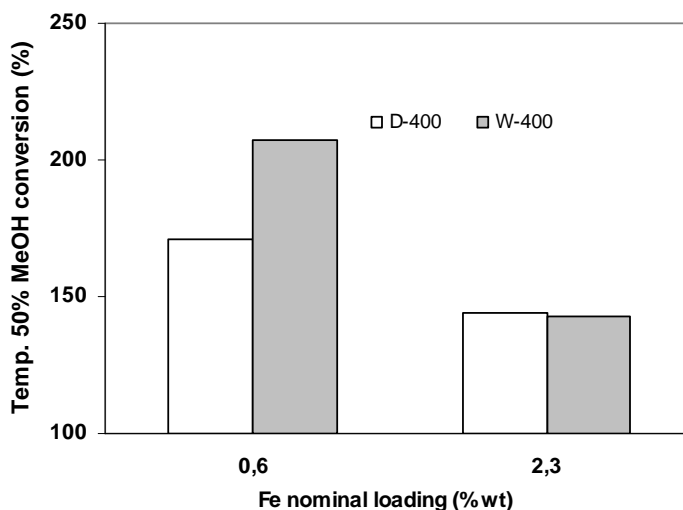


Figure 5.30: Temperature of 50% methanol conversion over thermal treated Au/FeO_x-Ce catalysts (Au=2% wt.) at different iron content and pretreatment conditions.

From these results it can be inferred that methanol oxidation activity is strongly dependent on the iron content and that wet air pretreatment leads to surface species less active in the reaction.

A detailed investigation on the nature of these different species obtained on bi-metallic catalysts starting from two different carbonyl is currently in progress to better understand and explain the observed phenomena. Several aspects have to be furtherly explored: verify which kind of phase or species are obtained starting from the two different clusters, how they change depending on different treatment conditions and if a different interaction exist between the species present on the support varying the iron loading .

Fe_{0,6}Au₂-Ce samples were also tested in PROX reaction

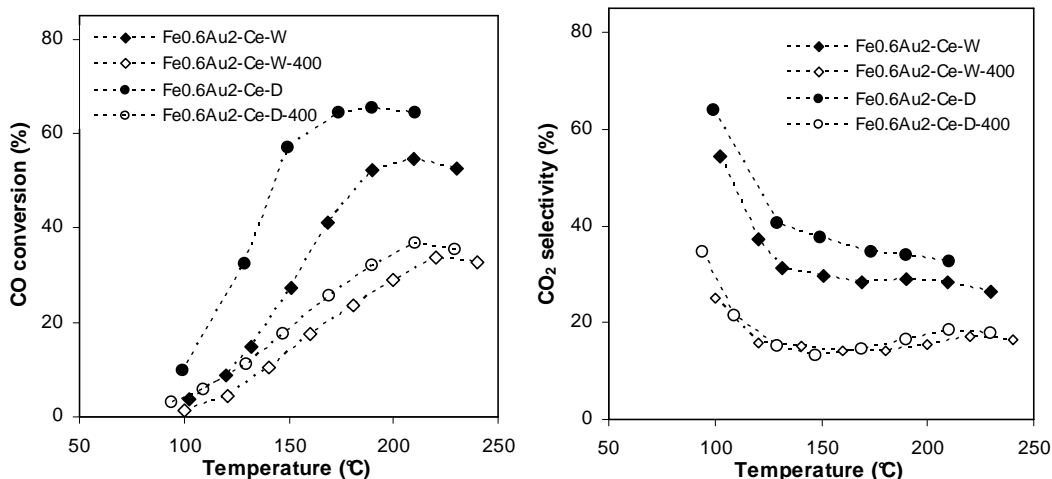


Figure 5.31: CO conversion and selectivity over thermal treated $\text{Fe}_{0.6}\text{Au}_2\text{-Ce}$ depending on pretreatment conditions.

CO conversion on this series of $\text{Fe}_{0.6}\text{Au}_2\text{-Ce}$ catalysts prepared under different conditions, follows the order $D > W > D-400 > W-400$.

Dried samples both in dry and wet air were more active than the thermal treated ones, and the wet air pretreatment leads to a minor activity on CO oxidation.

CO_2 selectivity results, reported in Figure 5.31, follow the same trend, suggesting the presence of particularly active species on the dried samples which seems to disappear after thermal treatment at 400°C under nitrogen.

In this case, catalytic activity can not be justified in terms of Au crystal size. In fact, only a moderate effect of gold particle size on CO oxidation was observed, considering that a minor influence should be taken into account, since they are bigger than 5 nm in all samples (see Figure 5.32).

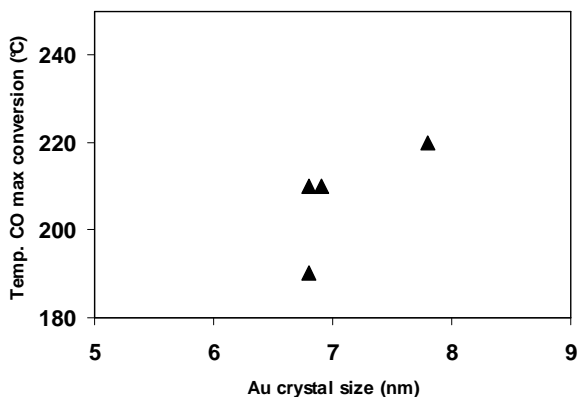


Figure 5.32: Temperature at the maximum of CO conversion depending on Au crystal size on $\text{Fe}_{0.6}\text{Au}_2$ -Ce catalyst treated under different conditions.

Moreover, a lower CO oxidation and CO_2 selectivity was obtained on $\text{Fe}_{0.6}\text{Au}_2$ -Ce-W suggesting a detrimental effect do to the wet air pretreatment.

The effect of iron content on CO PROX activity was also investigate, comparing the systems at different iron loading.

Figure 5.33 compare CO conversion and selectivity obtained on samples with different iron loading, thermal treated at 400°C under N_2 ($\text{Fe}_{0.6}\text{Au}_2$ -Ce and $\text{Fe}_{2.3}\text{Au}_2$ -Ce).

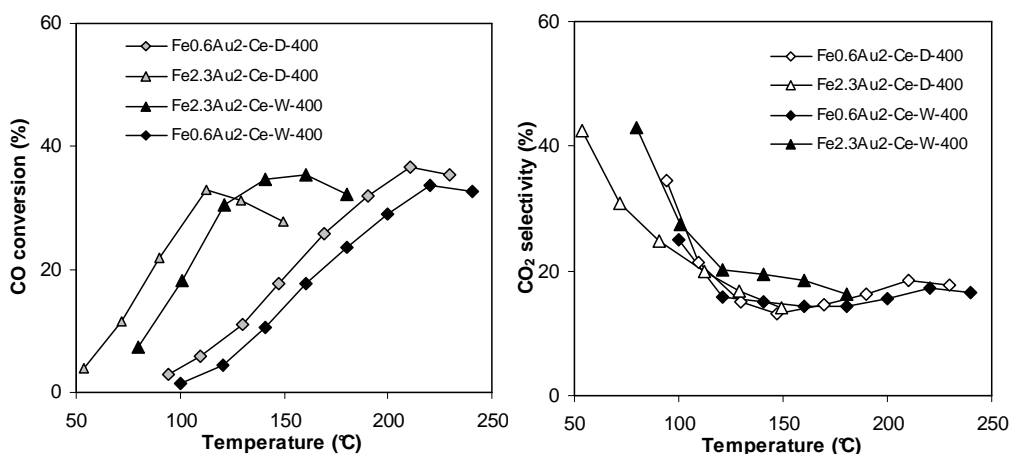


Figure 5.33: CO conversion (right) and selectivity (left) over thermal treated Au/ FeO_x -Ce (Au 2% wt.) containing different iron loading.

These results indicate that iron loading influence CO oxidation on thermal treated Au/FeO_x-Ce catalysts.

Samples with higher iron loading are active at lower temperature, but the maximum of CO conversion is almost the same for all samples. The higher activity obtained with higher iron content can be due to the FeO_x stabilization effect on gold dimensions, which also implies a larger Au/FeO_x interface where CO preferentially chemisorb. Moreover, data reported in literature clearly demonstrated that when gold nanoparticles are covered by FeO_x layer, as it was observed by XPS on our catalysts, the active sites in the CO oxidation are located on the iron oxide itself, promoted by gold underneath [17]. In this last case, higher catalytic activity is due the strong electronic effect occurring at FeO_x/Au interface coupling—through the FeO_x layer. A possible explanation of this effect, corroborated by results obtained on Pt/CeO₂ systems [18], its that the electron transfer from metal to oxide was considered to reduce enthalpy for oxygen vacancy formation in the oxide layer.

Nevertheless, CO₂ selectivity achieved on thermal treated samples seems to not depend on iron loading, suggesting that thermal treatment leads to the formation of similar species on which H₂ activation is equally favoured.

Minor differences on CO conversion were instead observed on just pretreated samples (see Figure 5.34).

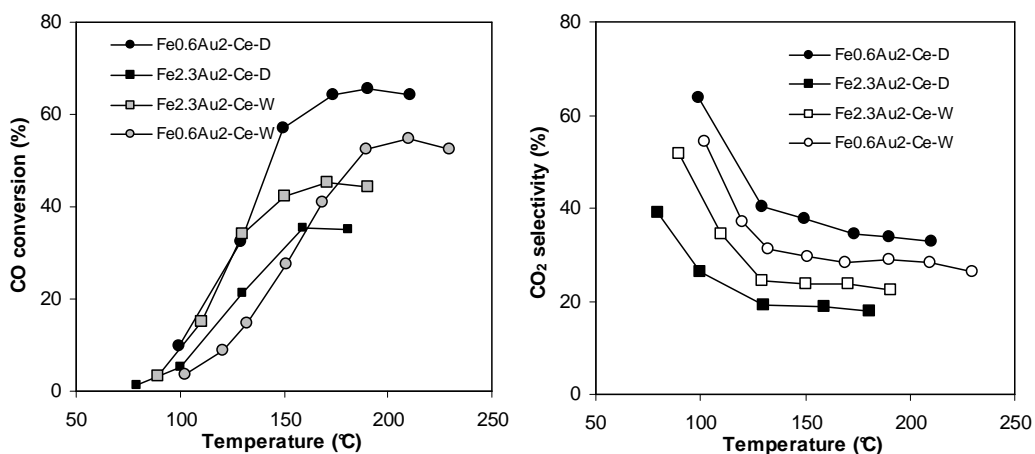


Figure 5.34: CO conversion (left) and selectivity (right) over pretreated Au/FeO_x-Ce (Au 2% wt.) containing different iron loading.

On these catalysts CO activation seems to occur at higher temperature but in the same range for all samples, probably due to the similar Au dispersion on the surface.

Actually, on the samples at lower iron loading a higher maximum of CO conversion was observed, corresponding also to a higher selectivity in CO PROX reaction.

In this case the iron content seems to be less influent on CO activation, however the formation of particularly active species during pretreatment, which changes under the effect of temperature, can not be excluded. In fact the interaction between Au and oxide layer is strongly influenced, rather than by Au particle size, also by the phase, dimension, morphology and shape of the oxide species.

A more detailed study is currently in progress in order to investigate on the nature of these species to find a correlation between their properties and the observed phenomena.

5.7 Bibliografia

- [1] S. Albonetti, R. Bonelli, R. Delaigle, C. Femoni, E. M. Gaigneaux, V. Morandi, L. Ortolani, C. Tiozzo, S. Zacchini, F. Trifirò, *Appl. Cat. A: Gen.* 372 (2010) 138.
- [2] T.J. Collins, *BioTechniques* 43 (2007) 25.
- [3] S. Albonetti, R. Bonelli, R. Delaigle, C. Femoni, E. M. Gaigneaux, V. Morandi, L. Ortolani, C. Tiozzo, S. Zacchini, F. Trifirò, *Appl. Cat. A: Gen.* 372 (2010) 138.
- [4] K. Z. Li, H. Wang, Y.G. Wey, *J. Phys. Chem. C* 113 (2009) 15288.
- [5] K. Z. Li, H. Wang, Y.G. Wey, *J. Phys. Chem. C* 113 (2009) 15288.
- [6] H. Kaneko, T. Miura, H. Ishihara, S. Taku, T. Yokoyama, H. Nakajima, Y. Tamaura, *Energy* 32 (2007) 656.
- [7] S. Scirè, S. Minicò, C. Crisafulli, C. Satriano, A. Pistone, *Appl. Cat. B: Env* 40 (2003) 43.
- [8] S. Scirè, S. Minicò, C. Crisafulli, S. Galvagno, *Cat. Comm.* 2 (2001) 229.
- [9] S. Minicò, S. Scirè, C. Crisafulli, R. Maggiore, S. Galvagno, *Appl. Cat. B: Env.* 28 (2000) 245.
- [10] C-H. Wang, S-S. Lin, *Appl. Cat.A: Gen.* 268 (2004) 227.
- [11] B. de Rivas, J. Gutierrez-Ortiz, R. Lopez-Fonseca, J. R. Gonzalez-Velasco, *Appl. Cat.A: Gen.* 314 (2006) 54.
- [12] B. de Rivas, J. I. Gutierrez-Ortiz, R. Lopez-Fonseca, J. R. Gonzalez-Velasco, *Appl. Catal. A: Gen.* 314 (2006) 54.
- [13] F. Moreau, G.C Bond, *Top. Catal.* 44,1-2, (2007) 95.
- [14] S. Carrettin, Y. Hao, V. Aguilar-Guerrero, B. C. Gates, S. Trasobares, J. J. Calvino, A. Corma, *Chem. Eur. J.* 13 (2007) 7771.
- [15] S. Scirè, C. Crisafulli, S. Minicò, G. G. Condorelli, A. Di Mauro, *J. Mol. Cat. A: Chem.* 284 (2008) 24.
- [16] A. C. Gluhoi, N. Bogdanchikova, B. E. Nieuwenhuys, *J. Catal* 229 (2005) 154.
- [17] L. Gucci, K. Frey, A. Beck, G. Peto, C. S. Daroczi, N. Kruse, S. Chenakin, *Appl. Cat. A: Gen* 291 (2005) 116.

[18] C. Hardacre, R. M. Ormerod, R. M. Lambert, *J. Phys. Chem.* 98 (1994)10901.

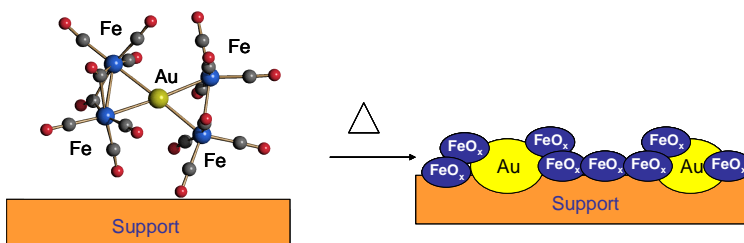
6. CONCLUSIONS

Au/FeO_x and FeO_x catalysts supported on titania and ceria were prepared by impregnation of carbonyl clusters as precursors of highly dispersed active phase. Au/FeO_x were obtained by employing bi-metallic carbonyl cluster salts [NEt₄]₄[Au₄Fe₄(CO)₁₆] (Fe/Au=1) and [NEt₄][AuFe₄(CO)₁₆] (Fe/Au =4), while FeO_x samples were prepared by employing the homometallic [NEt₄][HFe₃(CO)₁₁] cluster. Particular attention was made in the optimization of a suitable thermal treatment in order to achieve, along with a good Au and Fe metal dispersion, the formation of appropriate species with good catalytic properties.

The innovative preparation method used for the synthesis of CeO₂ and TiO₂ supported materials resulted in small gold metallic nanoparticles surrounded by highly dispersed iron oxide species, essentially in an amorphous phase.

Starting from both [NEt₄]₄[Au₄Fe₄(CO)₁₆] and [NEt₄][AuFe₄(CO)₁₆] salts, a very similar metal dispersion can be achieved either on ceria or on titania. Accordingly, the use of different metal oxides as supports does not seem to influence Au and Fe dispersion on the surface. The results herein described confirmed that FeO_x species can stabilize small Au particles. In fact, keeping constant the gold content but introducing a higher iron amount by means of [NEt₄][AuFe₄(CO)₁₆] salts, gave higher gold dispersion than using [NEt₄]₄[Au₄Fe₄(CO)₁₆] cluster.

A kind of encapsulation of gold atoms by iron oxide species was obtained since the Au/Fe surface ratio was found much lower than bulk ratio (Scheme 1).



A strong interaction between gold and oxide species was observed, both for iron oxide and the supports, especially for ceria species, denoted by a significantly enhanced reducibility.

All prepared catalysts were tested in the total oxidation of VOCs, using toluene and methanol as probe molecules for aromatic and alcohol compounds, and in the PROX reaction.

Different catalytic behaviour was observed on titania and ceria catalysts, on both toluene and methanol combustion and the wider variance was observed overall on toluene reactivity.

In the case of TiO_2 supported catalysts, toluene combustion was improved due to the higher oxygen mobility resulting from enhanced oxygen activation due to FeO_x and Au/FeO_x species dispersed on titania. The presence of Au was found to moderately improve FeO_x -Ti activity, due to the low toluene tendency to adsorb on gold-based catalysts; conversely an enhanced selectivity toward the combustion reaction was achieved due to the enhanced O_2 activation and Au ability on CO oxidation.

In the case of ceria catalysts, bare CeO_2 itself was found to be more active than both FeO_x and Au/FeO_x supported materials. However, on the latter catalysts, the introduction of gold was found to moderate the deactivation effect due to FeO_x species. In fact, ceria catalytic performances on toluene oxidation are due to its ability to adsorb toluene and O_2 . Since oxygen mobility is not a key factor in toluene combustion, CeO_2 activity is strongly decreased by FeO_x surface coverage which reduce the toluene adsorption on ceria sites, while the positive effect of gold was due to its ability to strongly enhance oxygen mobility on the catalyst surface. In fact, even if this latter aspect is not a key factor in toluene combustion, it has however an important role on this reaction being involved in the reaction pathway, that follows Mars van Krevelen mechanism.

More similar performances were obtained for both ceria and titania catalysts on methanol total oxidation.

In this case, the results obtained on differently supported catalysts, indicate that the oxygen mobility is the determining factor in the reaction.

In fact, on both TiO_2 and CeO_2 catalysts, the introduction of gold and consequently the higher oxygen mobility due to the weakening of both Fe-O and Ce-O bonds

leads to improved methanol combustion. Moreover, the catalytic activity was found to follow the same trend observed for catalysts reducibility.

Regarding PROX reaction it was verified that titania based catalysts are less active than ceria ones, due to the lower reducibility of titania compared to ceria. In fact the availability of lattice oxygen involved in CO total oxidation is much higher in the latter material.

However, the CO conversions observed for these samples are relatively low respect to literature data. These scarce results are probably due to the very low Au/Fe surface ratio inferred from XPS data.

CO preferential oxidation was found to strongly depend on Au particle size but also on the reducibility of surface oxygen, influenced from the different species which can be formed.

Actually, the effect of gold on the reducibility of oxide species present on the catalyst surface was clearly observed in all Au/FeO_x-Ce catalysts, especially for samples at lower metal content, on which higher CO conversion was achieved.

With the aim to improve Au/FeO_x-Ce performances in CO PROX the effect of samples thermal treatment and pretreatment was investigated.

In general, lowering of the catalyst thermal treatment temperature leads to more hydroxylated iron oxide species, responsible for higher CO oxidation activity.

A more detailed study was also carried out on Au/FeO_x-Ce catalyst pretreatment conditions. The aim of this study was basically to better-control the bi-metallic cluster decomposition over the support, avoiding Fe(CO)₅ loss. In fact, for both titania and ceria catalyst series, the real iron loading was always found to be lower than the theoretical one due to the evolution of Fe(CO)₅ during catalyst thermal treatment. A wet air pretreatment was then performed in order to force the iron oxidation simultaneously with the cluster decomposition, being favoured by the presence of water, instead of escaping from the support surface in the form of Fe(CO)₅.

Iron loss was found to be smaller for samples pretreated in wet air, confirming the possibility of limiting the evolution of Fe(CO)₅ and consequently reducing iron loss.

Conversely, a detrimental effect on gold dispersion was observed, due to the fast iron oxidation induced by water which could lead to local higher temperature, responsible of gold sintering.

CO PROX oxidation activity was found to be affected by the pretreatment conditions, depending on gold particles dimensions. On the other hand the influence of different FeO_x species on CO conversion and selectivity should be taken into account.

With the intent to obtain a higher Au/Fe surface atomic ratio and consequently a larger gold sites availability, the bi-metallic cluster salt $[\text{NEt}_4]_4[\text{Au}_4\text{Fe}_4(\text{CO})_{16}]$ (Fe/Au=1) was employed to prepare Au/ FeO_x -Ce materials with constant Au loading but lower iron content. In this way the iron content effect was also investigated.

The gold dispersion on samples at minor iron loading was slightly lower than at higher iron content, thus the stabilization effect due to FeO_x species on gold particles was confirmed.

In this case, catalytic activity do not only depend on Au crystal size since a moderate effect of gold particle size on CO oxidation was observed. Iron content seems not to strongly affect CO activation; however the formation of particularly active species during pretreatment, which changes under the effect of temperature, can not be excluded. In fact the interaction between Au and oxide layer is strongly influenced, rather than by Au particle size, also by the phase, dimension, morphology and shape of the oxide species.

The novel preparation method by employing carbonyl bi-metallic Fe-Au clusters with a well defined structure resulted in well dispersed gold nanoparticles anchored to the support via an iron layer. In this way a good stabilization of gold particles was achieved and, at the same time, the beneficial effect of gold on iron oxide reducibility was obtained.

These results indicate the possibility for this preparation method to find further applications in order to obtain a good Au dispersion over supports on which stabilization of gold nanoparticles is difficult. A first attempt on Au/ FeO_x supported SBA-15 mesoporous silica prepared by bi-metallic carbonyl cluster impregnation has been made and some preliminary promising results have been obtained.

Nevertheless, a careful optimization of thermal treatment in presence of steam, in order to improve Au dispersion and simultaneously favour the presence of more active iron species is still necessary.

A detailed investigation on the nature of these different species obtained on bi-metallic catalysts starting from two different carbonyl bi-metallic clusters is currently in progress to better understand and explain the observed phenomena and find a

correlation between catalyst properties and their catalytic performances. Several aspects have to be furtherly explored: to verify which kind of phase or species are obtained starting from the two different clusters, how they change depending on different treatment conditions and if a different interaction exists between the species present on the support varying the iron loading.